ENDOCYTIC RECYCLING AND REGULATION OF THE EARLY-TO-RECYCLING ENDOSOME TRANSITION

BY OU LIU

A dissertation submitted to the

Graduate School—New Brunswick

Rutgers, The State University of New Jersey

And

The Graduate School of Biomedical Sciences

in partial fulfillment of the requirements for the

Joint Degree of Doctor of Philosophy

Graduate Program in Cell and Developmental Biology

Written under the direction of

Dr. Barth D. Grant

and approved by

_____

_____

_____

_____

New Brunswick, New Jersey

October, 2015

ABSTRACT OF THE DISSERTATION

Endocytic recycling and regulation of the early-to-recycling endosome transition

by Ou Liu

Dissertation Director: Dr. Barth D. Grant

Endocytic recycling is the process by which cells return internalized cargos and receptors back to plasma membrane. Efficient recycling of cargos requires ordered transport of cargos from early endosome to recycling endosome. This is mainly achieved through the coordination of small GTPase RAB-5 and RAB-10. The small GTPase RAB-5 is a master regulator of cargo sorting at the early endosome and RAB-10 is a key resident of the recycling endosome. Countercurrent cascades of GEFs and GAPs for Rab proteins have been proposed to mediate Rab conversion, a process in which early acting Rabs are inactivated by later acting Rabs. Here we demonstrate that a downstream Rab protein, RAB-10, binds to and recruits a RAB-5 GAP, TBC-2, onto endosomes to inactivate the upstream Rab, RAB-5. This process is critical for proper relay of cargos from RAB-5 controlled early endosomes to RAB-10 regulated recycling endosomes. Lack of TBC-2 disrupted RAB-5/RAB-10 interaction and caused accumulation of recycling cargo hTAC-GFP in a malfunctioned hybrid early-recycling endosome compartment. Furthermore, our study showed that this cargo transition process from early to recycling endosome also requires the concerted effort by a BAR-domain protein AMPH-1, which acts as a binding partner and a contributor to the recruitment of TBC-2 on endosomes. In addition, the *C. elegans* Rac1 homolog CED-10 can also bind and recruit it to

endosomes. Taken together, our worked showed that RAB-10, AMPH-1 and CED-10 act in a concerted manner and recruits TBC-2 to inactivate RAB-5. These interactions are essential for early-to-recycling endosome transition and endocytic recycling.

We further demonstrated here that RAB-10, recruits CNT-1, the *C. elegans* homolog of mammalian ACAP1 and ACAP2 (Arf6 GTPase-activating proteins) to inactivate ARF-6 and downregulate endosomal PI(4,5)P2, a key phosphoinositide in membrane traffic.

Acknowledgements

Looking back, the past six years have been a memorable journey to me. Six years ago, as a young student who freshly graduated from college, I left my home country and began my exploratory journey in science in the United States.

I would like to give my heartfelt thanks to Dr. Barth Grant, my Ph.D. mentor. I thank Barth for his brilliant ideas as a scientist and providing me a supporting and encouraging environment for doing scientific research. Barth trained me with great patience and taught me research skills that helped to shape my ways of thinking in science. Doing science does not guarantee stepping forward all the time even with a lot of hard work. I'm especially grateful for Barth's support and encouragement over the time when experiments simply don't work. Barth has always been by my side to help and teach me how to troubleshoot. From Barth, I have learned that sometimes we need to take a step back in order to prepare for better marching forward. I learned to keep faith and persistence even when faced with setbacks and despair.

I would also like to thank members of my committee Dr. Chris Rongo, Dr. Richard Padgett and Dr. Maureen Barr. I genuinely appreciate their kind help and constructive advice during our meetings and through my graduate years. Their generous support is a valuable asset to me.

I thank the current members of the Grant lab, Adenrele(Dee) Akintobi, Dr. Anne Norris, Peter Schweinsberg for a cooperative working environment. I'm also grateful to have learned from former lab members. I appreciate their constant help and useful input for my projects.

Without the support of my family, I would never have been able to accomplish this challenging task. My parents constantly give me their support, encouragement and unconditional love and share with me my joy and bitter throughout the years. I'm

fortunate enough to have met my husband, Bin Guo, in graduate school. He is always by my side to help, encourage me and influence me to work hard. He is always with me through late night experiments and he always managed to bring sunshine to my life even when I'm disappointed and despaired from failures. I'm especially grateful to the love and support my family gives me.

Dedication

To my family

Table of Contents

Chapter 1.

Introduction

An overview of endocytosis

Cells internalize extracellular materials, fluid, macromolecules, membrane components, receptors and their associated ligands through endocytosis. Endocytosis is a process by which cells uses budding vesicles to selectively take in macromolecules such as nutrients and intercellular signals from the outside environment. This process plays a key role in removing lipids and proteins from the plasma membrane, maintaining the homeostasis of the plasma membrane and counterbalancing secretion (Sato et al., 2014).

Internalization of receptors and ligands occurs mainly through two major pathways: the canonical clathrin-dependent pathway (CDE) and a less well-understood clathrin-independent pathway (CIE). In the clathrin-dependent pathway, cargos are selected for internalization through recognition of their cytoplasmic signal sequences by clathrin adaptors. The most common internalization signals are dileucine-based [DE] xxxL [LI] and tyrosine-based YxxΦ (where Φ is a bulky hydrophobic amino acid) motifs that are recognized by the major endocytic clathrin adaptor, AP2. Some other internalization signals through CDE include post-translational modifications such as ubiquitination and phosphorylation (Kelly and Owen, 2011). In addition, many clathrin adaptors also functions by binding directly to the negatively charged lipid phosphatidylinositol-4, 5-phosphate PI(4,5)P2 which is enriched on the plasma membrane (Traub, 2009). AP2 exists in "locked" cytosolic form in which its binding sites for internalization sequence are blocked. Upon binding to PI (4, 5) P2, AP2 undergoes a large-scale conformational change and reveals its cargo binding sites. It is through this mechanism cargo internalization is restricted to required sites on the plasma membrane but not on other membrane systems (Jackson et al., 2010). After cargo recognition, adaptor proteins recruit clathrin and form a cage-like structure described as clathrin-coated pits (CCP). Invaginated CCPs pinch off into vesicles, uncoat and fuse with one another and early endosomes. Iron-bound transferrin receptors (TFRs) and low-density lipoproteins (LDLRs) are well-characterized cargos that enter the cell through CDE pathway. In contrast, the clathrin-independent endocytosis occurs through a variety of poorly understood pathways. One type of CIE is dynamin-dependent and involves caveolin

and cytoplasmic coat components termed cavins. ADP-ribosylation factor 1(ARF1), CDC42 and actin polymerization regulate another mode of dynamin-independent CIE pathway. Another dynamin-independent CIE pathway is regulated by ARF6 GTPase and mediates the entry of cargo proteins like major histocompatibility complex (MHC) class I proteins and interleukin 2 receptor α-subunit (TAC) into cells (Grant and Donaldson, 2009; Howes et al., 2010).

Pathways of membrane trafficking

The cellular uptake process is balanced in part by endocytic recycling processes that return much of endocytosed proteins and lipids back to the plasma membrane. The balance between endocytic uptake and recycling is subjected to tight regulation and exerts significant impact on a variety of cellular processes including nutrient uptake, plasma membrane repair, cell adhesion and junction formation, cell polarity and migration, cytokinesis and signal transduction (Grant and Donaldson, 2009). Molecular players and mechanisms underlying how certain cargos are sorted from others and recycled back to the plasma membrane remain to be better characterized.

After internalization into cells, cargos from both CDE and CIE pathways converge at the early endosome where sorting occurs. From early endosomes, cargos can be returned directly to plasma membrane through a rapid recycling pathway. Some other cargos are delivered to recycling endosomes for further sorting and returned back to plasma membrane (Grant and Donaldson, 2009; Hsu and Prekeris, 2010b). There is another route called the retrograde pathway where cargos are cycled from endosomes to the Golgi (Bonifacino and Rojas, 2006). Still some other cargos labeled by ubiquitin are transported from early endosomes to late endosomes and finally to lysosomes for degradation (Raiborg and Stenmark, 2009). Large cytoplasmic components are targeted to lysosome for degradation via autophagy, a process in which cytoplasmic macromolecules are engulfed into a double-membrane cytosolic vesicle referred to as an autophagosome and targeted to fusion with the lysosome for degradation (Melendez and Levine, 2009).

Rab Proteins as key regulators of membrane trafficking

Proper and efficient membrane trafficking requires coordination of a series of events: budding of vesicular or tubular organelles from donor membranes, transporting them to their acceptor membranes, docking and fusion of donor organelle with acceptor organelle to achieve transfer of cargo between different membranous stations. The key coordinators for all these events mentioned above are the Rab GTPases (Stenmark, 2009). Rab proteins constitute the largest family of the Ras GTPase superfamily. In humans, there are approximately 70 Rab GTPases and about three quarters are involved in endocytic trafficking. In worms, there are 31 genes encoding Rab or Rab-like proteins and these genes are commonly involved in targeted movement of vesicles. Rab GTPases act as molecular switches and cycle between an "active" GTP-bound and an "inactive" GDP-bound state. The switch is controlled by guanine nucleotide exchange factors (GEFs), which promote the binding of GTP, and GTPase-activating proteins (GAPs), which catalyze the hydrolysis of the bound GTP to GDP. Upon translation, Rab proteins associate with Rab escort protein (REP) and are presented to Rab geranylgeranyl transferase (RabGGT). Modification of two C-terminal cysteines on Rabs with geranylgeranyl moieties confers a membrane insertion ability to Rab proteins. GDP dissociation inhibitor (GDI) binds to the GDP-bound form of prenylated Rabs and masks the isoprenyl anchor, thereby sequestering Rab proteins in the cytosol. A GDI displacement factor (GDF) maybe required to dissociate GDI from Rabs, thereby preparing Rabs ready for GEF-stimulated GTP binding (Hutagalung and Novick, 2011b). Through the shift between active membrane-bound form and inactive cytosolic form, Rab proteins perform their roles as master regulators of membrane traffic.

Rab proteins regulate a diverse array of membrane transport processes such as vesicle formation, movement, tethering and fusion by signaling through various effectors. Rab effectors interact preferentially with a GTP-bound form of their respective Rabs. Subtle variations within and outside the conserved Rab switch region (Switch I and Switch II) convey specificity for binding of effectors to corresponding Rabs. Rab proteins can

recruit Rab effectors that bind specifically to certain receptors and cause concentration of cargo on a subset of endosomes. Rabs can also have effectors from both donor and acceptor organelles to promote fusion. Still, some Rabs interact with actin- or microtubule-based structures directly (Echard et al., 1998) or indirectly bridged by interaction of effectors with actin/microtubule motors (Grosshans et al., 2006b). Intriguingly, under some circumstances Rab GEFs and Rab effectors can form a complex to create a positive feedback loop which couples Rab localization and activation of downstream Rab effector function.

Membrane compartmentalization and achieving specificity in membrane trafficking

One major challenge in membrane trafficking is to transfer a variety of cargos with different destinations between distinct membranous organelles in a specific and tightly regulated manner that guarantees precision and efficiency. Sorting and relaying diverse cargos in this highly demanding manner entails accurate spatial and temporal regulation of the function of trafficking machinery. The assembly of a protein complex promoting the relay of cargo at one step also needs to be reversible. There is accumulating evidence showing that this formidable task is achieved at several different levels of regulation by Rab GTPases.

First, the Rab GDP-GTP cycle renders Rab proteins eligible candidates for acting as molecular switches for turning “on” and “off” the machinery for a certain step of membrane trafficking. Facilitated by guanine-nucleotide exchange factors (GEFs) and GTPase-activating proteins (GAPs), Rab proteins can shuffle between GTP-bound “active” state and the GDP-bound ”inactive” state. The two different states allow the Rab to behave as both a soluable cytosolic proteins and an integral-membrane protein. Therefore, in times of need, Rab proteins can become GTP-bound and insert to membranes for recruitment of a cohort of its binding partners to implement a series of downstream effects. After having fulfilled its mission, the Rab protein can convert to its GDP-bound form, be removed from the membrane, and sequestered in the cytosol

for storage.

Second, Rab GTPases can interact with one another and weave into a complicated but effective network, coordinating between different steps of membrane trafficking. Several modes of coordination of Rab proteins have been revealed. In one case, different Rab proteins are localized to distinct membrane microdomains. For instance, studies have characterized RAB4, RAB5 and RAB11 domains that do not overlap over time (de Renzis et al., 2002). The segregation of Rab proteins likely comes from feedback loops with Rab effectors that contributes to the sorting of cargos into distinct routes. Alternatively, Rab interactions are commonly associated with Rab effector coupling. Rab effectors have been found to contain separate binding sites for two or more different Rab GTPases. Through shared Rab effectors, the functions of multiple Rab proteins can be orchestrated in a concerted manner to promote and maintain working machinery for certain routes of membrane trafficking. Additionally, another noteworthy theory concerning transition of different Rab-defined compartments is the Rab cascade model. In this model, it has been proposed that an upstream Rab recruits as its effector the GEF for a downstream Rab to promote its association with the membrane. The downstream Rab may then recruit the GAP that inactivates the upstream Rab (Hutagalung and Novick, 2011b). A schematic illustration of the proposed Rab cascade model is shown below.

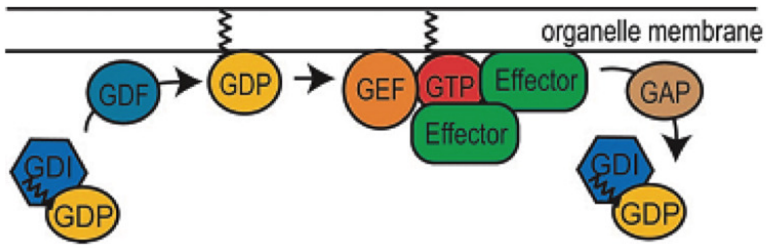

Figure 1: The nucleotide and membrane attachment/detachment cycles of Rab GTPases (Grosshans et al., 2006b).

Several examples have been shown to corroborate this Rab cascade model. In the event that RAB-5 positive early endosome matures into RAB-7 positive late endosome, it has been demonstrated that SAND-1/Mon1 acts as the mediator protein to negatively regulate the activity of the upstream Rab, RAB-5, and positively regulate the downstream

Rab, RAB-7. SAND-1 interacts with and removes the guanine-nucleotide exchange factor (GEF) of RAB-5, RABX-5 from the early endosome to disrupt the positive feedback loop for RAB-5. (Poteryaev et al., 2010). SAND-1 act as a RAB-7 GEF to facilitate the endosomal association of RAB-7. (Nordmann et al., 2010)

Third, through interaction with Rab effectors, Rab proteins function to specify the identity of membrane compartments. The identity is conferred both by protein recruitment and controlling membrane lipid composition. Each membrane compartment has its own associated protein complex and characteristic lipid compostion. Rab proteins control the lipid composition by recruiting as its effectors the kinases and phosphatases of phosphotidylinositides. For example, RAB-5 can recruit the class III PI3K to produce PI3P on early endosomes. Lipid that are specifically enriched on certain populations of endosomes also provide a platform for binding of Rab effectors. As in the example mentioned above, RAB-5 effectors EEA-1, rabenosyn 5 and rabankyrin 5 contain PI3P-binding FYVE domain. Thus defining the structural and functional identity of an organelle requires coincidence detection of the presence proper protein and lipid components. This constitutes a competent system that ensures precision and efficacy for transporting various cargos to their appropriate destination.

Through the above-mentioned complex regulated machinery, Rab proteins contribute to maintain organelle identity in the face of formidable challenges posed by large flow of cargo exchange between different cellular compartments. RAB-5 and the early endosome

The small GTPase RAB-5 is a canonical master regulator of the early endosome (Bucci et al., 1992). Regardless of the various routes of endocytosis, all the cargos converge to the early endosome for sorting. Therefore RAB-5 labeled early endosomes serve as the central hub of a complex network of proteins that undergoes a series of events including membrane fusion and fission, tethering and motility (Zeigerer et al., 2012). The activity of RAB-5 is controlled by guanine-nucleotide exchange factors which activate it and GTPase-activating protein that inactivates it. The catalytic Vps9 domain identifies Rab5/RAB-5 exchange factors (Carney et al., 2006). Distinct aspects of RAB-5 activity may require different RAB-5 GEF proteins for activation of RAB-5. For instance,

both RME-6 and RABX-5 proteins in *C. elegans* contain the Rab5/RAB-5 GEF Vps9 domain. However, they are involved in different facets of RAB-5 function. RME-6 localizes mainly to clathrin-coated pits and binds to clathrin adaptor APA-2. It is suggested that RME-6 activates RAB-5 on the nascent endocytic vesicles derived from clathrin-coated pits and mediate the fusion of nascent endocytic vesicles to early endosome (Sato et al., 2005). On the other hand, RABX-5 is thought to promote homotypic fusion of early endosomes and maturation of early endosome into late endosome along the degradation pathway. In particular, SAND-1 and its associated proteins remove RABX-5 from early endosomes as the RAB-5 labeled early endosomes mature into RAB-7 labeled late endosomes (Poteryaev et al., 2010).

RAB-5 builds its functional connections with various membranous compartments through a cohort of effector proteins. One effector of RAB-5 is the tethering factor early endosome antigen (EEA-1) which forms parallel coiled-coil dimers and has both amino- and carboxy- terminal RAB-5 binding sites thereby facilitating tethering of RAB5 labeled early endosomes (Stenmark, 2009). Another tethering complex that binds to RAB-5 contains RABS-5 (Rabenosyn5) and its binding protein VPS-45 (Sato et al., 2014).

RAB-10/Rab10 and the recycling endosome

Our lab set forth to characterize the molecular components of endocytic recycling pathway focusing on the processes employing RAB-10 as a master regulator in polarized epithelial cells. Previous work has indicated that RME-1, a fou *C. elegans*nding member of the C-terminal Eps15-homology (EH)-domain proteins (EHDs), mediates transport of cargo from recycling endosomes to plasma membrane. Loss of RME-1 results in accumulation of gigantic fluid-filled recycling endosomes in the worm intestine (Grant et al., 2001a). Our lab has also reported that RAB-10 is localized to a subset of endosomes. The number of early endosomes labeled by GFP-RAB-5 was found to increase in rab-10 mutant and the gigantic vacuoles present in rab-10 mutant worm intestine were weakly positive for GFP-RAB-5 and strongly positive for ARF-6-GFP, a marker for recycling endosomes. Based on the fact that GFP-RME-1 appears more diffusive in rab-10 mutants, and rme-1 mutants do not display increased number of RAB-5 labeled

early endosomes, we proposed that RAB-10 resides on a subset of basolateral early and recycling endosomes where it can regulate basolateral cargo recycling upstream of RME-1 (Chen et al., 2006b). In the intestinal cells of *C. elegans*, RAB-10 has partial localization with RAB-5 and RAB-10 localizes adjacently to RME-1 labeled recycling endosomal structures. Our studies in *C. elegans* suggests that RAB-10 function from the junction of early endosome to recycling endosome. rab-10 mutants did not affect other pathways such as degradation pathway and apical recycling pathway (Chen et al., 2006a).

Some other studies also reported different roles for RAB-10/RAB10 in both endocytic and biosynthetic pathways. In *C. elegans* neuron cells, RAB-10 has been shown to regulate the recycling of glutamate receptor AMPARs after clathrin-independent endocytosis (Glodowski et al., 2007b). RAB-10 also regulate the secretion of neuropeptides in neurons (Sasidharan et al., 2012). In polarized MDCK cells, Rab10 is found to localize to only a fraction of basolateral sorting endosomes and mainly to common recycling endosomes. It is thought to negatively regulate rapid recycling from basolateral sorting endosomes by mediating the transport from basolateral sorting endosomes to common endosomes (Babbey et al., 2006b). In adipocytes, Rab10 has been shown to be a substrate for RabGAP AS160 and responsible for the translocation of glucose transporter GLUT4 to plasma membrane upon insulin stimulation (Sano et al., 2007a). Additionally, in MDCK cells, Rab10 is reported to function cooperatively with Rab8 and mediate the biosynthetic transport from Golgi to basolateral plasma membrane (Schuck et al., 2007b). Also, the replenishment of Toll-like receptor (TLR) 4/receptor complex to plasma membrane requires Rab10. In nonpolarized cells, the function of RAB-10 in membrane traffic might be redundant with its closest homolog RAB-8 (Shi et al., 2010b). It was observed that rab-10 and rab-8 double mutants caused many worms to arrest at larvae stage, while the single mutants for either rab-10 or rab-8 are viable and fertile. We can conclude from the above-mentioned examples that although expressed ubiquitously among several tissues, the function of small Rab GTPases can differ with cell type.

The function of RAB-10 in the basolateral recycling pathway and its relationship with

RAB-8 was further illustrated in the study of a RAB-10 effector protein called EHBP-1. EHBP-1 binds to GTP-bound form of RAB-10 through its C-terminal coiled-coil domain. RAB-10 colocalizes with EHBP-1 on punctate endosomes. Loss of EHBP-1 results in accumulation of enlarged intestinal vacuoles filled with fluid-phase markers similar to the phenotype of a *rab-10* mutant (Chen et al., 2006b; Shi et al., 2010c). In *ehbp-1* mutant background, an obvious disruption in the recycling of CIE-dependent cargo hTAC was observed, whereas only minor effect was found for the recycling of CDE-dependent cargo hTFR. This preferential selectivity on cargo by EHBP-1 resembles that of RAB-10, which also has stronger effect on the recycling of hTAC than hTFR (Chen et al., 2006b; Shi et al., 2010c). In interneurons, as previously found for RAB-10, EHBP-1 regulates the trafficking of AMPAR subunit GLR-1 from endosomes within the neurites to synaptic membranes (Glodowski et al., 2007b; Shi et al., 2010c). Also, loss of EHBP-1 leads to accumulation of RAB-5 positive endosomes and loss of tubular structures labeled by RME-1, similar to that in *rab-10* loss-of-function strain. Taken together, these shared phenotypes suggest that EHBP-1 and RAB-10 may function on the same basolateral recycling pathway in polarized cells. However, membrane association of EHBP-1 does not require RAB-10. Surprisingly, RAB-10 (but not RAB-8) appears very diffusive in ehbp-1 mutant, implying that EHBP-1 functions to recruit RAB-10 on endosomes. This effect is more likely expected in a Rab-GEF mutant rather that in Rab-effector mutant. In the germline, *ehbp-1*mutant animals display larval arrest and adult sterility which can be phenocopied by simultaneous loss of both RAB-10 and RAB-8. It is also found that in *ehbp-1* mutant, or *rab-8/rab-10*(RNAi), plasma membrane localized SNARE SNB-1 is trapped intracellularly in endosomes. These results indicate that EHBP-1 may function with RAB-8 and RAB-10 together in non-polarized germ cells. In mammalian cells, EHBP1 has been reported to function with Eps15-homology (EH)-domain proteins EHD1 and EHD2 and affect insulin-regulated GLUT4 recycling and distribution of transferrin receptor (Guilherme et al., 2004a; Guilherme et al., 2004b). Another evidence for a better understanding of how RAB-10 regulates the recycling pathway comes from the interaction between RAB-10 and CNT-1, the only *C.elegans* homolog of mammalian Arf6 GTPase-activating protein ACAP1 and ACAP2

(Shi et al., 2012). Mammalian Arf6 regulates the recycling of cargos that entered the plasma membrane from the clathrin-independent endocytic (CIE) pathway, and rab-10 mutants caused block of recycling of the Arf6-dependent cargo hTAC (Brown et al., 2001; Radhakrishna and Donaldson, 1997). Mammalian Arf6 functions in part by activating type I phosphatidylinositol-4-phosphate 5 kinase which converts PI(4)P into PI(4,5)P2 (Brown et al., 2001; Radhakrishna and Donaldson, 1997) RAB-10 (GTP) interacts with the C-terminal ankyrin repeats of CNT-1. CNT-1 colocalizes with both RAB-10 and ARF-6 on endosomes and it becomes very diffusive in *rab-10* mutants, but not in mutants of other closely related Rabs such as *rab-8* and *rab-35* mutants. This suggests that RAB-10 functions to recruite CNT-1 onto endosomes to negatively regulate the activity of ARF-6. It turns out that this function loop affects the level of PI(4,5)P2 of on recycling endosomes. In arf-6 mutants, the PI(4,5)P2 level was reduced, while in *rab-10* or *cnt-1* mutants, the PI(4,5)P2 level increased. Since PI(4,5)P2 is the characteristic lipid on the recycling endosome, changing its composition on the recycling endosome strongly influences the recruitment of other relevant proteins that function in the recycling pathway by sensing the membrane PI(4,5)P2 level. In summary, one of the roles of RAB-10 in the endocytic recycling pathway occurs by the recruitment an ARF-6 GAP protein called CNT-1 by RAB-10 to regulate the PI(4,5)P2 level of the recycling endosome (Shi et al., 2012).

With a wide range of implications in membrane trafficking processes, it is of great interest to further study the molecular components and mechanisms involved in RAB-10/Rab10-dependent endocytic pathways.

TBC-2, a RABGAP involved in endocytic recycling

Most known Rab GAPs share a Tre-2/Bub2/Cdc16(TBC) catalytic domain (Bernards, 2003). There are 21 predicted TBC domain proteins in *C. elegans* (www.wormbase.org) and TBC-2 is one of them. TBC-2 is a RabGAP family protein which contains an N-terminal PH domain followed by a central coiled-coil domain and a C-terminal TBC domain. (Itoh et al., 2006) TBC-2 is most similar to human TBC1D2 (also known as PARIS-1 or Armus) and TBC1D2B (Frasa et al., 2010a; Zhou et al., 2002). PARIS-1

contains a TBC domain and has been found to express differentially in normal prostate cells and prostate cancer cells, indicating that PARIS-1 potentially plays a role in regulation of cell differentiation and growth (Zhou et al., 2002). Armus contains a PH domain which mediates its localization at cell-cell contacts. It is also shown to bind to Rac1, a Rho subfamily small GTPase through its central coiled-coil domain. And the C-terminal RABGAP domain has GAP activity towards Rab7 both *in vitro* and *in vivo*. Armus is reported to integrate Rac1 and Rab7 function in Arf6-dependent degradation of E-Cadherin. (Frasa et al., 2010b)

Studies in the *C. elegans* showed that TBC-2 is crucial for the removal of RAB-5 from phagosomes and maintaining a proper level and duration for PI(3)P to label phagosomes. Loss of TBC-2 caused less recruitment of RAB-7 and lysosome-associated membrane protein LMP-1 onto cell corpses-containing phagosomes. All of the above-described processes are critical for phagosome maturation and the efficient removal of cell corpse (Li et al., 2009). Another study in *C. elegans* showed that TBC-2 regulates RAB-5/RAB-7- mediated trafficking and has strongest GAP activity towards RAB-5 *in vitro*. (Chotard et al., 2010a)

In a recent publication from our lab, we have identified that a Rho-GTPase CED-10, together with its bipartite guanine-nucleotide exchange factor CED-5/CED-12, regulates endocytic recycling by recruiting TBC-2 onto endosomes. Loss of CED-10 or TBC-2 caused abnormal accumulation of both CDE cargo hTFR and CIE cargo hTAC in the worm intestine. In this study, we found that abnormally accumulated recycling cargo hTAC caused by *tbc-2* mutant background co-localizes with EHBP-1, a marker for recycling endosome. We further reasoned that if the abnormal accumulation of recycling cargos in *tbc-2* mutant background is caused by a lack of down-regulation of RAB-5 activity through TBC-2's RAB-5 GAP activity, overexpression of constitutively active form of RAB-5 should cause a similar cargo accumulation defect as in *tbc-2* mutant background. Consistent with this hypothesis, we found that overexpression of GTP-locked RAB-5 (Q78L) mimics the intracellular accumulation of recycling cargos including hTAC and hTFR as in *tbc-2* mutant (Sun et al., 2012a) A bioinformatics study on the interactome of Src homology 3 (SH3) domain protein has identified

AMPH-1, the only *C. elegans* homolog of Amphiphysin/BIN1 family of BAR-domain proteins, as a potential binding partner to TBC-2 (Xin et al., 2013). Using AMPH-1 SH3 domain as bait and randomly short peptide sequences expressed as prey in phage display analysis, a sequence within TBC-2 (146-160Aa) came out as the fourth best match in the whole genome for this AMPH-1 SH3 domain consensus target sequence. The binding between full-length TBC-2 protein and AMPH-1 SH3 domain was further confirmed to be a direct interaction. This interaction is also characterized to be specifically for the SH3 domain in AMPH-1 as another SH3 family protein SDPN-1 SH3 failed to bind to TBC-2. Interesting enough, *C. elegans* AMPH-1 has been reported previously to function in the endocytic recycling pathway by binding to RME-1, a regulator of basolateral recycling at a later step (Pant et al., 2009). In particular, during the cargo recycling process, RME-1 and AMPH-1 together promote the formation of narrower tubules than that generated by each protein individually. Taken together, it is of particular interest to further characterize the role of TBC-2 as a RABGAP in mediating endocytic recycling processes and investigate the molecular mechanism behind ordered transition of cargos along different Rab-defined endosomal compartments.

C. elegans as a model for studying membrane traffic

C. elegans is a small free-living nematode worm and it was first brought to the research community as a good potential experimental model organism to study development and behavior by Syndey Brenner in 1974 (Brenner, 1974). *C. elegans* has several advantages to serve as an excellent organism for genetics analysis:

(1) Compared to other higher organisms, it has relatively simple anatomy and genetic organization

(2) The life cycle of *C. elegans* is 3.5 days grown on agar plate seeded with *E. coli*

(3) Mutations can be induced by chemical mutagens or the recently developed CRISPR/Cas9 (Friedland et al., 2013; Paix et al., 2014) system to study behavior and morphological changes

(4) Strains can be kept as frozen stocks

C.elegans has proved to be an excellent model organism to study membrane trafficking. Almost all of the genes involved in membrane trafficking events that have been identified in mammalian studies are conserved in worm genome. The molecular mechanisms of how these genes function in the endocytic pathways also preserve well from *C. elegans* to mammalian systems. Moreover, for the genes that have multiple copies in the mammalian systems there is usually one corresponding *C.elegans* homolog. This is an advantage since only single mutants in *C.elegans* are sufficient to characterize the function of this gene. Taking advantage of this excellent genetic system of *C.elegans*, we can perform epistasis analysis to elucidate complex biochemical pathways.

The *C.elegans* intestine is our main choice of tissue to study membrane trafficking events. It is a relatively simple polarized epithelial tube consisted of 20 epithelial cells that are paired up to form nine rings. The worm intestine mains two distinct plasma membrane domains: basolateral and apical compartments which are separated by apical junctions. The intestinal cells of *C.elegans* present us the opportunity to study trafficking events in live intact polarized epithelial cells with the assistance of confocal imaging facilities.

Chapter 2.

CED-10/Rac1 Regulates Endocytic Recycling Through the RAB-5 GAP TBC-2

AUTHOR CONTRIBUTIONS

This chapter was published as presented here in *Plos Genetics* (Sun et al., 2012). I participated in the experimental design, performed some *C. elegans* related experiments (Figure 1M-M″, 1N-N″, 1O-O″, Figure 3J-L, Figure 5 K-K″, Figure 6). Dr. Lin Sun performed *C. elegans* related experiments (Figure 1A-L, Figure 2, Figure 3A-I, M-O, Figure 4C-J, Figure 5A-J and supplement figures). Farhad Karbassi and Marc-André Sylvain performed the biochemical experiments (Figure 4A-B) Dr. Barth D. Grant, Dr. Lin Sun, Christian E. Rocheleau and I designed the experiments and wrote the paper. Dr. Barth D. Grant, trained me to perform the experiments.

SUMMARY

Rac1 is a founding member of the Rho-GTPase family and a key regulator of membrane remodeling. In the context of apoptotic cell corpse engulfment, CED-10/Rac1 acts with its bipartite guanine nucleotide exchange factor, CED-5/Dock180-CED-12/ELMO, in an evolutionarily conserved pathway to promote phagocytosis. Here we show that in the context of the *C. elegans* intestinal epithelium CED-10/Rac1, CED-5/Dock180, and CED-12/ELMO promote basolateral recycling. Furthermore, we show that CED-10 binds to the RAB-5 GTPase activating protein TBC-2, that CED-10 contributes to recruitment of TBC-2 to endosomes, and that recycling cargo is trapped in recycling endosomes in *ced-12*, *ced-10*, and *tbc-2* mutants. Expression of GTPase defective RAB-5(Q78L) also traps recycling cargo. Our results indicate that down-regulation of early endosome regulator RAB-5/Rab5 by a CED-5, CED-12, CED-10, TBC-2 cascade is an important step in the transport of cargo through the basolateral recycling endosome for delivery to the plasma membrane.

INTRODUCTION

The *C. elegans* intestine has proven to be a powerful model system for the study of epithelial cell membrane trafficking mechanisms. The worm intestine is a simple epithelial tube consisting of 20 enterocyte cells that form nine "donut-like" intestinal rings (McGhee, 2007). Each of these 20 cells is terminally differentiated, and each intestinal cell is maintained for the life of the animal without replacement (McGhee, 2007).

Like mammalian intestinal epithelial cells, *C. elegans* enterocytes display apicobasal polarity with defined apical junctions separating the apical and basolateral domains (McGhee, 2007). The apical enterocyte membranes, which form the intestinal lumen, display a prominent microvillar brush border, with an overlying glycocalyx and underlying subapical terminal web rich in actin and intermediate filaments (McGhee, 2007). The basolateral membrane is in contact with the pseudocoelom (body cavity) and is responsible for the exchange of molecules between the intestine and other tissues of the body.

In previous studies we established three model transmembrane cargo markers for the analysis of basolateral endocytic trafficking in the *C. elegans* intestine: hTAC-GFP, hTfR-GFP, and MIG-14-GFP (Chen et al., 2006a; Pant et al., 2009; Shi et al., 2010a; Shi et al., 2007; Shi et al., 2009). hTAC (human IL-2 receptor alpha-chain) enters cells via clathrin-independent endocytosis (CIE), while hTfR (human transferrin receptor) and MIG-14 (Wntless) enter cells via clathrin-dependent endocytosis (CDE) (Grant and Donaldson, 2009; Pan et al., 2008; Yang et al., 2008). However, while hTAC and hTfR recycle via the recycling endosome in an RME-1/EHD-dependent manner, MIG-14 recycles via retrograde recycling to the Golgi in a retromer-dependent manner (Caplan et al., 2002; Chen et al., 2006a; Grant and Caplan, 2008; Lin et al., 2001; Pan et al., 2008; Shi et al., 2009; Yang et al., 2008). Thus comparison of the effects of any endocytic transport mutant on these three cargo proteins can give insight into which steps in receptor traffic are affected.

Here we focus on the function of the *C. elegans* Rac1 homolog CED-10 in regulation of epithelial cell endocytic trafficking. During engulfment of dead apoptotic cells, CED-10

functions in a pathway with associated proteins CED-12/ELMO, CED-5/DOCK180, and CED-2/CrkII, promoting cytoskeletal reorganization that is thought to be important for pseudopod formation/function (Kinchen and Ravichandran, 2007). CED-12 and CED-5 form a bipartite guanine-nucleotide exchange factor for CED-10, and are thus thought to promote conversion of inactive CED-10(GDP) to active CED-10(GTP) (Brugnera et al., 2002). CED-2 physically associates with CED-5 and is thought to function as an adapter, potentially linking the protein complex to certain apoptotic corpse receptors such as MOM-5/Frizzled and/or Integrins, but not the CED-1 corpse receptor (Cabello et al.; Reddien and Horvitz, 2000).

Mammalian Rac1 has been reported to become GTP-loaded on endosomes, and to require Arf6-dependent recycling for membrane ruffling and its localization to the leading edge of migrating cells (Donaldson et al., 2009; Koo et al., 2007; Palamidessi et al., 2008; Radhakrishna et al., 1999). Despite the known association of activated Rac1 with early and recycling endosomes, little is known of the potential role of Rac1 in regulating endosome function. In this study we define an important requirement for CED-10/Rac1 in basolateral recycling in the intestinal epithelia. This function of CED-10/Rac requires CED-5 and CED-12, but not CED-2. Furthermore we connect this recycling function of CED-10 to Rab-GAP TBC-2, indicating a mechanism for the down-regulation of the RAB-5 GTPase as endocytic cargo reaches the recycling endosome.

RESULTS

Loss of CED-10/Rac1, CED-12/Elmo, or CED-5/Dock180 leads to intracellular accumulation of recycling cargo

In order to determine if CED-10/Rac1 is required for endocytic transport, we assayed the effect of a strong Rac1 loss-of-function mutant, *ced-10 (n3246)*, on the subcellular distribution of three endocytic cargos, using confocal microscopy in the adult intestine (Reddien and Horvitz, 2000). The *C. elegans* intestine is known to express CED-10/Rac1 at high levels, but CED-10/Rac1 function has not been previously investigated in this tissue (Lundquist et al., 2001).

Interestingly, we observed strong intracellular accumulation of recycling receptor hTfR-GFP in the *ced-10* mutant background, similar to that we had previously observed in known endocytic recycling mutants such as *rme-1* and *amph-1* (Figure 1A and 1B, quantified in 1D) (Chen et al., 2006a; Pant et al., 2009). The abnormal intracellular accumulation of hTfR-GFP in the *ced-10(n3246)* mutant was completely rescued by transgenic expression of CED-10 using an intestine-specific promoter, indicating that the effect of CED-10 on recycling is cell autonomous and is not mediated by indirect effects via other tissues (Figure 1C and 1D). We also observed abnormal accumulation of another recycling cargo protein, hTAC-GFP, in *ced-10* mutants, and found that accumulated intracellular hTAC-GFP colocalized with recycling endosome marker EHBP-1 (Figure 1I, 1J, 1L, and 1N-1N″) (Shi et al., 2010a). TAC and TfR are thought to be internalized independently, meet in the endosomal system, and then recycle from the recycling endosome to plasma membrane in separate carriers (Naslavsky et al., 2003, 2004; Shi et al., 2007; Weigert et al., 2004). Taken together our results indicated trapping of multiple types of cargo in the recycling arm of the endocytic pathway in ced-10/Rac1 mutants.

Furthermore, we found that *ced-12(tp2)* and *ced-5(n1812)* mutants displayed the same aberrant intracellular accumulation of hTfR-GFP and hTAC-GFP found in *ced-10* mutants, indicating that the CED-12/CED-5 Rac exchange factor complex is also required for the recycling process (Figure 1E, 1F, 1H, 1K and 1L; Figure S2A-S2D and S2I). The

abnormal intracellular accumulation of hTfR-GFP in the ced-12 mutant was completely rescued by transgenic expression of CED-12 using an intestine-specific promoter, again indicating an intrinsic requirement for CED-12 in the intestinal cells (Figure 1G and 1H).

Importantly, *ced-10* and *ced-12* mutants had no effect on the subcellular localization of MIG-14-GFP, indicating that CED-10/Rac1 and CED-12/ELMO are somewhat cargo specific in their effects, and are not required for retrograde recycling from endosomes to the Golgi (Figure S1A-S1G). Since MIG-14 shares its uptake route with hTfR, but is not thought to enter the recycling endosome, these results suggest that CED-10/Rac1 is required for specific membrane trafficking events associated with recycling endosome dependent cargo.

No defect in hTAC-GFP or hTfR-GFP localization was found in *ced-2(e1752)* mutants, indicating that CED-2 is not required for the endocytic transport of these cargos (Figure S3A-S3D, S3I). Since CED-2 is required for phagocytic dead cell engulfment, this result indicates that the observed defects in endocytic traffic are not indirect effects of failed phagocytosis. This is also consistent with previous studies of the *C. elegans* intestinal cells, indicating that after embryogenesis the intestinal cells are not involved in the clearance of apoptotic cell corpses, do not perform phagocytosis, and do not migrate (Clokey and Jacobson, 1986; McGhee, 2007). Our results showing that CED-2 is not required in the intestine for hTfR and hTAC trafficking also indicates that not all CED-10 associated factors are shared between phagocytic and endocytic regulation.

Loss of CED-10, CED-12, or CED-5 disrupts endosome morphology

In order to help determine which step in trafficking is affected by loss of CED-10/Rac1 and its exchange factor CED-5/CED-12, we performed morphometric analysis of a wide-variety of marker proteins associated with endocytic organelles in the intestine of *ced-10* and *ced-12* mutant animals. This set of markers has been used successfully in previous studies to gain insight into the specific defects associated with endocytic transport mutants (Chen et al., 2006a; Pant et al., 2009; Shi et al., 2010a; Shi et al., 2007; Shi et al., 2009). We noted over-accumulation of GFP-tagged early endosome

regulator RAB-5 in *ced-10* and *ced-12* mutants (Figure 2A-2C, quantified in 2M and Figure S4). The average GFP-RAB-5 puncta intensity increased by about 8-fold and 12-fold, respectively, in *ced-10* and *ced-12* mutants (Figure 2M). We also noted in both mutants abnormal morphology of basolateral recycling endosomes labeled by GFP-RAB-10, ARF-6-GFP, GFP-RME-1, and SDPN-1-GFP (Figure 2D-2L, quantified in 2M, 2N, Figure S4, and Figure S5A-S5C, quantified in S5J). By contrast, markers for late endosomes (GFP-RAB-7), and apical recycling endosomes (GFP-RAB-11) were unperturbed (Figure S5D- S5I and S5K). We found that *ced-5* mutants, but not *ced-2* mutants, also displayed defective recycling endosome morphology (Figure S2E-S2H, S3E-S3H, S2J and S3J). Taken together with the cargo accumulation results, these specific changes in endosomal morphology indicate that a particular branch of the endocytic pathway, including the early endosomes and basolateral recycling endosomes, but not late endosomes or apical recycling endosomes, require CED-10/Rac1 activity for their normal function.

CED-10 and CED-12 are associated with early and recycling endosomes

If CED-10 and CED-12 function directly in endosomal regulation, then we would expect to find them associated with endosomes in wild-type cells. Thus we sought to determine the subcellular localization of CED-10 and CED-12 in the intestinal epithelial cells using functional tagged forms of the proteins. GFP-CED-10 localized strongly to the apical domain (likely to the microvilli) and to intracellular puncta in the cytoplasm (Figure 3A). CED-12-RFP colocalized well with GFP-CED-10 to the intracellular puncta (Figure 3B and 3C). However, CED-12-RFP also strongly labeled a subapical band that displayed significant overlap with the GFP-CED-10 labeled apical band (Figure 3A, 3B and 3C). It is not clear if the partial apical overlap represents the presence of both proteins on certain subapical structures, or rather represents two distinct apical localizations for CED-10 and CED-12 that are very near one-another. The simplest interpretation of these results is that the functionally important site of CED-10/CED-12 interaction for the recycling of basolateral cargo is on the intracellular puncta (endosomes - see below), although we cannot exclude important interactions on

other subcellular compartments.

We identified the intracellular puncta labeled by CED-10 as endosomes by performing a series of colocalization studies with a previously established set of intestine-specific compartment markers (Chen et al., 2006a; Pant et al., 2009; Shi et al., 2010a; Shi et al., 2007; Shi et al., 2009). CED-10 appeared specifically enriched on endosomes along the early and recycling pathway. We observed direct overlap of intestinal GFP-CED-10-labeled puncta and a subset of early endosomes marked by RFP-RAB-5 (Figure 3D, 3E and 3F). GFP-CED-10 showed the strongest colocalization with recycling endosome marker RFP-RAB-10 (Figure 3J, 3K and 3L), and displayed less overlap with later acting recycling endosome protein RFP-RME-1 (Figure 3G-3I). Similarly, we also observed colocalization between CED-12-GFP and markers of early endosomes and recycling endosomes (Figure S6J-S6L, and data not shown). Little overlap was observed between GFP-CED-10 and markers for late endosomes (GFP-RAB-7), the Golgi (MANS-GFP), or multi-vesicular bodies (GFP-HGRS-1/Hrs) indicating specificity in endosome-type associated with CED-10 (Figure S6A-S6I).

In order to confirm the endosomal localization of CED-10 we assayed for changes in the localization of GFP-CED-10 in rab-10 and rme-1 mutant backgrounds where the morphology of specific types of endosomes is specifically disrupted. Indeed we found that loss of either RAB-10 or RME-1 disrupted GFP-CED-10 localization (Figure 3M-3O). In *rab-10* and *rme-1* mutants, GFP-CED-10 labeled the grossly enlarged endosomes that were produced (Figure 3M-3O). Since our previous work showed that *rme-1* mutants accumulate enlarged basolateral recycling endosomes without affecting early endosomes, and *rab-10* mutants accumulate enlarged early endosomes and display reduced numbers of recycling endosomes, our results further indicate the residence of CED-10/Rac1 on both early and recycling endosome types (Chen et al., 2006a; Shi et al., 2007).

TBC-2 functions with CED-10 to mediate recycling

While most Rac1 effectors are thought to be plasma membrane localized, recent work identified the TBC-domain Rab-GAP protein Armus (TBC1D2) as an endosome associated Rac1 effector (Frasa et al., 2010a). This work showed that active GTP-bound Rac1 binds to Armus, regulating the trafficking of E-cadherin, and thus cell adhesion, in MDCK cells (Frasa et al., 2010a). The *C. elegans* homolog of Armus is TBC-2, a TBC-domain protein recently shown to function as a RAB-5 GAP important for the regulation of endocytosis and phagocytosis in vivo (Chotard et al., 2010 ; Li et al., 2009). Genetic analysis indicated that in the absence of TBC-2, RAB-5 activity is abnormally high, and early and late endosomes of the intestine are enlarged (Chotard et al., 2010). The enlargement of late endosomes in *tbc-2* mutants could be phenocopied by expression of constitutively active RAB-5(Q78L), and could be suppressed by depletion of RAB-5, RAB-7, or the HOPS complex. Thus it was proposed that hyperactive RAB-5 in *tbc-2* mutants leads to increased RAB-7 activity, and apparent increased lysosomal degradative activity (Chotard et al., 2010).

Previous studies did not determine if TBC-2/Armus is important for endocytic recycling. Since Rab GTPases generally function sequentially as cargo progresses along membrane trafficking pathways, one might expect that de-activation of the early acting GTPase RAB-5 is required to allow proper functioning of recycling endosomes associated with later acting GTPases such as RAB-10 (Hutagalung and Novick, 2011a). Thus we sought to determine if TBC-2 functions with CED-10/Rac1 in *C. elegans*, and if TBC-2 function is required for endocytic recycling.

In agreement with the work on mammalian Armus, we observed clear and consistent interactions between GFP::TBC-2 and CED-10 in GST pull-down experiments from *C. elegans* lysates. We found that GFP::TBC-2 interacts with a constitutively active mutant form of CED-10, G12V, or wild-type CED-10 loaded with GTPγS, but not wild-type CED-10 loaded with GDP (Figure 4A and 4B). Thus TBC-2 interacts specifically with activated CED-10, indicating that the physical interaction between Rac1/CED-10 and Armus/TBC-2 is evolutionarily conserved.

To determine if CED-10 is important for TBC-2 recruitment to endosomes, we examined the subcellular localization of GFP-TBC-2 in *ced-10* and *ced-12* mutants. We found that the normal punctate endosomal distribution of GFP-TBC-2 was disrupted in animals lacking CED-10 or CED-12 (Figure 4C-4E). The intensity of GFP-TBC-2 endosomal labeling was reduced by 6 to 7-fold in *ced-10* and *ced-12* mutants (Figure 4I). These results indicate that CED-10 and CED-12 are required in vivo for the efficient recruitment of TBC-2 to endosomal membranes, likely through direct binding of CED-10 (GTP) to TBC-2.

To determine if TBC-2 is important for endocytic recycling, we analyzed the localization of recycling endosome markers and recycling cargo markers in the *tbc-2(tm2241)* deletion mutant. We found that basolateral recycling endosome markers GFP-RME-1 and SDPN-1-GFP were severely perturbed in *tbc-2* mutants in a manner similar to that found in *ced-10*, *ced-12*, and *ced-5* mutants (Figure 5E-5H and 5J). Loss of TBC-2 also resulted in intracellular accumulation of hTAC-GFP and hTfR-GFP, similar to the phenotype observed in *ced-10, ced-12*, and *ced-5* mutants (Figure 5A-5D and 5I). hTAC-GFP in *tbc-2* mutants colocalized with recycling endosome marker EHBP-1-MC, indicating cargo trapping in recycling endosomes (Figure 5K-5K″). Furthermore, we reasoned that if the role of TBC-2 in recycling was to convert RAB-5(GTP) to RAB-5(GDP), then expression of GTPase-defective RAB-5 should also interfere with cargo recycling. Consistent with this model we found strong intracellular accumulation of hTAC-GFP and hTfR-GFP in the intestinal cells of animals expressing GTPase-defective RAB-5(Q78L) (Figure 6A-6F). Taken together these results indicate that the recycling of clathrin- independent cargo hTAC and clathrin-dependent cargo hTfR require TBC-2-depedent RAB-5 down-regulation. These results indicate that TBC-2 function is critical for the basolateral endocytic recycling pathway.

We also sought further evidence that TBC-2 functions downstream of CED-10/Rac1 in the recycling pathway. We reasoned that if the ced-10 recycling phenotype is due to poor recruitment of TBC-2 to endosomes, then overexpression of TBC-2 might ameliorate ced-10 mutant defects. Indeed, we found that the overexpression of RFP-tagged TBC-2 completely rescued the abnormal accumulation of recycling cargo hTfR-GFP in ced-10

mutant animals (Figure 4F-4H and 4J). These results strongly suggest that TBC-2 is a key CED-10/Rac1 effector required for endocytic recycling.

DISCUSSION

Rab conversion has recently emerged as a general principle of membrane traffic, acting as a key regulator of vectorial transport of cargo along the secretory and endocytic pathways (Hutagalung and Novick, 2011a). Countercurrent cascades of Rab GEFs and Rab GAPs have been proposed to mediate such Rab conversion (Hutagalung and Novick, 2011a). In the simplest form of such a cascade, the early acting Rab recruits the GEF for the next Rab along the pathway, while the later acting Rab recruits the GAP for the earlier acting Rab, producing a directional exchange of Rab-GTPases as cargo progresses along the pathway.

One well-studied Rab conversion event occurs during the early to late endosome transition, and during phagosome maturation, via a RAB-5 to RAB-7 switch (Kinchen and Ravichandran; Poteryaev et al.; Rink et al., 2005). RAB-5(GTP) recruits the SAND-1(Mon1)/CZZ-1 heterodimer, which in turn acts to displace RABX-5 (Rabex-5), a key RAB-5 GEF (Kinchen and Ravichandran; Poteryaev et al.). SAND-1/Mon1 also aids in RAB-7 recruitment, in part through interactions with the HOPS complex, a shared RAB- 5/RAB-7 effector (Poteryaev et al.). Recent evidence in yeast further indicates that the Mon1/Czz1 dimer is a Ypt7 (Rab7) GEF, acting to activate Ypt7 (Rab7) as the endosome matures (Nordmann et al.).

TBC-2 also appears to play a role in this process as a RAB-5 GAP. *tbc-2* null mutants produce grossly enlarged early and late endosomes, a phenotype very similar to that produced upon expression of constitutively active RAB-5(Q78L) (Chotard et al.) . These *tbc-2(-)* phenotypes can be suppressed by partial knockdown of RAB-5, RAB-7, or components of the HOPS complex, suggesting that TBC-2 is normally required to dampen the RAB-5 driven cascade that activates RAB-7 (Chotard et al.).

Importantly, our current study shows that TBC-2 also strongly influences the recycling

arm of the endocytic pathway, through interaction with CED-10/Rac1. This is particularly interesting because little is known of how the transition from early endosome to recycling endosome is achieved or how Rab GEFs and GAPs might be involved. Most studies on the early endosome to recycling endosome transition have focused on the joint Rab5/Rab4 effector Rabaptin5, or the neuron-specific Rab4 effector GRASP-1 (Deneka et al., 2003; Hoogenraad et al.). Our results indicate that CED-10/Rac1 resides on early and recycling endosomes where it is likely activated by the CED-5/CED-12 bipartite GEF. This is reminiscent of the activation of Rac1 by a different Rho-GEF, Tiam1, on endosomes of migrating mammalian cells (Palamidessi et al., 2008). Our results are the first to clearly show that CED-10/Rac1 is required for the recycling process, and is not simply a recycling cargo. Furthermore our work provides mechanistic insight into this requirement, showing that CED-10 acts to recruit TBC-2 to endosomal membranes. These results indicate that down-regulation of RAB-5 by TBC-2 is an important aspect of cargo recycling, and may serve as part of a program for Rab conversion along the recycling pathway. This is consistent with early work on Rab5 indicating that overexpressed Rab5(Q78L) inhibits transferrin recycling in HeLa cells (Stenmark et al., 1994). It remains unclear if direct down-regulation of RAB-7 is also important to promote recycling, since the TBC-2 homolog Armus was originally described as a Rab7 GAP, and *C. elegans* TBC-2 displays some GAP activity toward RAB-7 in vitro, albeit at a lower level than its activity toward RAB-5 (Chotard et al., 2010; Frasa et al., 2010a). In one important respect the *ced-10* mutant phenotype differs from that of *tbc-2* null mutants, in that RAB-7-positive late endosomes appear insensitive to CED-10 activity (Figure S5G and S5H). This suggests that while TBC-2 is generally important for regulating RAB-5, its interaction with CED-10 is mainly important for regulating RAB-5 along the recycling arm of the endocytic pathway. The specificity of the ced-10 mutant phenotype suggests that TBC-2 maintains some activity and membrane localization that is CED-10 independent, perhaps by direct lipid binding and/or interactions with additional endosomal proteins (Li et al., 2009).

The mechanisms that give rise to recycling endosomes are not clear, but most work suggests that recycling endosomes are formed from fission products that leave the early

endosome as it matures toward a late endosome (Grant and Donaldson, 2009; Hsu and Prekeris, 2010a). Fission products released from the Trans-Golgi also contribute to the recycling endosome (Ang et al., 2004). Once endosomal and Golgi-derived fission products fuse with one another and with pre-existing recycling endosomes, they would be expected to take on new recycling endosome-specific characteristics, including changing their phosphoinositide content and Rab-GTPase activities. Given the plethora of evidence that RAB-10 regulates basolateral recycling in many polarized cells, as first shown in the *C. elegans* intestine, one possibility is that the CED-10/TBC-2 interaction acts to promote a RAB-5 to RAB-10 transition (Babbey et al., 2006a; Chen et al., 2006a; Schuck et al., 2007a). In addition, endosomes are thought to contain functionally distinct subdomains (Sonnichsen et al., 2000; Thompson et al., 2007). The recycling endosome may maintain a RAB-5 positive fusogenic domain for incoming vesicles, and likely maintains multiple distinct tubular budding domains that accumulate outgoing cargo destined for different cellular compartments such as the basolateral plasma membrane, apical plasma membrane, and Golgi (Thompson et al., 2007). Thus another possible role for CED-10 to TBC-2 signaling is to provide negative feedback from RAB-10 to RAB-5 that maintains distinct RAB-10 and RAB-5 subdomains on the common recycling endosome. Both the Rab transition or subdomain maintenance models are consistent with the partial overlap in localization of RAB-5 and RAB-10 observed on basolateral endosomes of the *C. elegans* intestine, and both models predict that RAB-10 will be involved in recruiting or activating CED-10 and TBC-2 on recycling endosomes (Chen et al., 2006a). Future work will be directed at testing these models.

Interestingly, previous work in MDCK cells expressing constitutively active Rac1(V12) suggested that Rac1 could play a role in regulating the function of the common recycling endosome (Jou et al., 2000). In that work Jou et al. identified a Rac1(V12)-induced morphological defect in recycling endosomes that contain both apical and basolateral cargos. However pulse-chase analysis in Rac1(V12) MDCK cells defined defects in apically-directed common endosome-dependent functions (basolateral-to-apical transcytosis, apical recycling, and apical secretion), but surprisingly found no defect in

basolateral recycling. The physiological relevance of these results were unclear because expression of dominant negative Rac1(N17) did not affect recycling, and efficient knock-down methods were not available at that time to directly assay Rac1 loss-of-function. It would be of interest to revisit the MDCK system to investigate more fully the role of Rac1 and Armus in Rab5 down-regulation at the common recycling endosome, directly assaying for phylogenetic conservation of the mechanisms that we have defined here in the *C. elegans* intestine.

Our data connecting CED-10 to TBC-2 also has important implications for phagocytosis/engulfment, since CED-10/Rac1 and TBC-2 are both known to function early in the apoptotic corpse phagocytosis pathway. The potential importance of an interaction between CED-10 and TBC-2 during that process remains unexplored, but a function in promoting endocytic recycling may contribute to lamellipodia formation (Li et al., 2009; Struckhoff and Lundquist, 2003). RAB-10 has also recently been implicated in regulating phagosome maturation, and thus may be relevant to understanding the phagocytic functions of CED-10/Rac1 and TBC-2 (Cardoso et al.).

MATERIALS AND METHODS

General methods and strains

All *C. elegans* strains were derived originally from the wild-type Bristol strain N2. Worm cultures, genetic crosses, and other *C. elegans* husbandry were performed according to standard protocols (Brenner, 1974). Strains were maintained at 20℃. A complete list of strains used in this study can be found in Table S1—under a subheading "Transgenic and mutant strains used in this study".

Plasmid and transgenic worm strain construction

The CED-10 expression plasmid was created by PCR amplification and Gateway cloning of the *ced-10* cDNA, lacking a start codon, into the Gateway entry vector pDONR221 (Invitrogen, Carlsbad, CA). To create N-terminally tagged GFP or RFP/mCherry transgenes for CED-10 or RAB-5(Q78L) for expression specifically in the worm intestine, Gateway destination vectors were used that contain the promoter region of the intestine- specific gene vha-6 cloned into the *C. elegans* pPD117.01 vector, a Gateway cassette followed by a GFP or RFP/mCherry coding sequence and then the *unc-119* gene of C. briggsae.

To construct C-terminally tagged GFP or mCherry transgenes for CED-5/-12 for expression in the worm intestine, cDNA sequences of *C. elegans ced-5* and *ced-12* lacking a stop codon were cloned individually into Gateway entry vector pDONR221 by PCR and BP reaction, and then transferred into intestinal expression vectors by Gateway recombination cloning LR reaction according to the manufacturer's instructions (Invitrogen, Carlsbad, CA). All plasmids used in this study were sequenced and complete plasmid sequences are available on request.

Low copy integrated transgenic lines for all of these plasmids were obtained using the microparticle bombardment method (Praitis et al., 2001).

Microscopy and image analysis

Live worms were mounted on 2% agarose pads containing 100 mM tetramisole (MP Biomedicals, OH) in M9 buffer. Most GFP versus mCherry/RFP colocalization experiments were performed on L3 and L4 larvae expressing GFP and mCherry/RFP markers. Young adult hermaphrodites expressing GFP were used for taking confocal images. Images taken in the DAPI channel were used to identify broad-spectrum intestinal autofluorescence caused by lipofuscin-positive lysosome-like organelles (Clokey and Jacobson, 1986; Hermann et al., 2005).

Multi-wavelength fluorescence images were obtained using an Axiovert 200M (Carl Zeiss MicroImaging, Oberkochen, Germany) microscope equipped with a digital CCD camera (C4742-12ER, Hamamatsu Photonics, Hamamatsu, Japan). Metamorph software version 6.3r2 (Universal Imaging, West Chester, PA) was utilized for image acquisition and Z-stacks of images were deconvolved with AutoDeblur Gold software ver 9.3 (AutoQuant Imaging, Watervliet, NY).

To obtain images of GFP fluorescence without interference from autofluorescence, the spectral fingerprinting function of a Zeiss LSM510 Meta confocal microscope system (Carl Zeiss MicroImaging) was used as described previously (Chen et al., 2006a). Quantification of confocal images was performed with MetaMorph software version 6.3r2. The same threshold values were used for all images within a given experiment. For each marker comparison, at least six animals were analyzed. Three randomly selected regions of per animal were analyzed using circular regions of defined area. Quantification of fluorescence intensities or object count was performed. The average total intensity or average puncta number was calculated. Student's t-test was used to determine the difference between the different groups.

Preparation of worm extracts, GST protein purification and pull-downs

Worm extracts were prepared from a mixed-stage population of wild-type and *tbc-2(tm2241)*; vhIs12[$P_{vha\text{-}6}$::GFP::tbc-2 + Cb-unc-119] animals. Worms were grown on egg plates, harvested with 0.1M NaCl, floated in 30% fresh sucrose solution, and washed

three times with 0.1M NaCl. The worm pellet was frozen in liquid nitrogen and stored at -80℃. Frozen worm pellets were thawed on ice. An equal volume of fresh ice-cold lysis buffer (50 mM HEPES pH7.4, 1 mM EGTA, 150 mM KCl, 1 mM $MgCl_2$, 10% glycerol, 0.2% Triton X-100, Protease inhibitors: Pepstatin, Leupectin, Aprotinin, Sodium Orthovanadate, and PMSF) was added. One mL of the suspension was subjected to 35 strokes in a 2-mL pyrex tissue homogenizer (Thermo Fisher Scientific, Waltham, MA) at 4℃. The suspension was centrifuged twice at 12,000g for 10 minutes and once for 20 minutes at 4℃. The resulting supernatant was recovered.

The plasmid pGEX-5X-CED-10 was constructed by PCR amplification of *ced-10* from a cDNA template (kindly provided by Dr. Erik Lundquist, University of Kansas) using the primers 5′-GAT CGG ATC CCC CAA GCG ATC AAA TGT GTC GT-3′ and 5′-GAT CCT CGA GTT ACT TGC TCT TTT TGG CTC TTT-3′. The resulting PCR product was cloned in plasmid pGEX-5X-2 (GE Healthcare Life Sciences, Buckinghamshire, England) using the *BamHI* and *XhoI* restriction sites.

To purify the GST proteins, overnight cultures (10 mL) of BL21 *E. coli* transformed with pGEX-5X-2 vectors were diluted 10-fold in 2X YT with 100 mg/mL ampicillin, grown for one hour at 37℃ with shaking. Protein expression was induced with 0.5 mM IPTG and shaking at 25℃ for 2 hours. The culture was centrifuged at 5,000g for 10 minutes at 4℃ and the pellet was resuspended in 10 mL ice-cold PBS, centrifuged at 3,000g for 10 minutes at 4℃, and the pellet was resuspended in 1 mL PBS containing 1 mM PMSF and 7 mM β-mercaptoethanol. Cells were sonicated 10 seconds on ice, freeze/thawed three times in liquid nitrogen and a 20℃ water bath, and mixed with 100 μL of 10% Triton X- 100. The sample was centrifuged at 12,000g for 5 minutes at 4℃. The supernatant was gently mixed with 100 μL of 50% glutathione sepharose beads coated with 5% BSA. The sample was centrifuged 500g for 60 seconds at room temperature and washed with 1 mL of ice-cold PBS two times, centrifuged for 10 seconds at room temperature and the pellet was resuspended in 1mL PBS was stored at 4℃ for not more than 4 weeks. For the pull-down assays, 10 μg of the purified GST-CED-10 (or GST as the negative control) was added to 800 μL of worm lysate, 20 μL of extra glutathione sepharose beads (3X washed with PBS and pre-coated with 5%

BSA), 0.2 mM GDP or GTPγS (Sigma- Aldrich, St. Louis, MO) and 10 mM $MgCl_2$, and then incubated for 2 hours rotating at 4℃. The mixture was washed 3 times with ice-cold lysis buffer (without protease inhibitors) and proteins were eluted in 60 μL 2X Laemmli buffer for 20 minutes at 65℃. The samples were centrifuged at 500g for one minute at room temperature and 25 μL of eluted proteins were carefully collected from the solution above the beads and analyzed by SDS-polyacrylamide-gel electrophoresis using 8% resolving gel and blotted onto nitrocellulose membrane (Bio-Rad Laboratories, Hercules, CA). GFP::TBC-2 was detected using a goat anti-GFP antibody (Rockland Inc., Gilbertville, PA) and a donkey anti-goat antibody (Santa Cruz Biotechnology, CA) at a 1:1000 and a 1:10,000 dilution, respectively. To detect GST and GST::CED-10 proteins, the nitrocellulose membrane was reprobed with a rabbit anti-GST antibody and a goat anti-rabbit antibody (Sigma- Aldrich, St. Louis, MO) at a 1:2000 and a 1:10,000 dilution, respectively.

ACKNOWLEDGEMENT

We thank Nilgun Tumer for first sparking our interest in CED-10 function in the intestine. We also thank Peter Schweinsberg for microparticle bombardment of plasmids into *C. elegans*, Zui Pan for generous advice on confocal microscopy, and Jung Hwa Seo for technical assistance. The *ced-10* cDNA was kindly provided by Erik Lundquist.

FIGURES

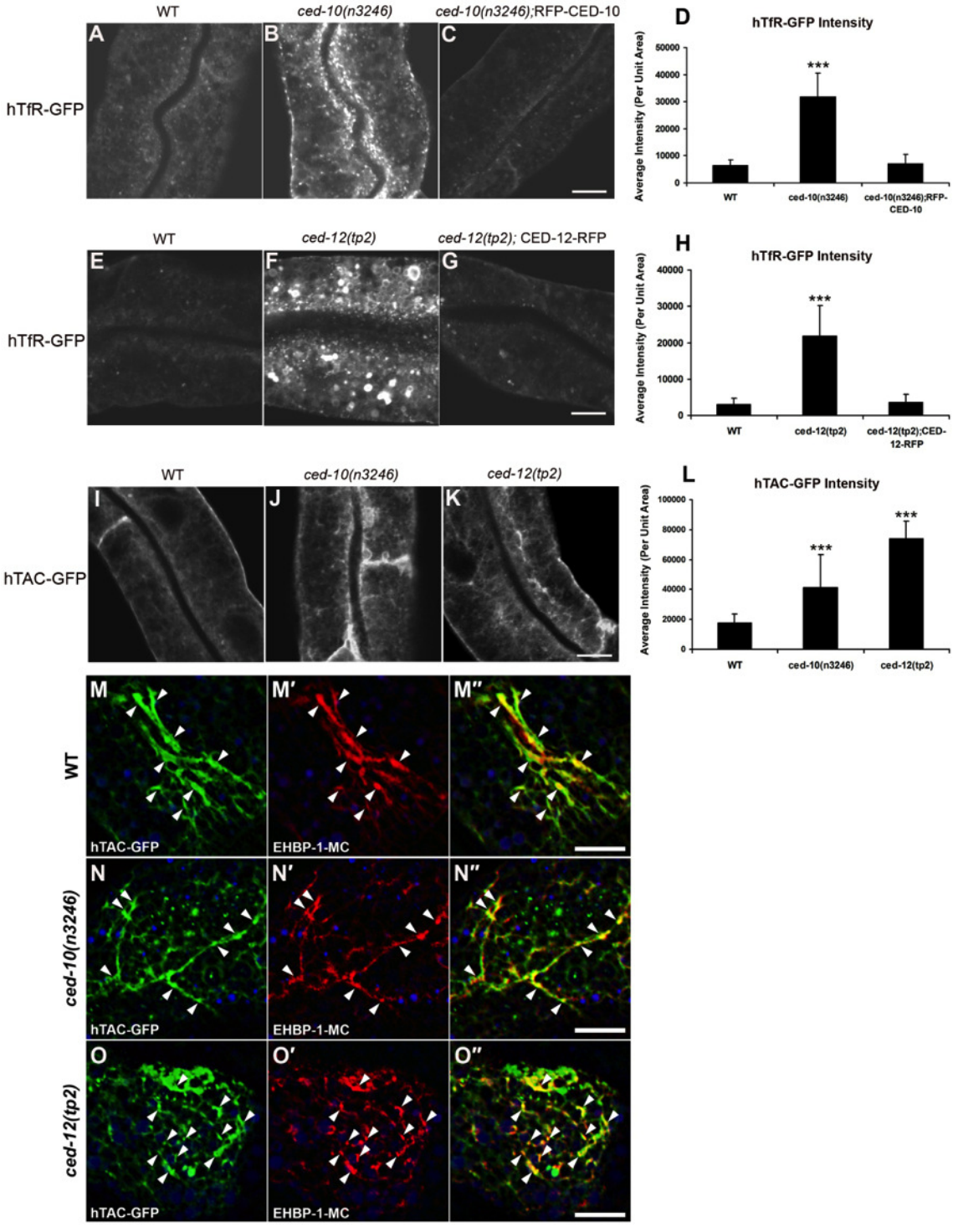
WT
ced-10(n3246)
ced-10(n3246);RFP-CED-10
hTfR-GFP
A
B
C
D
hTfR-GFP Intensity
Average Intensity (Per Unit Area)
***
WT
ced-10(n3246)
ced-10(n3246);RFP-CED-10
WT
ced-12(tp2)
ced-12(tp2); CED-12-RFP
hTfR-GFP
E
F
G
H
hTfR-GFP Intensity
***
WT
ced-12(tp2)
ced-12(tp2);CED-12-RFP
WT
ced-10(n3246)
ced-12(tp2)
hTAC-GFP
I
J
K
L
hTAC-GFP Intensity
***
***
WT
ced-10(n3246)
ced-12(tp2)
WT
ced-10(n3246)
ced-12(tp2)
M
M′
M″
N
N′
N″
O
O′
O″
hTAC-GFP
EHBP-1-MC

Figure 1: *ced-10* and *ced-12* mutants display abnormal trafficking of recycling cargo in the *C. elegans* intestine.

(A-C) Confocal images of the worm intestine in live intact animals expressing a GFP-tagged CDE cargo protein that recycles via the recycling endosome, the human transferrin receptor (hTfR-GFP). The *ced-10* mutant phenotype is rescued by intestine-specific expression of RFP-CED-10. (D) Quantification of hTfR-GFP puncta intensity. (E-G) Intracellular hTfR-GFP accumulates in *ced-12(tp2)* mutants. The CED-12 mutant phenotype is rescued by intestine-specific expression of CED-12-RFP. (H) Quantification of hTfR-GFP puncta intensity. (I-K) Representative confocal images of the worm intestine in living intact young adult animals expressing a GFP-tagged CIE cargo protein that recycles via the recycling endosome, the IL- 2 receptor alpha chain (hTAC-GFP). Wild type (N2), *ced-10(n3246)*, and *ced-12(tp2)* mutant animals are shown. (L) Quantification of hTAC-GFP intensity. (M-O″) Confocal images of the worm intestine in live intact animals expressing GFP-tagged IL-2 receptor alpha chain (hTAC-GFP) and mCherry-tagged *C. elegans* EHBP-1 (EHBP-1-MC), a recycling endosome marker. Wild-type animals (M-M″), *ced-10(n3246)* mutant animals (N-N″), and *ced-12(tp2)* mutant animals (O-O″) are shown. Error bars represent standard deviations from the mean (n = 18 each, 6 animals of each genotype sampled in three different regions of each intestine). Asterisks indicate a significant difference in the one-tailed Student's T-test (***p<0.0001). Scale bar, 10 μm.

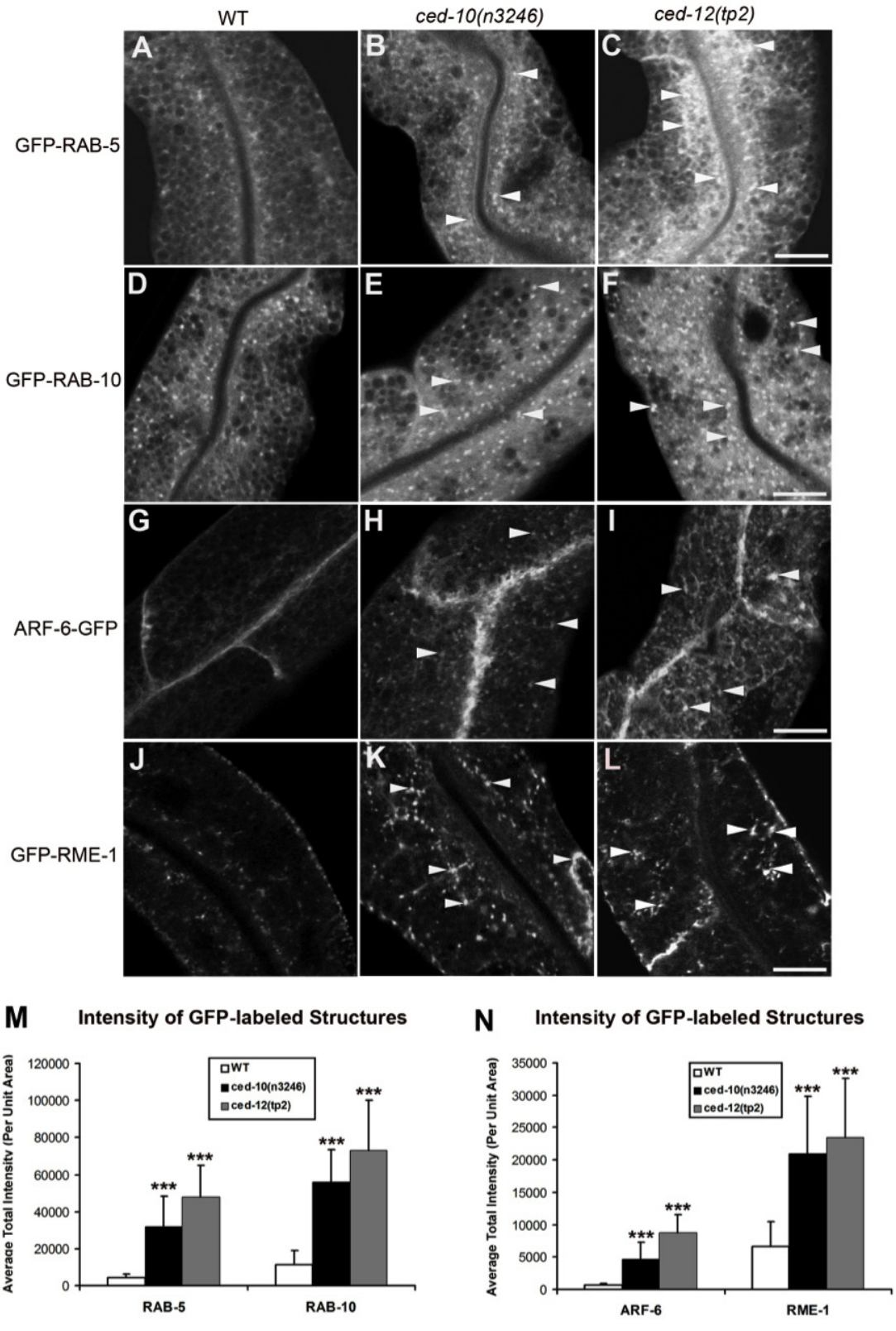
WT
ced-10(n3246)
ced-12(tp2)
A
B
C
GFP-RAB-5
D
E
F
GFP-RAB-10
G
H
I
ARF-6-GFP
J
K
L
GFP-RME-1
M
Intensity of GFP-labeled Structures
Average Total Intensity (Per Unit Area)
120000
100000
80000
60000
40000
20000
0
WT
ced-10(n3246)
ced-12(tp2)
***
***
***
***
RAB-5
RAB-10
N
Intensity of GFP-labeled Structures
Average Total Intensity (Per Unit Area)
35000
30000
25000
20000
15000
10000
5000
0
WT
ced-10(n3246)
ced-12(tp2)
***
***
***
***
ARF-6
RME-1

Figure 2: Abnormal accumulation of early and recycling endosomes markers in *ced-10(n3246)* and *ced-12(tp2)* mutants.

Representative confocal images are shown for GFP-RAB-5 (A-C), GFP-RAB-10 (D-F), ARF-6- GFP (G-I), and GFP-RME-1 (J-L). Quantifications of average puncta intensity are shown in (M-N). All images were collected from living intact young adult animals expressing GFP- tagged proteins specifically in the intestinal epithelial cells. Error bars represent standard deviation from the mean ($n = 18$ each, 6 animals of each genotype sampled in three different regions of each intestine). Asterisks indicate a significant difference in the one-tailed Student's *t*-test (***p$<$ 0.0001). Scale bar represents 10 μm.

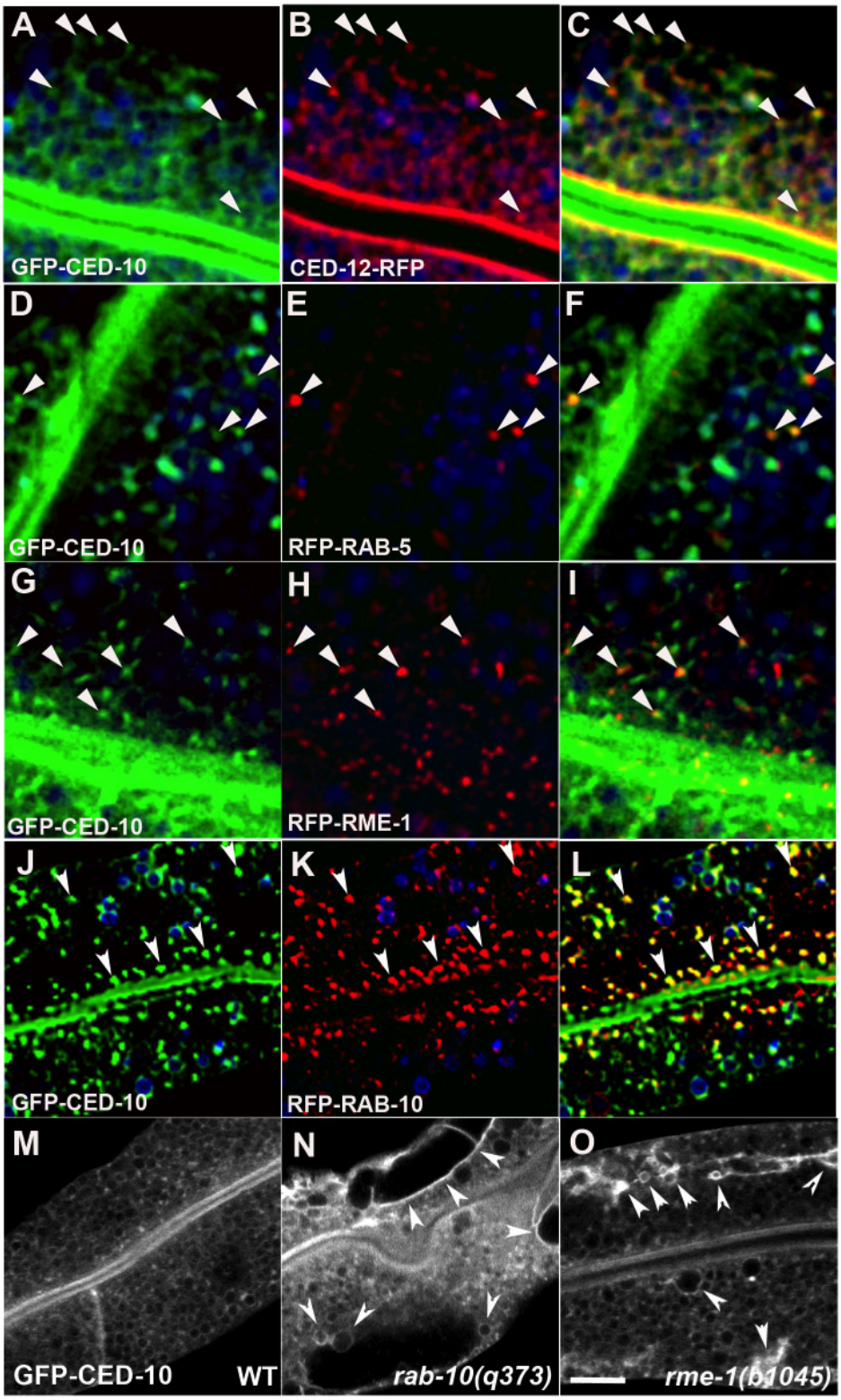
A
GFP-CED-10
B
CED-12-RFP
C
D
GFP-CED-10
E
RFP-RAB-5
F
G
GFP-CED-10
H
RFP-RME-1
I
J
GFP-CED-10
K
RFP-RAB-10
L
M
GFP-CED-10
WT
N
rab-10(q373)
O
rme-1(b1045)

Figure 3: CED-10 localizes to early and recycling endosomes, and colocalizes with CED-12, in the intestine.

All images are from wide-field deconvolved, or confocal, 3-D image stacks acquired in intact living animals expressing GFP and RFP tagged proteins specifically in intestinal epithelial cells. (A-C) GFP-CED-10 colocalizes with CED-12-RFP on intracellular puncta. Arrowheads indicate structures labeled by both GFP-CED-10 and CED-12-RFP. (D-F) GFP-CED-10 colocalizes with RFP-RAB-5 on a subset of early endosomes. Arrowheads indicate endosomes labeled by both GFP-CED-10 and RFP-RAB-5. (G-I) GFP-CED-10 partially colocalizes with RFP-RME-1 on basolateral recycling endosomes. Arrowheads indicate endosomes labeled by both GFP-CED-10 and RFP-RME-1. (J-L) GFP-CED-10 colocalizes extensively with RFP-RAB-10 on recycling endosomes. Arrowheads indicate endosomes labeled by both GFP-CED-10 and RFP-RAB-10. (M-O) GFP-CED-10 localizes to the abnormally enlarged endosomes present in *rab-10* and *rme-1* mutants. Arrows mark the grossly enlarged early and recycling endosomes. In each image autofluorescent lysosome- like organelles are shown in blue in all three channels, whereas GFP appears only in the green channel and RFP only in the red channel. Signals observed in the green or red channels that do not overlap with signals in the blue channel are considered bone fide GFP or RFP signals, respectively. Scale bar, 10 μm.

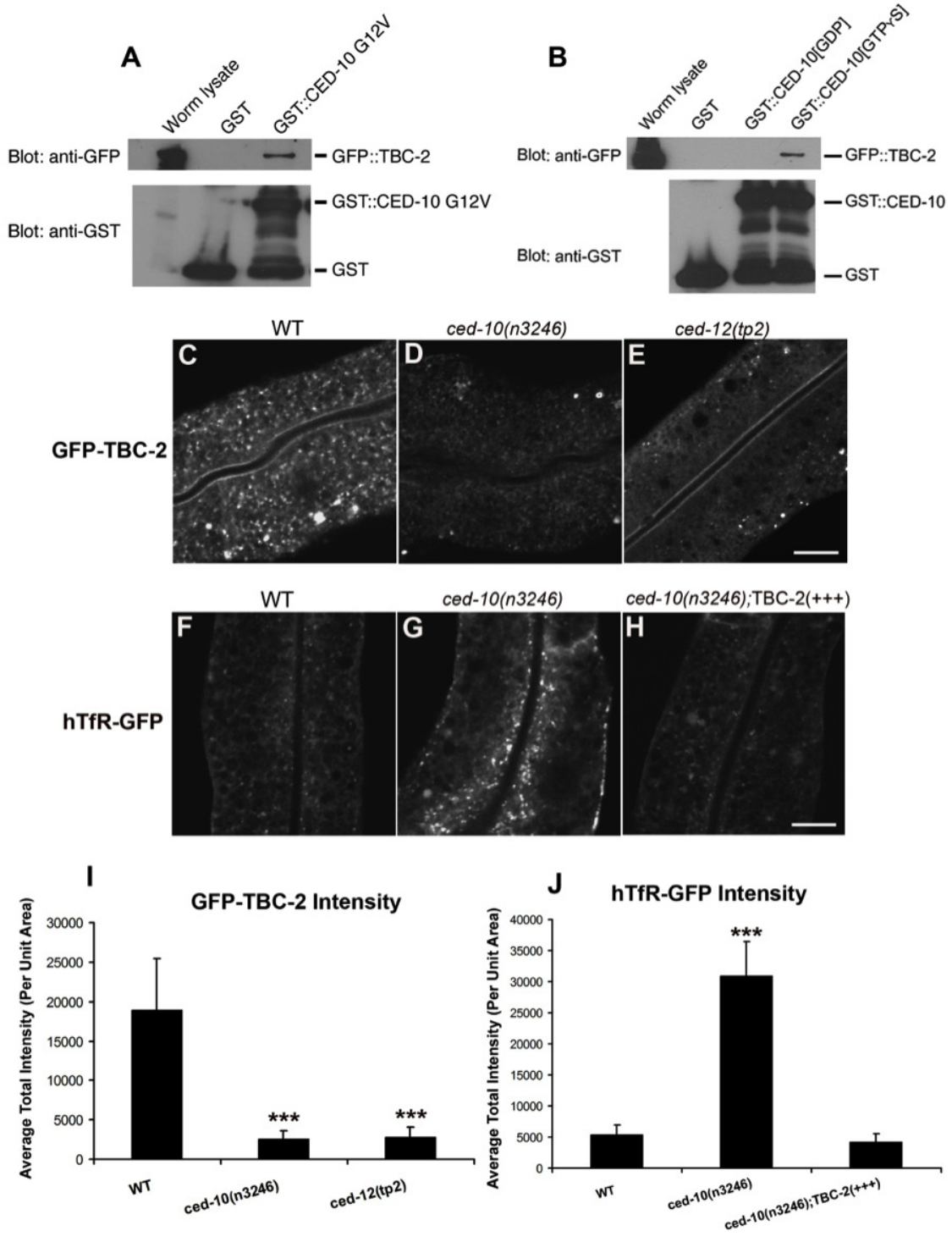
A
Worm lysate
GST
GST::CED-10 G12V
Blot: anti-GFP
GFP::TBC-2
Blot: anti-GST
GST::CED-10 G12V
GST
B
Worm lysate
GST
GST::CED-10[GDP]
GST::CED-10[GTPγS]
Blot: anti-GFP
GFP::TBC-2
Blot: anti-GST
GST::CED-10
GST
WT
ced-10(n3246)
ced-12(tp2)
C
D
E
GFP-TBC-2
WT
ced-10(n3246)
ced-10(n3246);TBC-2(+++)
F
G
H
hTfR-GFP
I
GFP-TBC-2 Intensity
Average Total Intensity (Per Unit Area)
30000
25000
20000
15000
10000
5000
0
***
***
WT
ced-10(n3246)
ced-12(tp2)
J
hTfR-GFP Intensity
Average Total Intensity (Per Unit Area)
40000
35000
30000
25000
20000
15000
10000
5000
0
***
WT
ced-10(n3246)
ced-10(n3246);TBC-2(+++)

Figure 4: TBC-2 is recruited to endosomes by CED-10.

(A) Glutathione beads loaded with recombinant GST or GST-CED-10(G12V), or (B) GST- CED-10(GDP) or GST-CED-10(GTPγS) were incubated with worm lysates containing GFP::TBC-2 and then washed to remove unbound proteins. Bound proteins were eluted and analyzed by Western blot using anti-GFP (top) or anti-GST (bottom) antibodies. Worm lysate represents 1% of the input. No GFP::TBC-2 was detected in non-transgenic worm lysates (not shown). (C-G) Representative confocal micrographs for GFP-TBC-2 and hTfR- GFP in various genetic backgrounds are shown. All images were collected from living intact adult animals expressing intestine-specific transgenes. (C-E) GFP-TBC-2 localization to endosomes is strongly reduced in *ced-10* and *ced-12* mutants. (F-H) hTfR-GFP overaccumulation in *ced-10* mutants is suppressed by overexpression of RFP-TBC-2. (I-J) Quantification of average puncta and tubule intensities for the indicated genotypes are shown. Asterisks indicate a significant difference in the one-tailed Student's T-test ($***p < 0.0001$). For all the presented data, error bars represent standard deviations from the mean ($n = 18$ each, 6 animals of each genotype sampled in three different regions of each intestine). Scale bar, 10 μm.

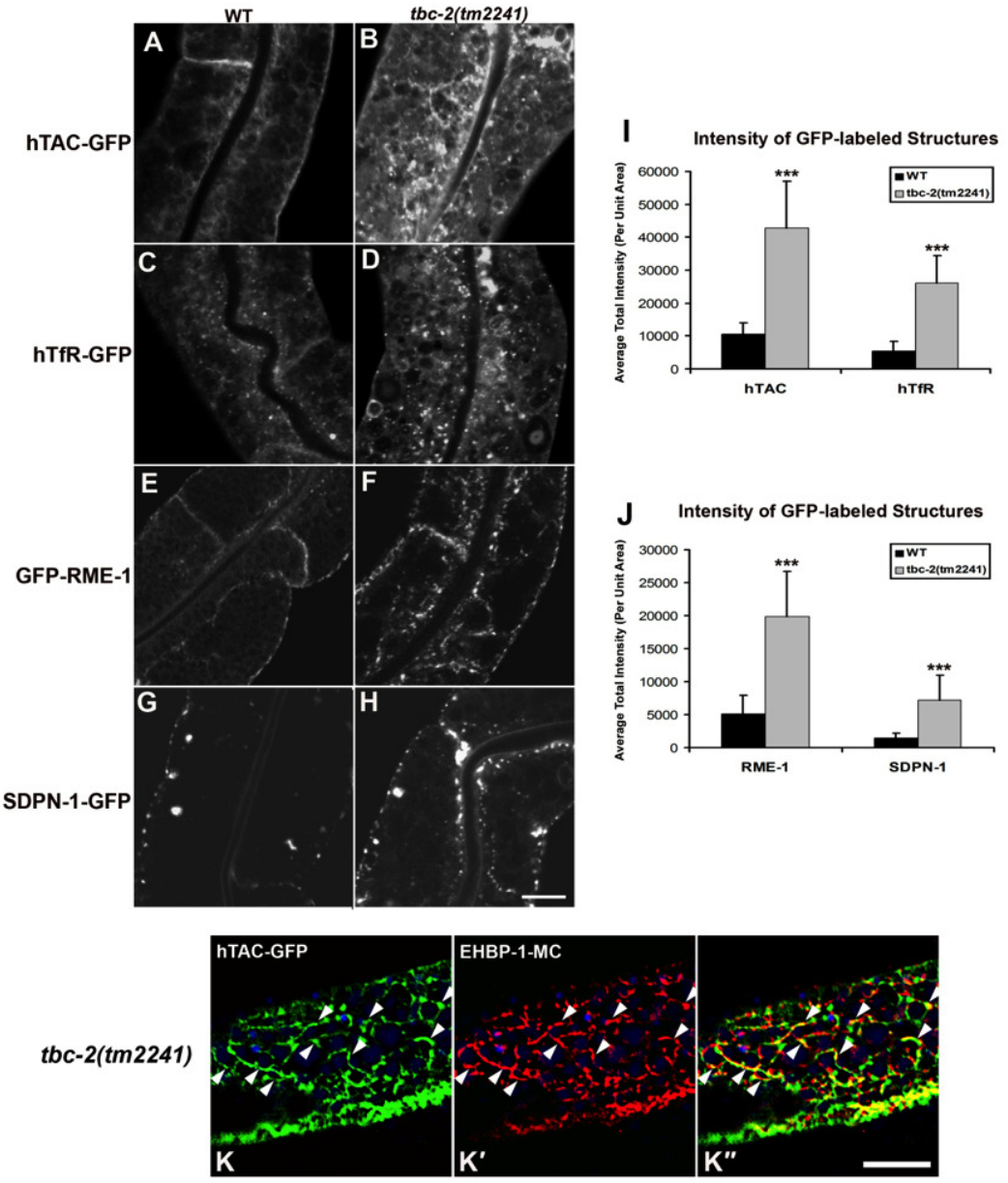
WT
tbc-2(tm2241)
A
B
hTAC-GFP
C
D
hTfR-GFP
E
F
GFP-RME-1
G
H
SDPN-1-GFP
I
Intensity of GFP-labeled Structures
Average Total Intensity (Per Unit Area)
60000
50000
40000
30000
20000
10000
0
***
***
WT
tbc-2(tm2241)
hTAC
hTfR
J
Intensity of GFP-labeled Structures
Average Total Intensity (Per Unit Area)
30000
25000
20000
15000
10000
5000
0
***
***
WT
tbc-2(tm2241)
RME-1
SDPN-1
tbc-2(tm2241)
hTAC-GFP
EHBP-1-MC
K
K'
K''

Figure 5: TBC-2 is required for recycling endosome morphology and function.

Representative confocal micrographs are shown for hTAC-GFP, hTfR-GFP, GFP-RME-1 and SDPN-1-GFP, in a *tbc-2* mutant background. All images were collected from living intact adult animals expressing intestine-specific transgenes. (A-D) Recycling cargos hTAC-GFP and hTfR-GFP over-accumulate in *tbc-2* mutants. (I) Quantification of hTAC-GFP and hTfR- GFP puncta and tubule intensity in the intestine of living intact wild-type and *tbc-2* mutant animals. (E-H) Recycling endosome markers GFP-RME-1 and SDPN-1-GFP also over- accumulate in tbc-2 mutants. (J) Quantification of puncta and tubule intensity of GFP-RME-1 and SDPN-1-GFP per unit area. (K-K″) Confocal images of the intestinal epithelium in live intact *tbc-2(tm2241)* mutant animals expressing recycling cargo hTAC-GFP and recycling endosome marker EHBP-1-MC. Autofluorescent lysosomes are shown in blue. Asterisks indicate a significant difference in the one-tailed Student's t test ($^{***}p < 0.0001$). Error bars represent standard deviations from the mean ($n = 18$ each, 6 animals of each genotype sampled in three different regions of each intestine). Scale bar, 10 μm.

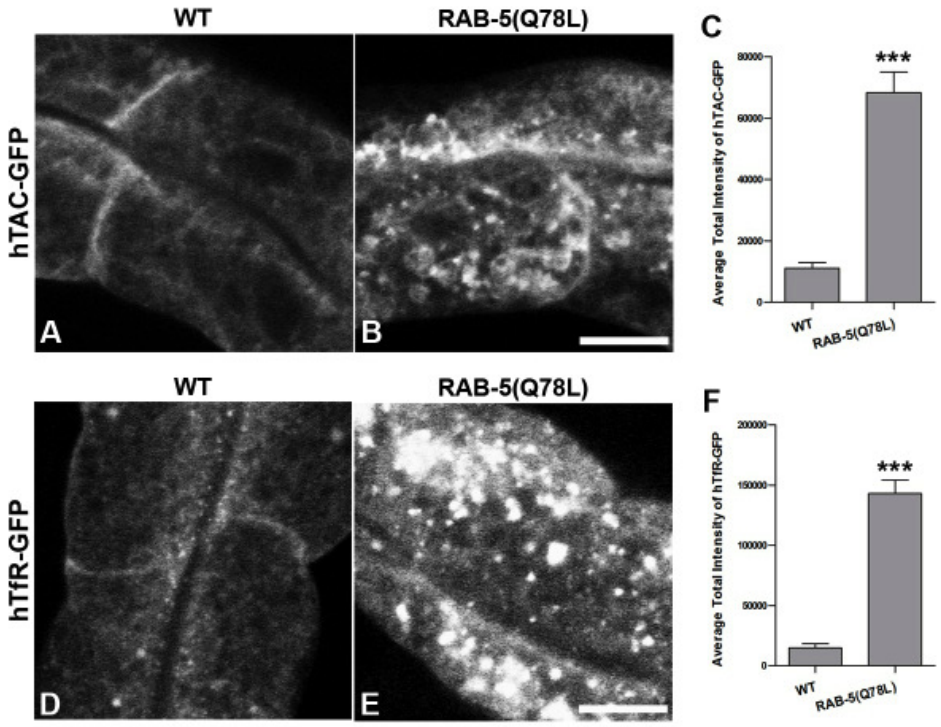

Figure 6: Expression of GTPase-defective RAB-5 interferes with the trafficking of recycling cargo.

(A and B) Confocal images of recycling cargo hTAC-GFP in the intestinal epithelium. Wild-type animals (A) and animals expressing of GTPase-defective RAB-5 (tagRFP-RAB-5(Q78L)) (B) are shown. (C) Quantification of hTAC-GFP puncta and tubule intensity. (D and E) Confocal images of recycling cargo hTfR-GFP in the intestinal epithelium. Wild-type animals (D) and animals expressing of GTPase-defective RAB-5 (tagRFP-RAB-5(Q78L)) (E) are shown. (F) Quantification of hTfR-GFP puncta intensity. Error bars represent standard deviations from the mean ($n = 18$ each, 6 animals of each genotype sampled in three different regions of each intestine). Asterisks indicate a significant difference in the one-tailed Student's T-test ($^{***}p < 0.0001$). Scale bar, 10 μm.

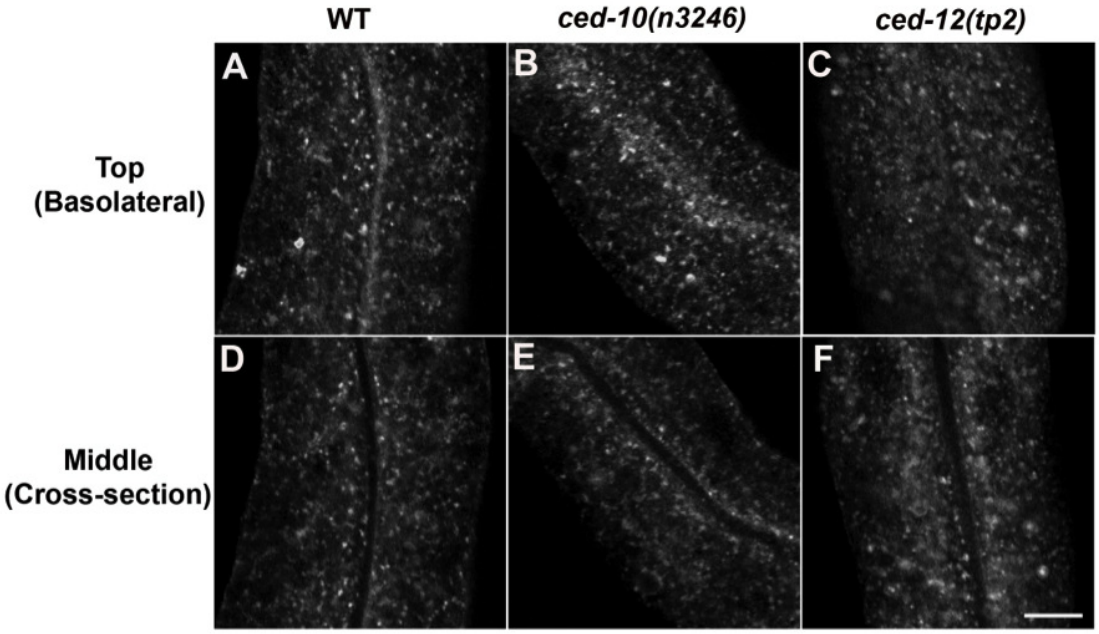
WT
ced-10(n3246)
ced-12(tp2)
A
B
C
D
E
F
Top
(Basolateral)
Middle
(Cross-section)

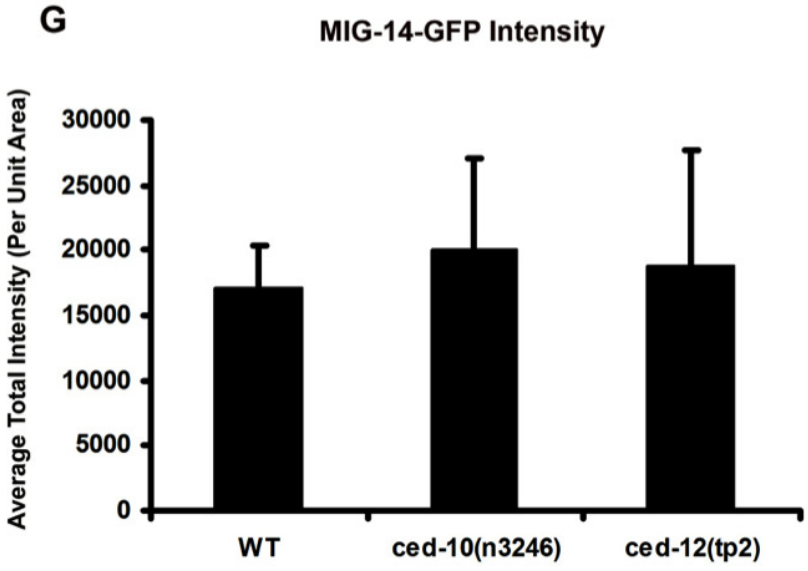
G
MIG-14-GFP Intensity
Average Total Intensity (Per Unit Area)
30000
25000
20000
15000
10000
5000
0
WT
ced-10(n3246)
ced-12(tp2)

Figure S1: No change in retrograde recycling cargo protein MIG-14-GFP was observed in *ced-10* and *ced-12* mutants.

Representative confocal micrographs of MIG-14(Wntless)-GFP expressed in the intestine of living intact animals, in the indicated genetic backgrounds, are shown (A-F). Average total MIG-14-GFP intensities are shown in (G). Error bars represent standard deviations from the mean ($n = 18$ each, 6 animals of each genotype sampled in three different regions of each intestine). Scale bar, 10 μm.

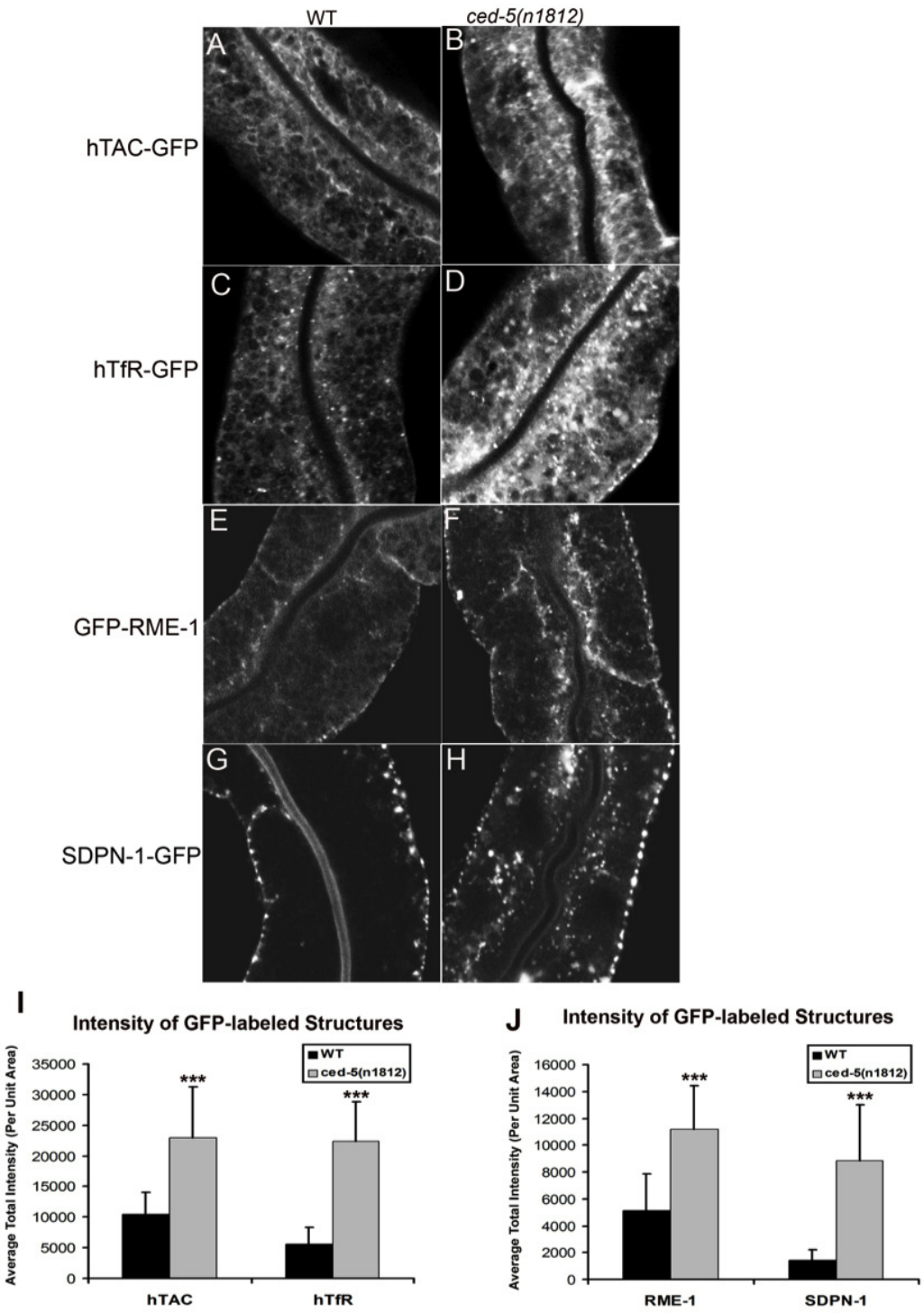
WT
ced-5(n1812)
A
B
hTAC-GFP
C
D
hTfR-GFP
E
F
GFP-RME-1
G
H
SDPN-1-GFP
I
Intensity of GFP-labeled Structures
Average Total Intensity (Per Unit Area)
35000
30000
25000
20000
15000
10000
5000
0
WT
ced-5(n1812)
***
***
hTAC
hTfR
J
Intensity of GFP-labeled Structures
Average Total Intensity (Per Unit Area)
16000
14000
12000
10000
8000
6000
4000
2000
0
WT
ced-5(n1812)
***
***
RME-1
SDPN-1

Figure S2: Recycling cargo hTfR and hTAC, and recycling endosome markers RME-1 and SDPN-1 accumulate in *ced-5* mutants.

(A,B) Recycling cargo hTAC-GFP over-accumulates in *ced-5*(*n1812*) mutants. (C,D) Recycling cargo hTfR-GFP accumulates in ced-5(*n1812*) mutants. (I) Quantification of hTAC-GFP and hTfR-GFP intensities in the intestine of living wild-type and ced-5 mutant animals. Asterisks indicate a significant difference in the one-tailed Student's t test ($***p < 0.0001$). (E,F) Recycling endosome marker GFP-RME-1 accumulates abnormally in *ced-5(n1812)* mutants. (G,H) Recycling endosome marker SDPN-1-GFP accumulates abnormally in *ced-5(n1812)* mutants. (J) Quantification of GFP-RME-1 and SDPN-1-GFP intensity in the intestine of living wild-type and *ced-5* mutants. Error bars represent standard deviations from the mean ($n = 18$ each, 6 animals of each genotype sampled in three different regions of each intestine). Scale bar, 10 μm.

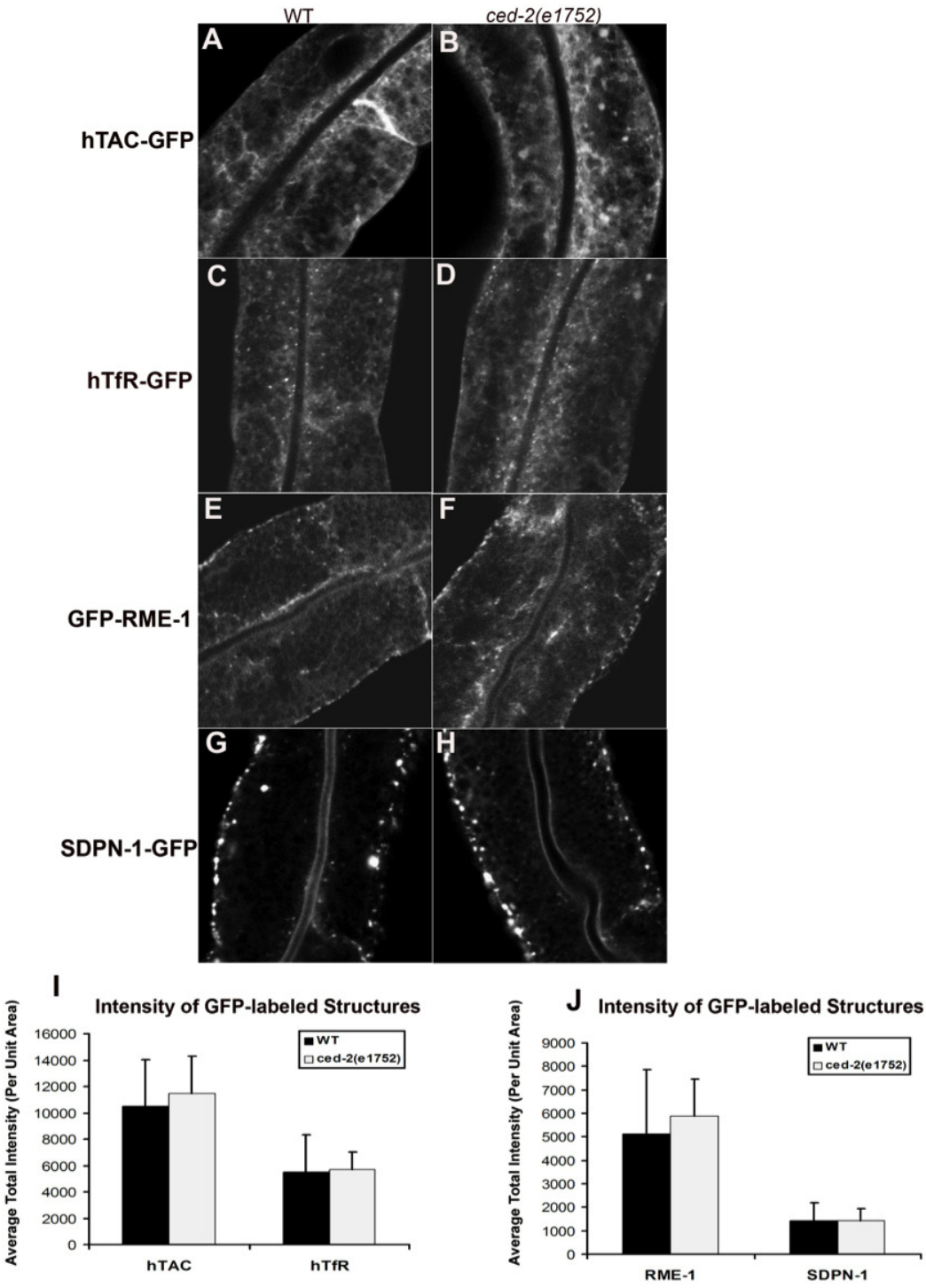
WT
ced-2(e1752)
A
B
hTAC-GFP
C
D
hTfR-GFP
E
F
GFP-RME-1
G
H
SDPN-1-GFP
I
Intensity of GFP-labeled Structures
Average Total Intensity (Per Unit Area)
16000
14000
12000
10000
8000
6000
4000
2000
0
WT
ced-2(e1752)
hTAC
hTfR
J
Intensity of GFP-labeled Structures
Average Total Intensity (Per Unit Area)
9000
8000
7000
6000
5000
4000
3000
2000
1000
0
WT
ced-2(e1752)
RME-1
SDPN-1

Figure S3: No change in the localization or intensity of recycling cargo hTfR and hTAC, or recycling endosome markers RME-1 and SDPN-1, in *ced-2* mutants.

(A-H) Recycling cargo hTAC-GFP and hTfR-GFP, and recycling endosome markers GFP-RME-1 and SDPN-1-GFP did not change distribution or intensity in *ced-2(e1752)* mutants. (I-J) Quantification of indicated marker intensities in the intestine of living wild-type and *ced-2* mutant animals. Error bars represent standard deviations from the mean ($n = 18$ each, 6 animals of each genotype sampled in three different regions of each intestine). Scale bar, 10 μm.

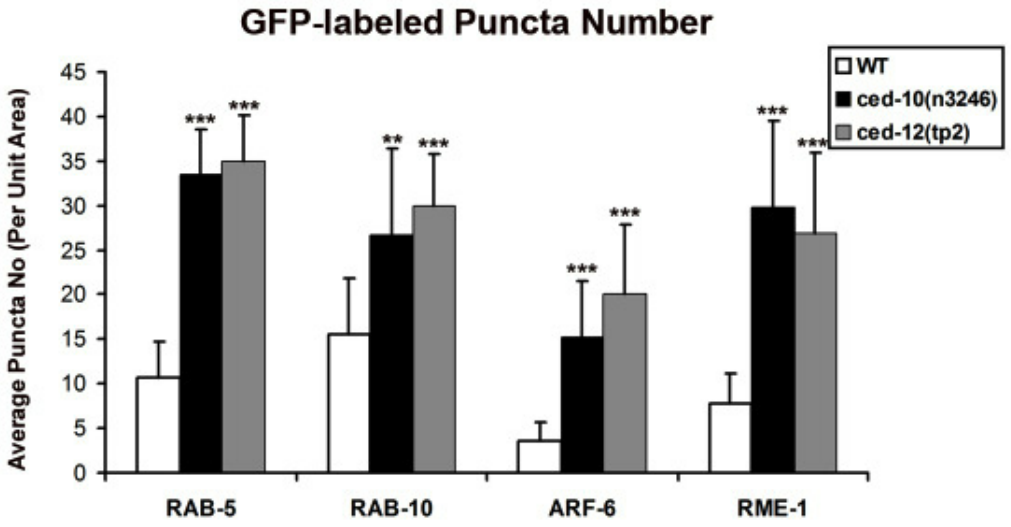

Figure S4: Quantification of endosome marker puncta number in *ced-10* and *ced-12* mutants.

Bar graph representation of puncta number, rather than puncta intensity, for the data shown in main figure 2. Asterisks indicate a significant difference in the one-tailed Student's t test (***$p < 0.0001$, **$p = 0.001$). Error bars represent standard deviations from the mean ($n = 18$ each, 6 animals of each genotype sampled in three different regions of each intestine).

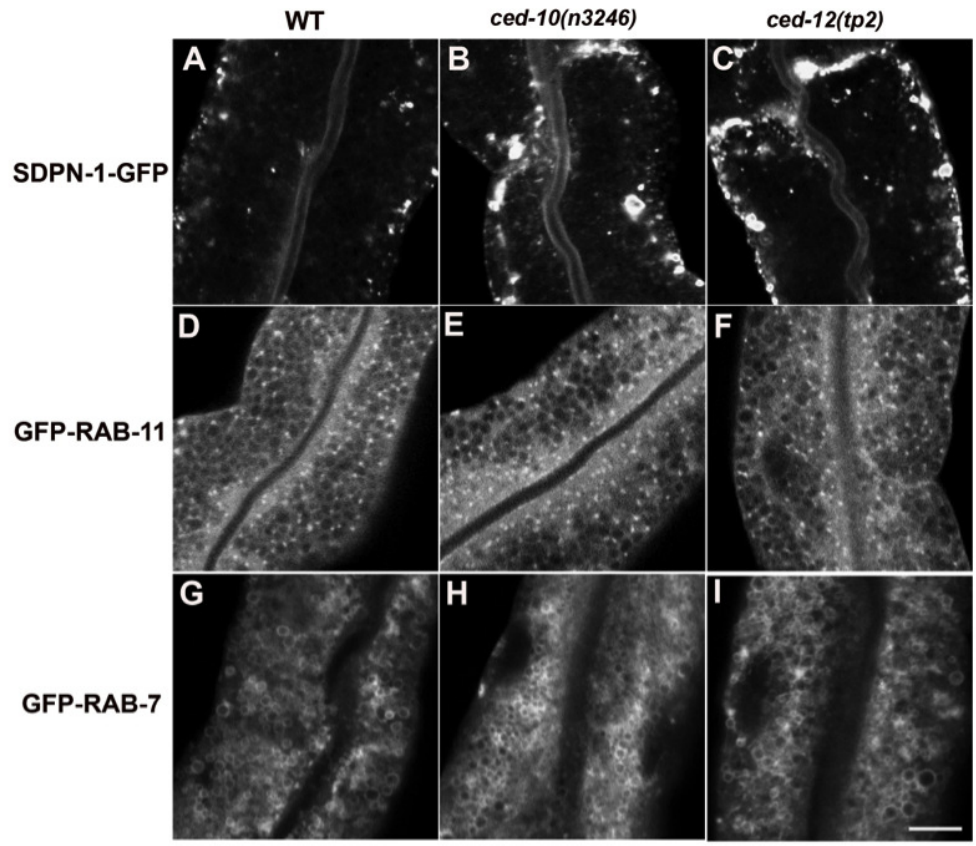
WT
ced-10(n3246)
ced-12(tp2)
A
B
C
SDPN-1-GFP
D
E
F
GFP-RAB-11
G
H
I
GFP-RAB-7

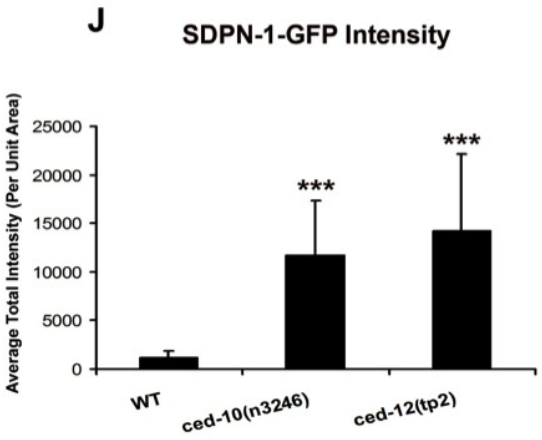
J
SDPN-1-GFP Intensity
Average Total Intensity (Per Unit Area)
25000
20000
15000
10000
5000
0
***
***
WT
ced-10(n3246)
ced-12(tp2)

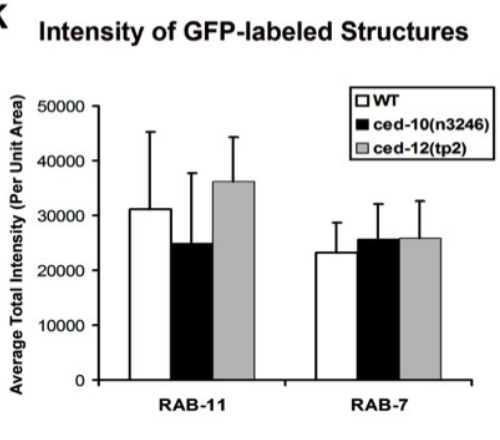
K
Intensity of GFP-labeled Structures
Average Total Intensity (Per Unit Area)
50000
40000
30000
20000
10000
0
WT
ced-10(n3246)
ced-12(tp2)
RAB-11
RAB-7

Figure S5: Further analysis of endosome markers in *ced-10(n3246)* and *ced-12(tp2)* mutants.

(A-C) Basolateral recycling endosome marker SDPN-1-GFP over-accumulates in *ced-10(n3246)* and *ced-12(tp2)* mutants. (D-F) Apical recycling endosome marker GFP-RAB-11 was not affected by *ced-10* and *ced-12* mutants. (G-I) Late endosome marker GFP-RAB-7 was not affected by *ced-10(n3246)* and *ced-12(tp2)* mutants. (J) Quantification of SDPN-1- GFP intensity in the intestine of living wild-type, *ced-10*, and *ced-12* mutants. The asterisk indicates a significant difference in the one-tailed Student's T-test ($^{***}p < 0.0001$). (K) Quantification of GFP-RAB-11 and GFP-RAB-7 intensity in the intestine of living wild-type, *ced-10*, and *ced-12* mutants. Error bars represent standard deviations from the mean ($n = 18$ each, 6 animals of each genotype sampled in three different regions of each intestine). Scale bar, 10 μm.

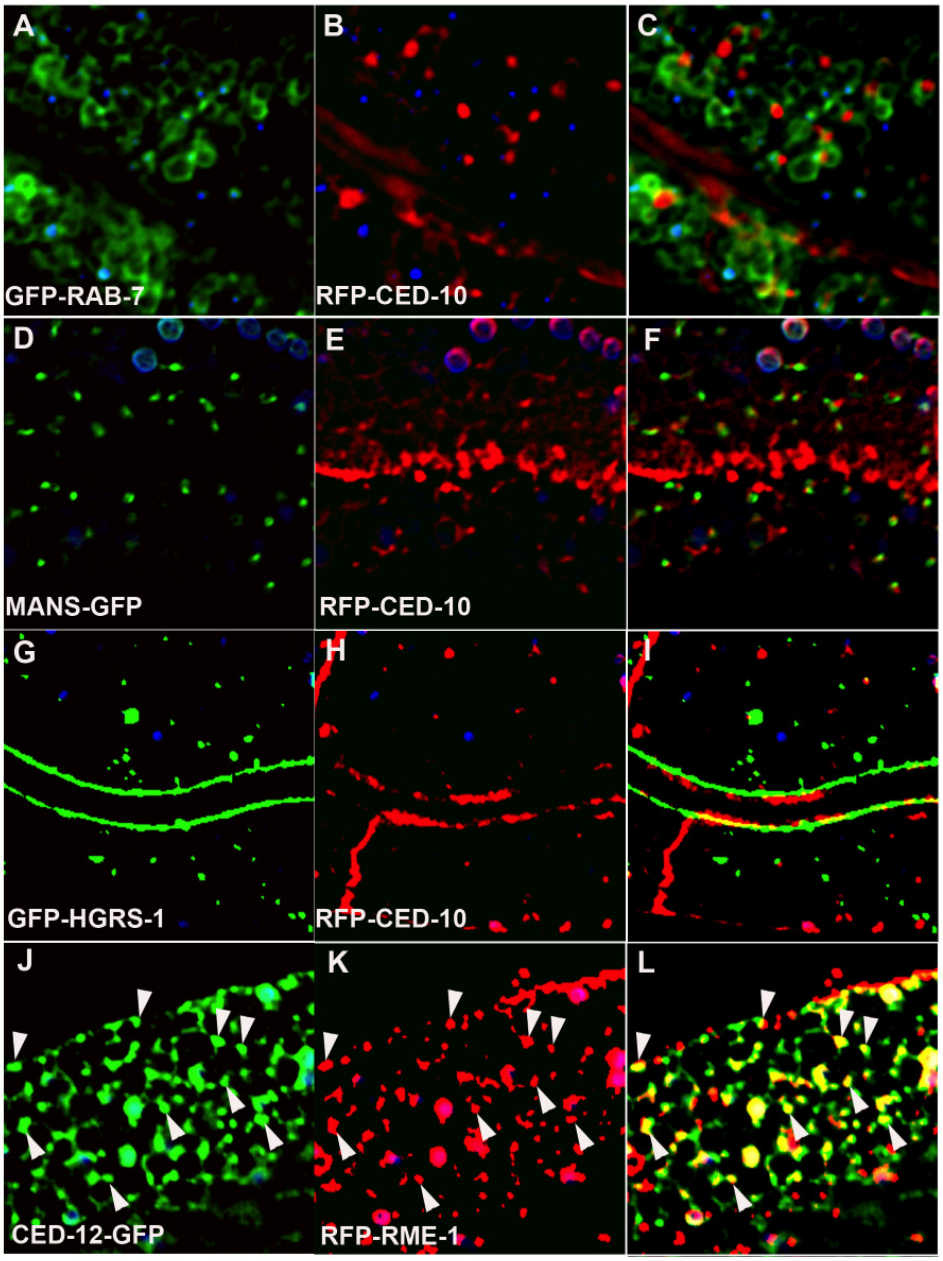
A
GFP-RAB-7
B
RFP-CED-10
C
D
MANS-GFP
E
RFP-CED-10
F
G
GFP-HGRS-1
H
RFP-CED-10
I
J
CED-12-GFP
K
RFP-RME-1
L

Figure S6: Further analysis of CED-10 and CED-12 localization in the intestine.

(A-C) RFP-CED-10 fails to colocalize with late endosome marker GFP-RAB-7. (D-F) RFP-CED-10 does not co-localize with the Golgi marker AMAN-2/Mannosidase-GFP, but often labels structures juxtaposed to the Golgi ministacks. (G-I) RFP-CED-10 and GFP-HGRS- 1 label different endosome types. Virtually no overlap was observed between RFP-CED-10 and GFP-HGRS-1 labeled multivesicular endosomes. (J-L) CED-12-GFP colocalizes with RFP- RME-1 on basolateral recycling endosomes. In each image autofluorescent lysosome-like organelles can be seen in all three channels with the strongest signal in blue, whereas GFP appears only in the green channel and RFP/mCherry only in the red channel. Signals observed in the green or red channels that do not overlap with signals in the blue channel are considered bone fide GFP or RFP/mCherry signals, respectively. Scale bar, 10 μm.

Transgenic and mutant strains used in this study

pwIs112[Pvha-6::hTAC::GFP] (Chen et al., 2006a)

pwIs717[Pvha-6::hTfR::GFP] (Chen et al., 2006a)

pwIs883[Pvha-6::EHBP-1::mCherry] (Shi et al., 2010b)

pwIs859[Pvha-6::mCherry::CED-10] (this work)

pwIs807[Pvha-6::CED-12::mCherry] (this work)

pwIs72[Pvha-6::GFP::RAB-5] (Chen et al., 2006a)

pwIs206[Pvha-6::GFP::RAB-10] (Chen et al., 2006a)

pwIs601[Pvha-6::ARF-6::GFP] (this work)

pwIs87[Pvha-6::GFP::RME-1] (Chen et al., 2006a)

pwIs731[Pvha-6::GFP::CED-10] (this work)

pwIs846[Pvha-6::RFP::RAB-5] (Shi et al., 2007)

pwIs852[Pvha-6::RFP::RME-1] (Shi et al., 2007)

pwIs414[Pvha-6::mCherry::RAB-10] (this work)

pwIs69[Pvha-6::GFP::RAB-11] (Chen et al., 2006a)

vhIs12[Pvha-6::GFP::TBC-2] (Chotard et al., 2010b)

vhIs1[Pvha-6::mCherry::TBC-2] (Chotard et al., 2010b)

pwIs722[Pvha-6::SDPN-1::GFP] (Shi et al., 2007)

pwIs765[Pvha-6::MIG-14::GFP] (Shi et al., 2009)

pwIs170[Pvha-6::GFP::RAB-7] (Chen et al., 2006a)

pwIs481[Pvha-6::MANS::GFP] (Chen et al., 2006a)

pwIs518[Pvha-6::GFP::HGRS-1] (Shi et al., 2009)

pwIs770[Pvha-6::CED-12::GFP] (this work)

pwIs950[Pvha-6::RFP::RAB-5(Q78L)] (this work)

pwIs954[Pvha-6::RFP::RAB-5(Q78L)] (this work)

ced-10(n3246) (Reddien and Horvitz, 2000)

ced-12(tp2) (Brugnera et al., 2002)

rab-10(q373) (Chen et al., 2006a)

rme-1(b1045) (Grant et al., 2001b)

ced-5(n1812) (Cabello et al., 2010)

ced-2(e1752) (Reddien and Horvitz, 2000)

tbc-2(tm2241) (Chotard et al., 2010b)

Table S1: Strain list: Summary of the transgenic and mutant strains used during this work.

Chapter 3.

RAB-10 and AMPH-1 regulate cargo transport from early-to-recycling endosome via the RAB-5 GAP TBC-2

AUTHOR CONTRIBUTIONS

This chapter was submitted for publication to *Plos Genetics*. I participated in the experimental design, performed all the experiments, analyzed the data. Dr. Barth D. Grant designed the experiments and trained me to perform experiments. Dr. Barth D. Grant and I wrote the paper.

SUMMARY

Ordered transport of cargos from early endosome to recycling endosome requires the coordination of small GTPase RAB-5 and RAB-10. Countercurrent cascades of GEFs and GAPs for Rab proteins have been proposed to mediate Rab conversion, a process in which early acting Rabs are inactivated by later acting Rabs. Here we demonstrate that a downstream Rab protein, RAB-10, binds to and recruits a RAB-5 GAP, TBC-2, onto endosomes to inactivate the upstream Rab, RAB-5. This process is critical for proper transport of cargos from RAB-5 controlled early endosomes to RAB-10 regulated recycling endosomes. Lack of TBC-2 disrupted RAB-5/RAB-10 interaction and caused accumulation of recycling cargo hTAC-GFP in a malfunctioned hybrid early-recycling endosome compartment. In addition, our study showed that this cargo transition process from early to recycling endosome also requires the concerted effort by a BAR-domain protein AMPH-1, which acts as a binding partner and a contributor to the recruitment of TBC-2 on endosomes.

INTRODUCTION

Endocytic recycling, the return of proteins and lipids from endosomes to the plasma membrane, plays a key role in many essential cellular processes including nutrient uptake, cell migration, cytokinesis, synaptic plasticity, immune response, and growth factor receptor modulation (Grant and Donaldson, 2009). In polarized epithelial cells an additional layer of complexity in the endocytic pathway contributes to formation and/or maintenance of the specialized apical and basolateral domains (Eaton and

Martin-Belmonte, 2014; Folsch et al., 2009). Both the apical and basolateral membranes deliver cargo to early endosomes, often referred to as apical early endosomes and basolateral early endosomes (Brown et al., 2000; Folsch et al., 2009; Wang et al., 2000). Basolaterally derived and apically derived cargo can reach common recycling endosomes, from which cargo is sorted for delivery to the basolateral plasma membrane or to apical recycling endosomes (Brown et al., 2000; Folsch et al., 2009; Wang et al., 2000). The apical recycling endosomes are thought to send their cargo to the apical plasma membrane. Small GTPases of the Rab superfamily play key roles in membrane transport, with at least one Rab protein regulating each transport step. In polarized epithelial cells Rab11 is primarily associated with the ARE and is thought to function in the transport of cargo from the ARE to the plasma membrane (Casanova et al., 1999; Folsch et al., 2009; Sobajima et al., 2014). Rab8 has also been implicated in apical recycling in the intestinal epithelia of mouse and worms (Sato et al., 2007).

Our attention was first brought to bear on the basolateral recycling pathway of C. elegans intestinal epithelia because of the accumulation of grossly enlarged basolateral vesicles in mutants lacking the recycling regulator RME-1/EHD (Grant et al., 2001b). In the case of rme-1 mutants, these enlarged vesicles accumulated recycling cargo and were positive for the endosomal recycling regulator ARF-6, but lacked early endosome marker RAB-5, suggesting that RME-1 functions at a late recycling step (Chen et al., 2006a; Grant et al., 2001b; Shi et al., 2012). Pulse-chase data in mammalian cells showed that loss of mRme- 1/EHD1 likewise resulted in a block in recycling endosome to plasma membrane transport (Caplan et al., 2002; Lin et al., 2001). Similarly rab-10 mutants first caught our attention because they displayed enlarged basolateral vesicles in the C. elegans intestine that accumulated recycling cargo (Chen et al., 2006a). However, in this case the enlarged endosomes were positive for RAB-5, indicating an earlier block in basolateral recycling, at the level of early endosome to recycling endosome transport (Chen et al., 2006a). We extended this work, identifying two RAB-10 effectors that function with RAB-10 in basolateral recycling, EHBP-1 and CNT-1 (Shi et al., 2010b; Shi et al., 2012). EHBP-1 strongly labeled the tubular elements of the recycling pathway, was required for strong RAB-10 endosomal recruitment, and may

link endosomes to the cytoskeleton (Guilherme et al., 2004c; Shi et al., 2010b). CNT-1/ACAP is recruited to endosomes by RAB-10 and regulates the activity of ARF-6, acting as part of a small GTPase regulatory loop (Shi et al., 2012). In turn ARF-6 regulates PI5-kinase, controlling PI(4,5)P2 levels on basolateral recycling endosomes, and the recruitment of downstream PI(4,5)P2 lipid binding proteins such as RME-1 (Brown et al., 2001; Shi et al., 2012).

C. elegans RAB-10 and human Rab10 are now known to contribute a wide range of endocytic recycling pathways. Like its *C. elegans* homolog, mammalian Rab10 functions in basolateral recycling in polarized MDCK cells, where Rab10 localized to the common recycling endosome (Babbey et al., 2006a).

C. elegans RAB-10 is also required for the postsynaptic recycling of glutamate receptors in interneurons (Glodowski et al., 2007a), and dense-core vesicle secretion of neuropeptides by motor neurons (Sasidharan et al., 2012). Mammalian Rab10 is required for toll-like receptor 4 recycling in activated macrophages (Wang et al., 2010), membrane insertion of plasmalemmal precursor vesicles during neuronal polarization and axonal growth (Deng et al., 2014; Wang et al., 2011), and insulin-stimulated glucose transporter recycling in adipocytes (Chen et al., 2012). Expression of human Rab10 in the *C. elegans* intestine rescues rab-10 mutant defects, indicating a high degree of functional conservation, suggesting that further elucidating RAB-10 function in the *C. elegans* will provide mechanistic insight into RAB-10/Rab10 function in many or all of these related processes (Chen et al., 2006a).

Countercurrent cascades of Rab GEFs and Rab GAPs have been proposed to mediate Rab conversion, a process by which Rab proteins interact, helping to establish vectorial transport of cargo along membrane trafficking pathways (Hutagalung and Novick, 2011a). In such cascades early acting Rab-GTPases recruit effectors that activate later acting Rab- GTPases, and in turn later acting Rab-GTPases recruit effectors that inactivate early acting Rab-GTPases (Hutagalung and Novick, 2011a). However little is known of how such cascades contribute to endocytic recycling. Here we show that RAB-10 recruits the RAB-5 GTPase-activating-protein TBC-2 to endosomes in a step necessary for early endosome to recycling endosome transport. This negative feedback

from RAB-10 to RAB-5 is required for the exit of recycling cargo from early endosomes. We also show that the BAR-domain protein AMPH-1 as a binding partner of TBC-2 important for recruitment of TBC-2 to endosomes, as part of the transition of cargo from the early to recycling endosome compartments, a poorly understood membrane transport step in any organism.

RESULTS

RAB-5 GAP TBC-2 is a RAB-10 binding partner

We have previously reported several proteins that function with RAB-10 in basolateral recycling in the C. elegans intestine, some of which we first identified via a yeast two-hybrid screen that used a predicted constitutively GTP-bound form of RAB-10 (Q68L) as bait (Shi et al., 2010b). In this same yeast two-hybrid screen we also identified a RAB-10(Q68L) interacting clone encoding full-length TBC-2, a GAP for the earlier acting endosomal GTPase RAB-5 (Caplan et al., 2002; Chotard et al., 2010b; Deng et al., 2014). The interaction between RAB-10(Q68L) and TBC-2 was positive in both Leu2 and β-galactosidase expression assays (Figure 1A). Using successive truncations of TBC-2 we narrowed the RAB-10 binding site to a 42 amino acid region of TBC-2 (amino acids 279-321) (Figure 1A- 1B, 1E). We noted several runs of highly charged residues in this region, and tested their importance for binding to RAB-10 in groups of 5 by alanine scanning. The interaction was abolished when alanine substitutions were imposed at TBC-2 positions aa283-287, aa288- 292, and aa294-298, indicating a requirement for these sequences in RAB-10 binding (Figure 1C). Taken together, our results indicate the presence of a sequence of 42 amino acids within the predicted coiled-coil domain of TBC-2 that provides a binding surface to interact with RAB-10, a key regulator of the basolateral endocytic recycling process. Since TBC-2 is known to act as a GAP for early endosome master regulator RAB-5, these results suggest a negative feedback loop from RAB-10 to RAB-5, potentially acting as part of a RAB cascade in the basolateral recycling pathway.

TBC-2 is highly enriched on RAB-10-positive endosomes

Intestinally expressed GFP-tagged TBC-2 labels abundant cytoplasmic puncta with the typical size and shape of endosomes (250-500nm diameter). If TBC-2 is a physiologically relevant binding partner for RAB-10, we would expect to find RAB-10 and TBC-2 on the same endosomes *in vivo*. Previous qualitative work indicated some localization of TBC-2 to early and late endosomes, but the extent of localization, and its relationship to recycling endosomes, remained unclear (Chotard et al., 2010b; Deng et al., 2014). To quantitatively test the subcellular localization of TBC-2 we conducted a series of co-localization studies in the intestinal epithelial cells where RAB-10 is known to function, using a set of previously established RFP markers for RAB-10 and a variety endocytic compartments. The degree of colocalization was measured using Pearson's correlation coefficient (Manders et al., 1992). Consistent with our binding data, we detected the greatest overlap of GFP-TBC-2 with RFP- tagged RAB-10(+) and RFP-RAB-10(Q68L), 60% and 70% respectively (Figure 2A-2A‴, 2B- 2B‴ and Figure 2D). The greater degree of colocalization with RAB-10(Q68L) is consistent with a model where RAB-10 helps to recruit TBC-2 onto endosomes. GFP-TBC-2 also colocalized very well (57%) with a previously characterized RAB-10 effector, CNT-1 (CNT- 1-mCherry) (Figure 2C-2C‴ and Figure 2D), which is also required for the recycling process (Shi et al., 2012). These results are consistent with TBC-2 acting with RAB-10 and CNT-1 in the basolateral endocytic recycling process.

GFP-TBC-2 also showed partial colocalization with early endosomal marker tagRFP-RAB-5 (34%) (Figure S2A-S2A‴ and S2D) and late endosomal marker tagRFP-RAB-7 (45%) (Figure S2B-S2B"' and Figure S2D). The degree of colocalization of TBC-2 with RAB-5 and RAB-7 was significantly less than that of TBC-2 with RAB-10. We also noted that GFP-TBC-2 displays hardly any colocalization with EHBP-1, another RAB-10 interacting protein that labels tubular aspects of the basolateral recycling endosome network (Figure S2C-S2C‴). Collectively, our results indicate that TBC-2 is enriched on a subpopulation of endosomes, where it could work with RAB-10 and RAB-5 to confer effective transport of cargo during the endocytic recycling process.

RAB-10 is required for the endosomal recruitment of TBC-2 in the intestinal epithelium

To further test the idea that an interaction with RAB-10 is important for TBC-2 function *in vivo*, we examined the effect of a *rab-10* loss-of-function mutant on the endosomal localization of GFP-TBC-2 in the intestinal epithelia. In the *rab-10* mutant background GFP- TBC-2 became very diffusive, losing its typical punctate endosomal localization, indicating a requirement for RAB-10 in TBC-2 endosomal recruitment (Figure 3A and 3B). We extended this analysis further, testing a form of TBC-2 impaired for RAB-10 binding (QRNNE 288-292 AAAAA) for function *in vivo*. In previous work we showed that TBC-2 is required for the normal recycling of model cargo hTfR-GFP (human transferrin receptor - GFP)(Sun et al., 2012b). In the absence of TBC-2, hTfR-GFP accumulates in enlarged intracellular structures (Figure 4A-4B, 4F). While expression of full length wild-type TBC-2 efficiently rescued the localization of hTfR-GFP in a *tbc-2* null mutant background (Figure 4C and 4F), we found that expression of the interaction defective form of TBC-2 failed to rescue the localization of hTfR-GFP in a *tbc-2* null mutant background (Figure 4E and 4F).

Physical interaction between TBC-2 and AMPH-1

In many cases peripheral membrane proteins of the endosome require multiple protein and/or lipid interactions to direct their localization. Recent work using phage-display to identify the binding preferences of all *C. elegans* SH3 domains suggested a link between TBC-2 and AMPH-1, a BAR-domain and SH3-domain protein that is the only *C. elegans* member of the Amphiphysin/BIN1 protein family (Pant et al., 2009; Xin et al., 2013). TBC-2 amino acid sequence 146-160 was identified as the fourth best match for the AMPH-1 SH3- domain binding consensus in the entire predicted *C. elegans* proteome (Xin et al., 2013). Previous work from our laboratory has shown that AMPH-1 participates in the basolateral recycling pathway (Pant et al., 2009; Xin et al., 2013). Thus we sought to further examine this potential interaction. We detected interaction of full-length TBC-2 with the AMPH-1 SH3 domain in a yeast 2-hybrid

assay (Figure 1D). Importantly, the interaction was abolished when key residues in the consensus sequence, prolines P150 or P153, or arginine R155, were mutated to alanine (Figure 1D and 1E). Despite losing their ability to interact with AMPH-1, the P150A, P153A, and R155A mutant forms of TBC-2 protein retained the ability to interact with RAB-10(Q68L) in the same two-hybrid assay, indicating that the mutant forms of TBC-2 were stable (Figure S1A). We conclude that the AMPH-1 SH3 domain has the potential to bind to the predicted target sequence in TBC-2 (Figure 1D and S1A).

AMPH-1 contributes to the endosomal recruitment of TBC-2

If an interaction between AMPH-1 and TBC-2 is important *in vivo*, we might expect to observe a change in TBC-2 localization in an *amph-1* mutant background. Indeed, when we examined the subcellular localization of intestinally expressed GFP-TBC-2 in an *amph-1* deletion mutant, we found that the normal punctate endosomal distribution of GFP-TBC-2 was severely disrupted (Figure 3A-3C, 3D). Instead, GFP-TBC-2 appeared quite diffusive in the absence of AMPH-1 (Figure 3C). We extended this analysis further, testing a form of TBC-2 impaired for AMPH-1 binding (P150A) for function *in vivo*, using the same hTfR-GFP localization assay described above. We found that while expression of full length wild-type TBC-2 efficiently rescued the localization of hTfR-GFP in a *tbc-2* null mutant background (Figure 4A-4C, 4F), the expression of the interaction defective form of TBC-2 failed to rescue the localization of hTfR-GFP in a *tbc-2* null mutant background (Figure 4A-B, 4D, 4F). Our results thus indicate that in addition to RAB-10, AMPH-1 also contributes to TBC-2 endosomal recruitment.

RAB-5 displays elevated membrane-association in *tbc-2*, *rab-10*, and *amph-1* mutants

If RAB-10 and AMPH-1 contribute to TBC-2 recruitment and function, then loss of RAB-10 or AMPH-1 would be expected to result in abnormally elevated levels of GTP-bound RAB-5. Furthermore, since the Rab protein nucleotide cycle is linked to Rab protein membrane association, an elevated "active" GTP-bound status for RAB-5 should result in an elevated level of membrane-bound RAB-5. This model predicts that in

tbc-2, *rab-10*, and *amph-1* mutants, where the RAB-5 GAP TBC-2 is either completely missing, or is mislocalized, RAB- 5 association with membranes should be increased. We tested this hypothesis biochemically, separating membranes from cytosol in *C. elegans* lysates using ultracentrifugation at 100,000g in the appropriate mutant backgrounds, comparing the amount of intestinally expressed GFP-RAB-5 present in each fraction by Western blot. Consistent with the predictions from this model, we observed an elevation in GFP-RAB-5 membrane-to-cytosol ratio in *tbc-2*, *rab-10*, and *amph-1* mutants (Figure 5A-5C). Loss of RAB-10 or AMPH-1 increased the membrane association of RAB-5 to a lesser extent than that caused by loss of TBC-2, suggesting that some localized TBC-2 remains in *rab-10* and *amph-1* mutants, although endosome localized TBC-2 is difficult to visualize by microscopy in such mutant backgrounds (Figure 5A and Figure 5C). In summary, our data supports a role for *rab-10* and *amph-1* in TBC-2 membrane recruitment that is required to complete the RAB-5 nucleotide cycle, removing RAB-5 from membranes. Since RAB-10 and AMPH-1 function in the recycling aspect of endocytic trafficking, these results suggest that removal of RAB-5 from endosomal membranes is an integral part of the recycling process, perhaps linked to cargo transition from early to recycling endosome transport.

Loss of TBC-2 or AMPH-1 alters the spatial coordination of RAB-5 and RAB-10

Previous work showed that RAB-5 and RAB-10 display significant spatial overlap in the C. elegans intestine, consistent with functional data indicating that RAB-10 is important for exit of recycling cargo from RAB-5-positive endosomes (Chen et al., 2006a). To better understand the relationship between RAB-5 and RAB-10, we assayed for changes in their relative colocalization in *tbc-2* and *amph-1* mutants. Similar to previously published results, we found that under wild-type conditions tagRFP-RAB-5 and GFP-RAB-10 both label punctate endosomal structures that partially colocalize (53%) (Figure 6A-6A‴, 6D). We detected dramatic morphological changes for both tagRFP-RAB-5 and GFP-RAB-10 labeled endosomes in a *tbc-2* mutant background. Aside from some remaining punctate structures, in *tbc-2* mutants tagRFP-RAB-5 and

GFP-RAB-10 tended to label very large pleiomorphic structures that were never observed in wild-type animals (Figure 6B-6B‴). Quantification of RAB-5 colocalization with RAB-10 showed a signficant increase (to 71%) in the degree of overlap of tagRFP-RAB-5 and GFP-RAB-10 in tbc-2 mutants (Figure 6D), mostly restricted to the grossly enlarged structures (Fig 6B-6B‴). amph-1 mutants also displayed a significant increase in tagRFP-RAB-5 spatial overlap with GFP-RAB-10 (Figure 6C-6C‴, 6D), although the morphological size and shape changes were less severe than those in *tbc-2* mutants (Fig 6C-6C‴). Taken together, these data suggest that TBC-2 and AMPH-1 cause recycling defects by altering the normal compartmentalization of RAB-5 and RAB-10 on endosomes.

Recycling cargo accumulates in RAB-5 labeled endosomes in *tbc-2* and *amph-1* mutants

Our previous work on RAB-10 function in the intestine showed that RAB-5 labeled endosomes in *rab-10* mutants are grossly enlarged and accumulate an additional model recycling cargo, hTAC-GFP (human TAC, IL-2 receptor alpha chain)(Chen et al., 2006a). hTAC-GFP strongly labels that tubular aspects of the basolateral recycling pathway at steady state, and depends upon RAB-10, RME-1, and ARF-6 for its recycling [10-11,13]. To better understand the step in recycling transport affected by TBC-2 and AMPH-1 we assayed the relative localization of hTAC-GFP to tagRFP-RAB-5 and tagRFP-RAB-10 in *tbc-2* and *amph-1* mutants. Under wild-type conditions, hTAC-GFP displays little steady-state overlap with tagRFP-RAB-5 (Figure 7A-7A‴). In *tbc-2* mutant animals, the tubular meshwork of hTAC-GFP appears disrupted, with hTAC-GFP mostly found in enlarged endosomes, many of which label for tagRFP-RAB-5 (Figure 7B-7B‴). We measured a striking increase in the degree of colocalization between hTAC-GFP and tagRFP-RAB-5 in TBC-2 mutants (Figure 7D). In animals lacking AMPH-1, we also detected a significantly larger degree of overlap between hTAC-GFP and tagRFP-RAB-5 in comparison to that of wild-type animals (Figure 7C-7C‴, 7D). Consistent with our previous reports, we observed partial overlap of hTAC-GFP with tagRFP-RAB-10, mostly restricted to punctate rather than tubular aspects of the hTAC-GFP

labeled endosomes (Figure 8A-8A‴). The degree of colocalization between hTAC-GFP and tagRFP-RAB-10 increased mildly in *tbc-2* mutant and was basically unaltered in amph-1 mutants (Figure 8A-8A‴, 8B-8B‴, 8C-8C‴, 8D) . Taking into account the aforementioned increase in colocalization between RAB-5 and RAB-10 in these mutant backgrounds, these data suggest that most hTAC-GFP in *tbc-2* mutant and in amph-1 mutant animals is trapped in the early endosome.

DISCUSSION

Given the continuous flow of proteins and membranes along the endocytic and exocytic pathways, cells face a formidable challenge in achieving accurate intracellular transport of membrane cargo. Such transport is likely to require tight regulation that enforces the directionality of sequential flow between membranous compartments (Hutagalung and Novick, 2011a). Rab GTPases serve as master regulators of membrane trafficking by controlling the structural and functional characteristics of intracellular organelles (Hutagalung and Novick, 2011a). The ability to switch between the "on" and "off" states through the Rab GTP/GDP cycle empowers Rab proteins to control the spatial and temporal regulation of cargo transport (Barr and Lambright, 2010). Rabs interact with a cohort of effector proteins that contribute to a variety of functions, ranging from vesicle tethering, their most widely observed role, to vesicle budding and movement, and regulating the activation state of other small GTPases (Grosshans et al., 2006a). An ordered relay of cargo between sequentially acting compartments is thought to entail coordination of Rab activation states, coordinating changes in organelle maturation and/or allowing distinct compartments to interact at the right time and the right place for cargo transfer (Wandinger-Ness and Zerial, 2014). A Rab cascade model has been proposed that likely defines a general principle in membrane transport. This model proposes that an upstream GTP-loaded Rab protein recruits the GEF for the next Rab-GTPase along a transport pathway, activating the downstream Rab. In turn a countercurrent activity is initiated by the downstream GTP-loaded Rab, which recruits the GAP for the upstream Rab to deactivate it (Hutagalung and Novick, 2011a). Together these activities are proposed to help enforce unidirectional flow. Such Rab

cascades have been proposed for maturation based transport steps, such as the early endosome to late endosome transition, as well as transport steps mediated by small vesicle transport between distinct compartments, such as ER to Golgi transport (Del Conte-Zerial et al., 2008; Poteryaev et al., 2010; Wang and Ferro-Novick, 2002).

While the molecular details of how such Rab cascades work are beginning to come to light in a small number of cases, little is known of how such activities influence endocytic recycling. In this study, we focused on the transition from early endosomes, controlled by RAB-5, to recycling endosomes, controlled by RAB-10, acting in the basolateral recycling pathway of the *C. elegans* intestinal epithelia. Our study shows that the downstream Rab, RAB-10, in its GTP-bound form, binds to RAB-5 GAP TBC-2 and is required for its recruitment to endosomes. Consistent with a RAB-10 to RAB-5 negative regulatory loop via TBC-2, loss of TBC-2 or RAB-10 increases association of RAB-5 with membranes, indicating abnormally high RAB-5 activation. Lack of TBC-2 also causes a dramatic morphological change in the RAB-5 labeled early endosomes. We observed accumulation of abnormally large, RAB-5-positive, pleomorphic endosome structures, many of which displayed increased overlap with RAB-10. Thus we propose that TBC-2 can serve as a bridge in the interaction between RAB-10 and RAB-5. This model suggests that without TBC-2, RAB-5 cannot be inactivated as part of the recycling pathway, and RAB-10 endosomes cannot properly separate from RAB-5 endosomes. Our cargo localization analysis shows that in *tbc-2* mutants the recycling cargo hTAC is mostly trapped in RAB-5 positive endosomes, indicating a defect in the exit of recycling cargo from early endosomes that cannot inactivate RAB-5. These results are reminiscent of the a counter-current GAP cascade in Saccharomyces cerevisiae that is required to restrict the spatial overlap of early and late Golgi Rabs Ypt1p and Ypt32p (Rivera-Molina and Novick, 2009).

Our study also showed that cargo transition from early endosomes to recycling endosomes requires the coordination of another regulator of the recycling pathway, BAR-domain protein AMPH-1. Like RAB-10, AMPH-1 contributes to endosomal recruitment of TBC-2. We also detected failure in proper separation of RAB-5 and RAB-10 and failure in the exit of recycling cargo from early endosomes in *amph-1* mutants, although

the endosomes did not appear as grossly enlarged as in *tbc-2* mutants. The AMPH-1 BAR domain binds directly to PI(4,5)P2 enriched membranes, can potentially sense membrane curvature, and can promote tubule formation (Pant et al., 2009). An interesting possibility is that AMPH-1 derived membrane tubules could be directly involved in cargo transfer. Our previous work also showed that AMPH-1 binds to RME-1, a later acting player in the basolateral recycling pathway, potentially acting to coordinate early and late aspects of recycling (Pant et al., 2009).

Our current study delineated distinct regions of TBC-2 bound by RAB-10 binding and AMPH-1. Combined with our previous work showing a connection of CED-10/Rac1 to TBC-2 and recycling (Sun et al., 2012b), our observations indicate that TBC-2 is a key feedback regulator of RAB-5, acting as a molecular nexus that integrates signals from recycling endosome regulators RAB-10, AMPH-1, and CED-10. The correct localization of peripheral membrane proteins is often maintained by multiple weak physical interactions, perhaps to more precisely position such proteins at points where multiple binding partners converge, a concept sometimes called coincidence sensing. Precise recruitment of TBC-2 to endosomes during recycling is likely to be quite important in the complex process of endosomal transport, where RAB-5 activity is essential for early aspects of the pathway but needs to be deactivated for later events. Such localization mechanisms may also be easily reversible, an important characteristic in dynamic situations.

In wild-type animals we found that RAB-5-labeled endosomes and RAB-10-labeled endosomes appear as distinct puncta that show partial overlap, suggesting that only a subpopulation of RAB-5 and RAB-10 labeled endosomes is interacting at any given time. This could imply the existence of transient interactions between RAB-5 and RAB-10 labeled endosomes that function to transfer cargo, removing recycling cargo as the early endosome matures into the late endosome. Such transient interactions between early and recycling endosomes have been proposed in other systems, although the detailed mechanisms remain obscure (Rodal et al., 2011). Interestingly that work also indicated a BAR domain protein (Nwk) was involved in early endosome to recycling endosome transport, perhaps indicating cargo transfer via membrane tubules.

More work will be required to understand the dynamic interactions between early and recycling endosomes that mediate cargo transfer.

MATERIAL AND METHODS

General Methods and Strains

All *C.elegans* strains were derived originally from the wild-type Bristol strain N2. Worm cultures, genetic crosses, and other *C.elegans* husbandry were performed according to standard protocols (Brenner, 1974). Strains expressing transgenes were grown at 20 ℃. A complete list of strains used in this study can be found in Table S1.

Bioinformatics Analyses

Secondary structures of TBC-2 protein were predicted using the Quick2D from the Bioinformatics Toolkit (Max-Planck Institute for Developmental Biology). (Web link: http://toolkit.tuebingen.mpg.de/quick2d)

Yeast Two-Hybrid Analyses

The yeast two-hybrid experiments were performed according to the procedure of the DupLEX-A yeast two-hybrid system (OriGene Technologies). All two-hybrid plasmids were generated as PCR products with Gateway attB1.1 and attB2.1 sequence extensions and were introduced into the Gateway entry vector pDONR221 by BP clonase II (Invitrogen) reaction. The bait vector pEG202-Gtwy and target vector pJG4-5-Gtwy have been described previously (Sato et al., 2005). Origene plasmid pSH18-34 (URA3, 8 ops.-LacZ) was used as a reporter in all yeast two-hybrid experiments. Constructs were introduced into the yeast strain EGY48 (MATα trp1 his3 ura3 leu2::6 LexAop-*LEU2*) included in the system.

Transformants were selected on plates lacking leucine, histidine, tryptophan, and uracil and containing 2% (wt/vol) galactose/1% (wt/vol) raffinose at 30 ℃ for 3d and were assayed for the expression of the *LEU2* reporter. The constructs of mutated forms of TBC-2 with alanine substitution were constructed by Q5® - Site Directed Mutagenesis

Kit (New England Biolabs, Inc.) using the cDNA sequence of TBC-2 as template.

Plasmids and Transgenic Strains

To construct GFP or RFP/mCherry fusion transgenes that express specifically in the worm intestine, we used a previously described *vha-6* promoter-driven vector modified with a Gateway cassette inserted at the Asp718I site just upstream of the GFP or RFP coding region (Chen et al., 2006a). The PCR products of the genes of interest were first cloned into the Gateway entry vector pDONR221 by BP reaction (Invitrogen). Then the pDONR221 carrying the sequence for the gene of interest were transferred into the intestinal expression vectors by Gateway recombination cloning LR clonase II (Invitrogen) reaction to generate N- terminal/C-terminal fusions (Chen et al., 2006a). Low-copy integrated transgenic lines for all of these plasmids were obtained by the microparticle bombardment method (Praitis et al., 2001). Transgenic strains pwEx142-144 were generated as following. Full-length TBC-2, TBC-2(P150A), and TBC-2(288-292AAAAA) was first cloned into pDONR221. pSM47 pSNX- 1::tagRFP, pDONR221 containing TBC-2, or TBC-2(P150A), TBC-2(288-292AAAAA), pCM1.36-TBB-2 3'-UTR was inserted into the pCFJ1001 vector via multi-site LR reaction. (Gateway® LR Clonase™ II Plus Enzyme by Life Technologies) Rescue plasmids pCFJ1001::pSNX-1::tagRFP::TBC-2 (full length, P150A, or 288-292AAAAA) (10ng/ul), pCFJ601 (50ng/ul) and pmyo-2::GFP (coinjection marker) (10ng/ul) were microinjected and resulting extrachromosomal arrays wereused in this study (Mello and Fire, 1995). The baits for yeast two-hybrid analysis pEG202-RAB-10(Q68L) and pEG202-AMPH-1(SH3) was constructed as described previously (Chen et al., 2006a; Pant et al., 2009). TBC-2 cDNA was cloned into prey plasmid pJG4-5-Gtwy. Complete plasmid sequences are available on request.

Microscopy and Image Analysis

Live worms were mounted on 2% agarose pads with 10mM levamisole as described previously (Sato et al., 2005). Multiwavelength fluorescence colocalization images were obtained using an Axio Imager.Z1 microscope (Carl Zeiss Microimaging) equipped with

a YOKOGAWA CSU-X1 spinning disk, Photometrics Evolve 512 EMCCD camera, captured using Metamorph software (Universal Imaging), and then deconvolved using AutoQuant X5 (AutoQuant Imaging). Images taken in the DAPI channel were used to identify broad-spectrum intestinal autofluorescence caused by lipofuscin-positive lysosome-like organelles (Clokey and Jacobson, 1986; Hermann et al., 2005). Quantification of colocalization images was done using the open source Fiji (Image J) software (Schindelin et al., 2012). GFP/RFP colocalization experiments were performed on L4 larvae expressing GFP and RFP markers as previously described. To obtain images of GFP fluorescence without interference from autofluorescence, we used argon 488-nm excitation and the spectral fingerprinting function of the Zeiss LSM710 Meta confocal microscope system (Carl Zeiss Microimaging). Quantification of images was performed with Metamorph Version 6.3r2 (Universal Imaging).

Membrane Fractionation Assay

Worms expressing intestinal GFP-RAB-5 in wild-type, *tbc-2(tm2241)*, *rab-10(q373)* and *amph-1(tm1060)* genetic backgrounds were synchronized and cultured on NGM. Mixed stage worms were washed off with M9 buffer, pelleted and resuspended in 500 μl of lysis buffer (50mM Tris-HCL PH 8.0, 20% Sucrose, 10% Glycerol, 2mM DTT and protease inhibitors). The worms are then disrupted using a Mini-Beadbeater-16 (BioSpec Products). Carcasses and nuclei were removed by centrifugation at 1000g for 5 min at 4℃. 200 μl of the postnuclear lysate was centrifuged at 100,000g for 1h. Pellets were reconstituted in the same volume of lysis buffer as that recovered as supernatant.

ACKNOWLEDGEMENT

We thank Carlos Chen for original identification of TBC-2 clones as RAB-10(Q68L) interactors in his yeast 2-hybrid screen. We thank Peter Schweinsberg for his technical assistance in making plasmid clones and biolistic transgenic lines. We than Helen Ushakov for DNA microinjections. This work was supported by NIH Grant GM067237 to B.D.G., and an Anne B. and James B. Leathem Summer Fellowships to O.L..

FIGURES

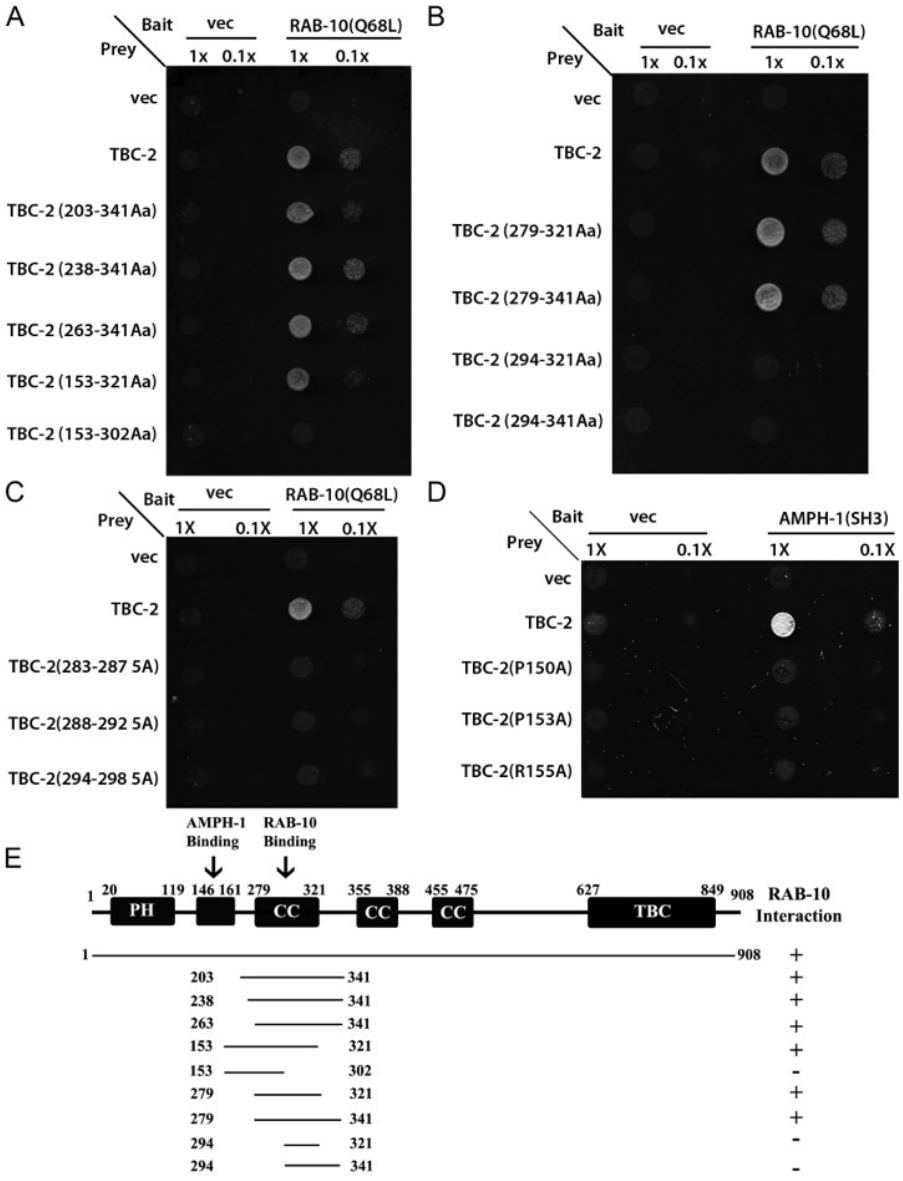
A
Bait
Prey
vec
RAB-10(Q68L)
1x 0.1x 1x 0.1x
vec
TBC-2
TBC-2 (203-341Aa)
TBC-2 (238-341Aa)
TBC-2 (263-341Aa)
TBC-2 (153-321Aa)
TBC-2 (153-302Aa)
B
Bait
Prey
vec
RAB-10(Q68L)
1x 0.1x 1x 0.1x
vec
TBC-2
TBC-2 (279-321Aa)
TBC-2 (279-341Aa)
TBC-2 (294-321Aa)
TBC-2 (294-341Aa)
C
Bait
Prey
vec
RAB-10(Q68L)
1X 0.1X 1X 0.1X
vec
TBC-2
TBC-2(283-287 5A)
TBC-2(288-292 5A)
TBC-2(294-298 5A)
D
Bait
Prey
vec
AMPH-1(SH3)
1X 0.1X 1X 0.1X
vec
TBC-2
TBC-2(P150A)
TBC-2(P153A)
TBC-2(R155A)
E
AMPH-1 Binding
RAB-10 Binding
1 20 119 146 161 279 321 355 388 455 475 627 849 908
PH
CC
CC
CC
TBC
RAB-10 Interaction
1 908 +
203 341 +
238 341 +
263 341 +
153 321 +
153 302 -
279 321 +
279 341 +
294 321 -
294 341 -

Figure 1: TBC-2 interacts physically with RAB-10 and AMPH-1.

(A) and (B) The interaction between TBC-2 and RAB-10(Q68L) requires a segment of TBC- 2(AA 279-321) containing a predicted coiled-coil domain. RAB-10 (Q68L) was expressed in a yeast reporter strain as a fusion to the DNA-binding domain of LexA (bait). Different truncations of TBC-2 were expressed in the same yeast cells as fusions to the B42 transcriptional activation domain (prey). Interaction between bait and prey was assayed by complementation of leucine auxotrophy (LEU2 growth assay). Colonies were diluted in liquid and spotted on solid growth medium directly (1X) or after further dilution (0.1X). (C) Alanine substitutions within the critical RAB-10-binding sequence of TBC-2 (positions aa283-287, aa288-292, aa294-298) abolished the interaction between TBC-2 and RAB-10 (Q68L). (D) Full-length TBC-2 interacts with AMPH-1. Mutation of key residues (prolines P150 or P153, or arginine R155) within TBC-2 (aa146-160), the predicted consensus sequence for AMPH-1 SH3-domain-binding, into alanine via site-directed mutagenesis disrupted the interaction between TBC-2 and the SH3 domain of AMPH-1. AMPH-1 SH3 domain was expressed as bait. Full-length and mutated forms of TBC-2 were expressed as prey. Their interactions were detected using the same two-hybrid assay as described in (A) and (B). (E) Schematic representation of TBC-2 domains and the truncated fragments of TBC-2 used in the Y2H analysis. Protein domains are displayed as dark boxes above the protein sequences (represented by dark lines). Amino acid numbers are indicated.

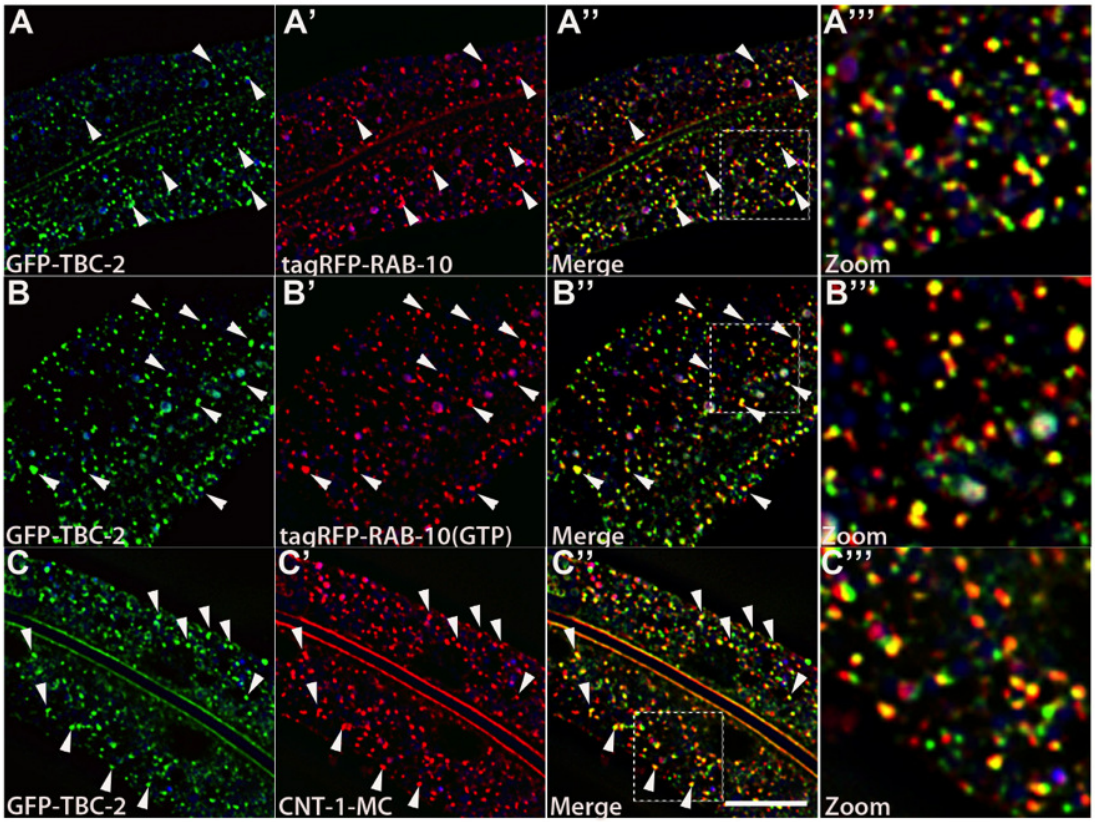
A
A'
A''
A'''
GFP-TBC-2
tagRFP-RAB-10
Merge
Zoom
B
B'
B''
B'''
GFP-TBC-2
tagRFP-RAB-10(GTP)
Merge
Zoom
C
C'
C''
C'''
GFP-TBC-2
CNT-1-MC
Merge
Zoom

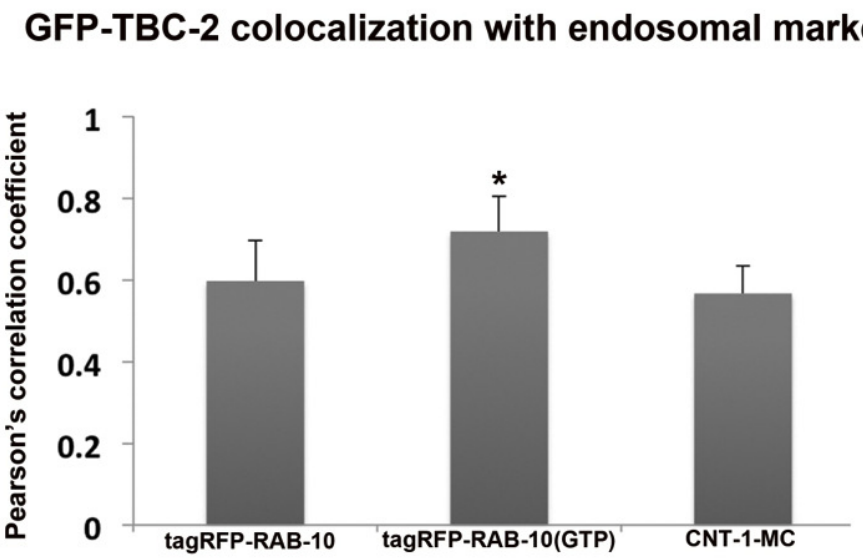
D
GFP-TBC-2 colocalization with endosomal markers
Pearson's correlation coefficient
1
0.8
0.6
0.4
0.2
0
*
tagRFP-RAB-10
tagRFP-RAB-10(GTP)
CNT-1-MC

Figure 2: TBC-2 colocalizes with RAB-10 and CNT-1 on endosomes.

All images are from deconvolved 3D confocal image stacks acquired in intact living animals expressing GFP- and RFP-tagged proteins specifically in intestinal epithelial cells. (A-A″) GFP-TBC-2 colocalizes well with tagRFP-RAB-10. Arrowheads indicate endosomes labeled by both GFP-TBC-2 and tagRFP-RAB-10. (A‴) Magnified image of A″ is designated by rectangular outline. (B-B″) GFP-TBC-2 colocalizes extensively with tagRFP-RAB-10(Q68L). Arrowheads indicate endosomes labeled by both GFP-TBC-2 and tagRFP-RAB-10 (Q68L). (B‴) Magnified image of B″ is designated by rectangular outline. (C-C″) GFP-TBC-2 colocalizes well with CNT-1-MC. Arrowheads indicate endosomes labeled by both GFP-TBC- 2 and CNT-1-MC. (C‴) Magnified image of C″ is designated by rectangular outline. In each image autofluorescent lysosome-like organelles appears in blue in all three channels, whereas GFP appears only in the green channel and RFP shows up only in the red channel. Signals observed in the green or red channels that do not overlap with signals in the blue channel are considered bone fide GFP or RFP signals respectively. (Scale bar: 10μm) (D) Pearson's correlation coefficient for colocalization of GFP-TBC-2 with tagRFP-RAB-10, tagRFP-RAB-10 (Q68L), and CNT-1-MC. $n = 6$. Error bars represent SEM. $^*P < 0.05$(student's t test).

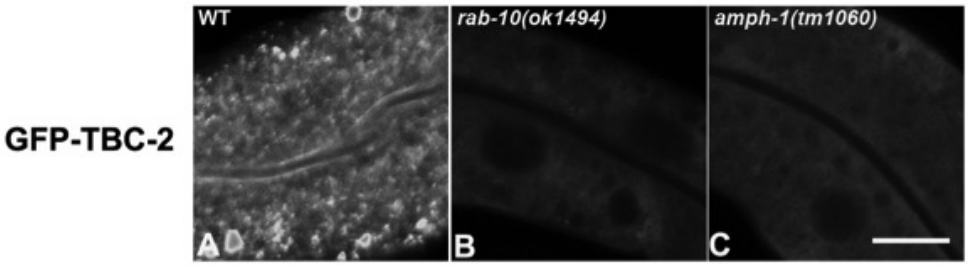
GFP-TBC-2
WT
rab-10(ok1494)
amph-1(tm1060)
A
B
C

D

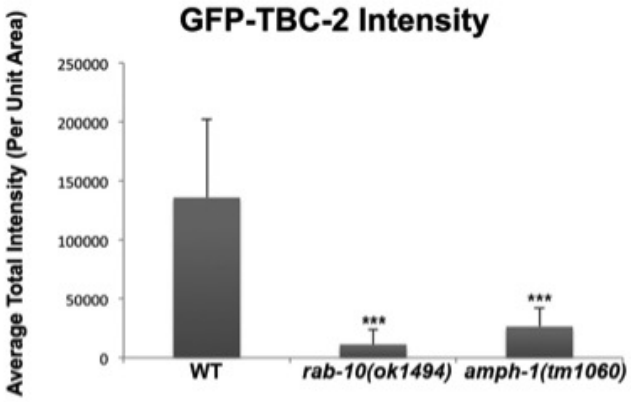
GFP-TBC-2 Intensity
Average Total Intensity (Per Unit Area)
250000
200000
150000
100000
50000
0
***
***
WT
rab-10(ok1494)
amph-1(tm1060)

Figure 3: RAB-10 and AMPH-1 contribute to the endosome recruitment of TBC-2.

All images were collected from living intact adult animals expressing intestine-specific transgenes. (A-C) Representative confocal images of GFP-TBC-2 in wild-type, *rab-10(ok1494)* mutant and *amph-1(tm1060)* mutant backgrounds are shown. The endosomal localization of GFP-TBC-2 is strongly reduced in *rab-10(ok1494)* and *amph-1(tm1060)* mutant backgrounds. (Scale bar: 10μm) (D) Quantification of the average total intensity of GFP- TBC-2 labeled structures. (n = 18 each, 6 animals of each genotype sampled in three different regions of each intestine.) Error bars represent SEM. ***$P < 0.001$(student's t test).

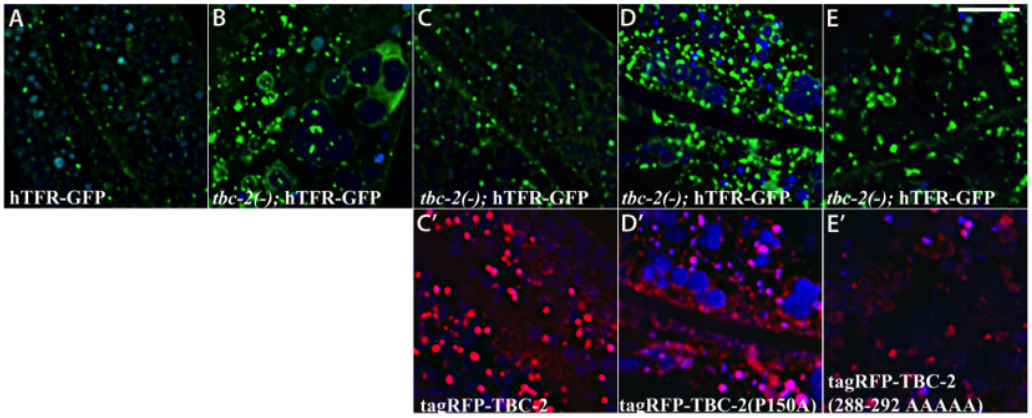
A
hTFR-GFP
B
tbc-2(-); hTFR-GFP
C
tbc-2(-); hTFR-GFP
D
tbc-2(-); hTFR-GFP
E
tbc-2(-); hTFR-GFP
C′
tagRFP-TBC-2
D′
tagRFP-TBC-2(P150A)
E′
tagRFP-TBC-2
(288-292 AAAAA)

F

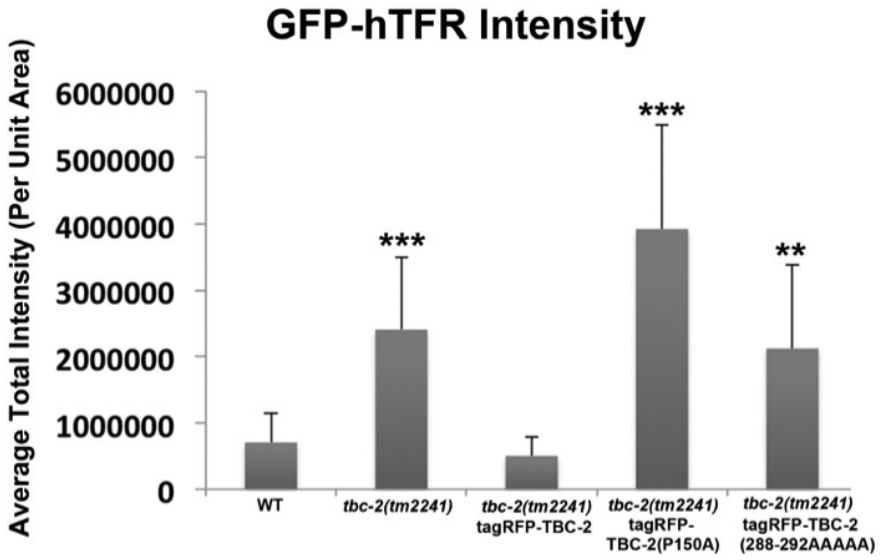
GFP-hTFR Intensity
Average Total Intensity (Per Unit Area)
6000000
5000000
4000000
3000000
2000000
1000000
0
***
***
**
WT
tbc-2(tm2241)
tbc-2(tm2241) tagRFP-TBC-2
tbc-2(tm2241) tagRFP-TBC-2(P150A)
tbc-2(tm2241) tagRFP-TBC-2 (288-292AAAAA)

Figure 4: Rescue of the cargo-recycling defect of *tbc-2* mutants requires intact RAB-10 and AMPH-1 interaction sequences.

All images are from deconvolved 3D confocal image stacks acquired in intact living animals expressing GFP- and RFP-tagged proteins. (A-E) Representative confocal images of the worm intestine expressing a GFP-tagged recycling cargo protein, the human transferrin receptor (hTFR-GFP). Loss of TBC-2 caused accumulation of hTFP-GFP on abnormally enlarged endosomal structures. The *tbc-2* mutant phenotype in cargo recycling is rescued by expression of RFP-tagged full-length TBC-2 in the worm intestine. However, expression of mutant forms of RFP-tagged TBC-2 defective either in AMPH-1-binding (TBC-2[P150A]) or in RAB-10-binding (TBC-2[288-292 AAAAA]) in the worm intestine failed to rescue the *tbc-2* mutant phenotype. (C′) Confocal image of the worm intestine expressing RFP-tagged wild-type TBC-2. (D′) Confocal image of the worm intestine expressing RFP-tagged mutant form of TBC-2 with alanine substitution at proline P150. (E′) Confocal image of the worm intestine expressing RFP-tagged mutant form of TBC-2 with five alanines replacing amino acids 288-292. (Scale bar: 10μm) (F) Quantification of the average total intestity of hTFR- GFP. In each image autofluorescent lysosome-like organelles appears in blue in all three channels, whereas GFP appears only in the green channel and RFP shows up only in the red channel. Signals observed in the green or red channels that do not overlap with signals in the blue channel are considered bone fide GFP or RFP signals respectively. ($n = 18$ each, 6 animals of each genotype sampled in three different regions of each intestine.) Error bars represent SEM. $^{**}P < 0.01$, $^{***}P < 0.001$(student's t test).

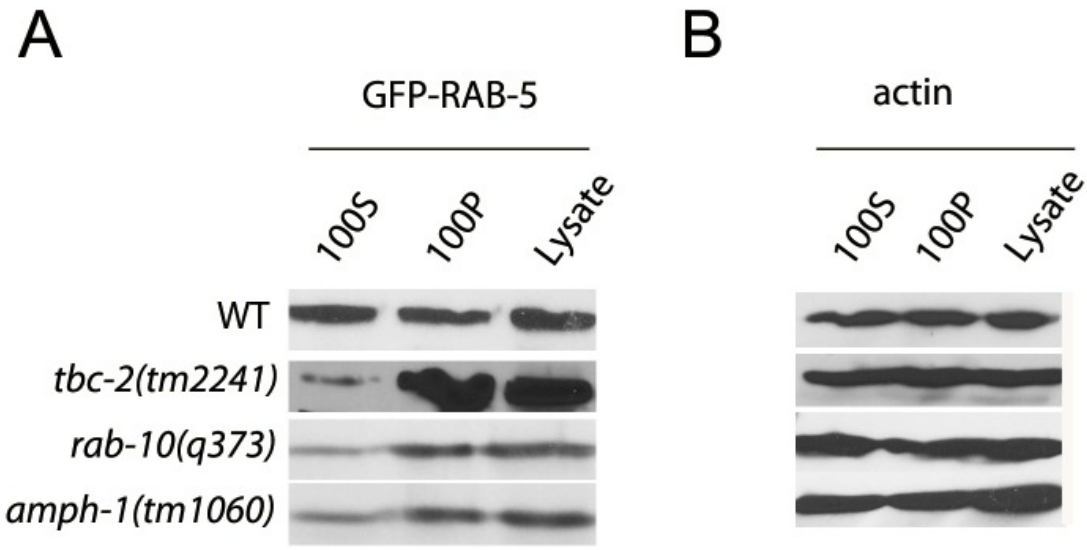
A
GFP-RAB-5
100S
100P
Lysate
WT
tbc-2(tm2241)
rab-10(q373)
amph-1(tm1060)
B
actin
100S
100P
Lysate

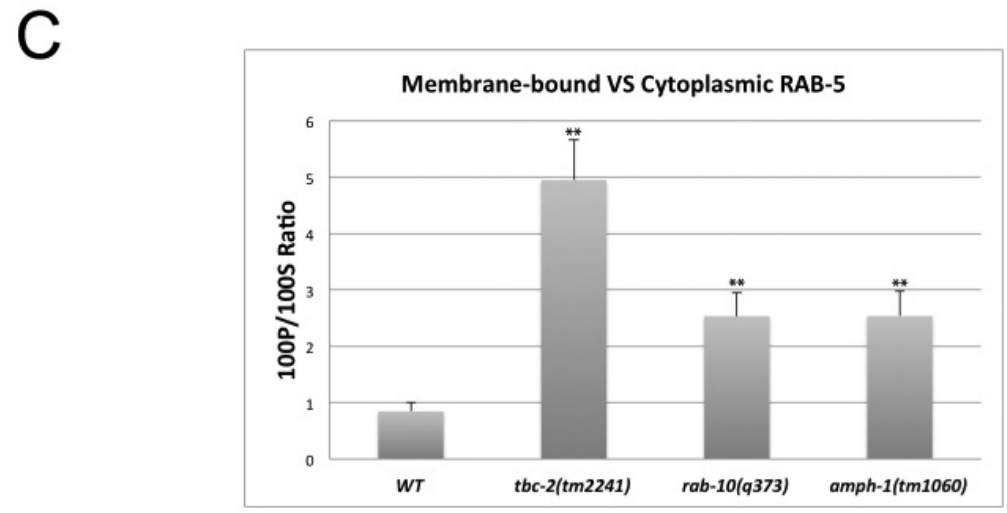
C
Membrane-bound VS Cytoplasmic RAB-5
100P/100S Ratio
0
1
2
3
4
5
6
**
**
**
WT
tbc-2(tm2241)
rab-10(q373)
amph-1(tm1060)

Figure 5: RAB-5 displays elevated membrane-association in *tbc-2*, *rab-10* and *amph-1* mutants

(A) The membrane-to-cytosol ratio of RAB-5 increased in *tbc-2*, *rab-10* and *amph-1* mutants. Post-nuclear worm lysates were subject to centrifugation at 100,000g for 1h. 100P corresponds to the pellets and 100S represents the supernatants after the 100,000g centrifugation. (B) Loading control with actin antibody. (C) Quantification of the membrane- to-cytosol ratio (100P/100S) of RAB-5 in appropriate genetic backgrounds. The ratio of membrane-bound VS cytosolic RAB-5 was determined by densitometry. The standard deviations from three independent experiments are shown. $^{**}P < 0.01$ (student's t test).

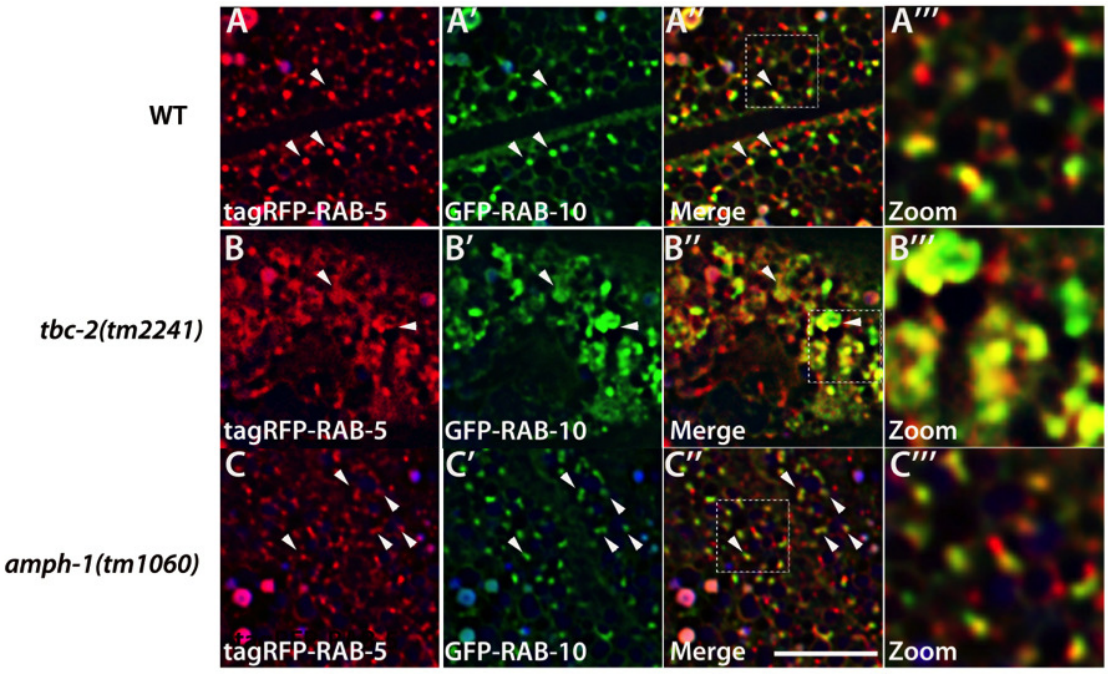
WT
tbc-2(tm2241)
amph-1(tm1060)
A
A′
A″
A‴
B
B′
B″
B‴
C
C′
C″
C‴
tagRFP-RAB-5
GFP-RAB-10
Merge
Zoom

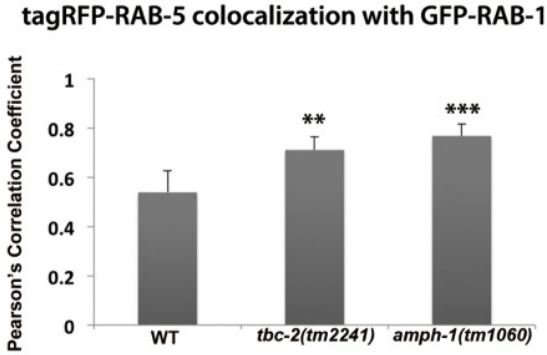
D
tagRFP-RAB-5 colocalization with GFP-RAB-10
Pearson's Correlation Coefficient
1
0.8
0.6
0.4
0.2
0
**
***
WT
tbc-2(tm2241)
amph-1(tm1060)

Figure 6: Loss of TBC-2 or AMPH-1 alters the spatial coordination of RAB-5 and RAB-10

All images are from deconvolved 3D confocal image stacks acquired in intact living animals expressing GFP- and RFP-tagged proteins specifically in intestinal epithelial cells. (A-A‴) Under wild-type conditions, tagRFP-RAB-5 and GFP-RAB-10 display partial colocalization (53%) on punctate endosomal structures. (B-B‴) In *tbc-2 (tm2241)* mutant animals, tagRFP-RAB-5 and GFP-RAB-10 label enlarged pleiomorphic structures and their degree of overlap increased to $\tilde{7}1\%$. (C-C‴) amph-1 mutants also displayed increased overlap between tagRFP-RAB-5 and GFP-RAB-10 ($\tilde{7}6\%$) with less severe morphological change than that caused by *tbc-2* mutants. In each image autofluorescent lysosome-like organelles appears in blue in all three channels, whereas GFP appears only in the green channel and RFP shows up only in the red channel. Signals observed in the green or red channels that do not overlap with signals in the blue channel are considered bone fide GFP or RFP signals respectively. (Scale bar: 10μm) (D) Pearson's correlation coefficient for colocalization of tagRFP-RAB-5 and GFP-RAB-10. $n = 6$. Error bars represent SEM. $^{**}P < 0.01$, $^{***}P < 0.001$(student's t test).

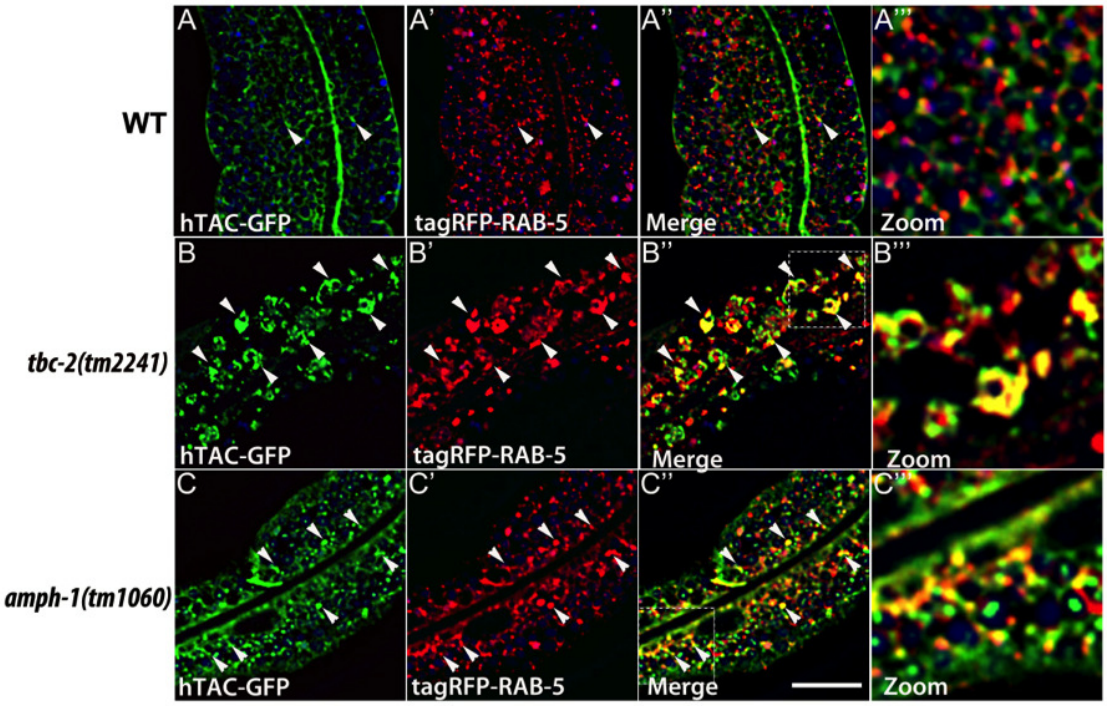
WT
tbc-2(tm2241)
amph-1(tm1060)
A
A'
A''
A'''
B
B'
B''
B'''
C
C'
C''
C'''
hTAC-GFP
tagRFP-RAB-5
Merge
Zoom

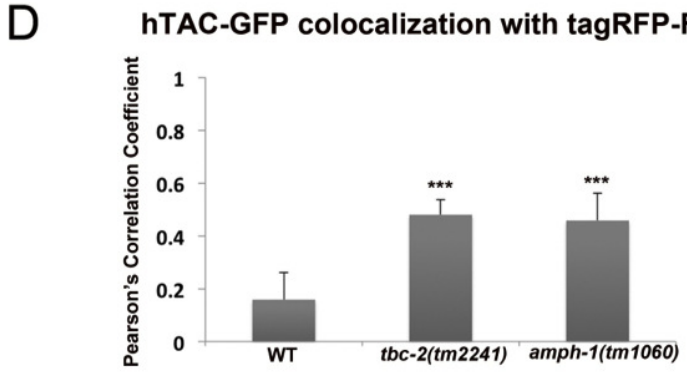
D
hTAC-GFP colocalization with tagRFP-RAB-5
Pearson's Correlation Coefficient
1
0.8
0.6
0.4
0.2
0
***
***
WT
tbc-2(tm2241)
amph-1(tm1060)

Figure 7: Recycling cargo accumulates in RAB-5 labeled endosomes in *tbc-2* and *amph-1* mutants

All images are from deconvolved 3D confocal image stacks acquired in intact living animals expressing a GFP-tagged recycling cargo protein, the IL-2 receptor alpha-chain (hTAC-GFP) and tagRFP-RAB-5 in wild-type animals (A-A‴), *tbc-2(tm2241)* (B-B‴) and *amph-1(tm1060)* mutants (C-C‴). (A-A‴) In wild-type animals, hTAC-GFP labels both punctate and tubular endosomal structures and has very little overlap with tagRFP-RAB-5. (B-B‴) In *tbc-2* mutants, hTAC-GFP and tagRFP-RAB-5 label abnormally enlarged endosomal structures. There is a striking increase in the degree of overlap between hTAC-GFP and tagRFP-RAB-5 in *tbc-2* mutants in comparison to that in wild-type animals. (C-C‴) In *amph-1* mutants, the degree of colocalization between hTAC-GFP and tagRFP-RAB-5 also increased. In each image autofluorescent lysosome-like organelles appear in blue in all three channels, whereas GFP appears only in the green channel and RFP appears only in the red channel. Signals observed in the green or red channels that do not overlap with signals in the blue channel are considered bone fide GFP or RFP signals respectively. (Scale bar: 10μm) (D) Pearson's correlation coefficient for colocalization of hTAC-GFP and tagRFP-RAB-5. $n = 6$. Error bars represent SEM. $^{***}P < 0.001$(student's t test).

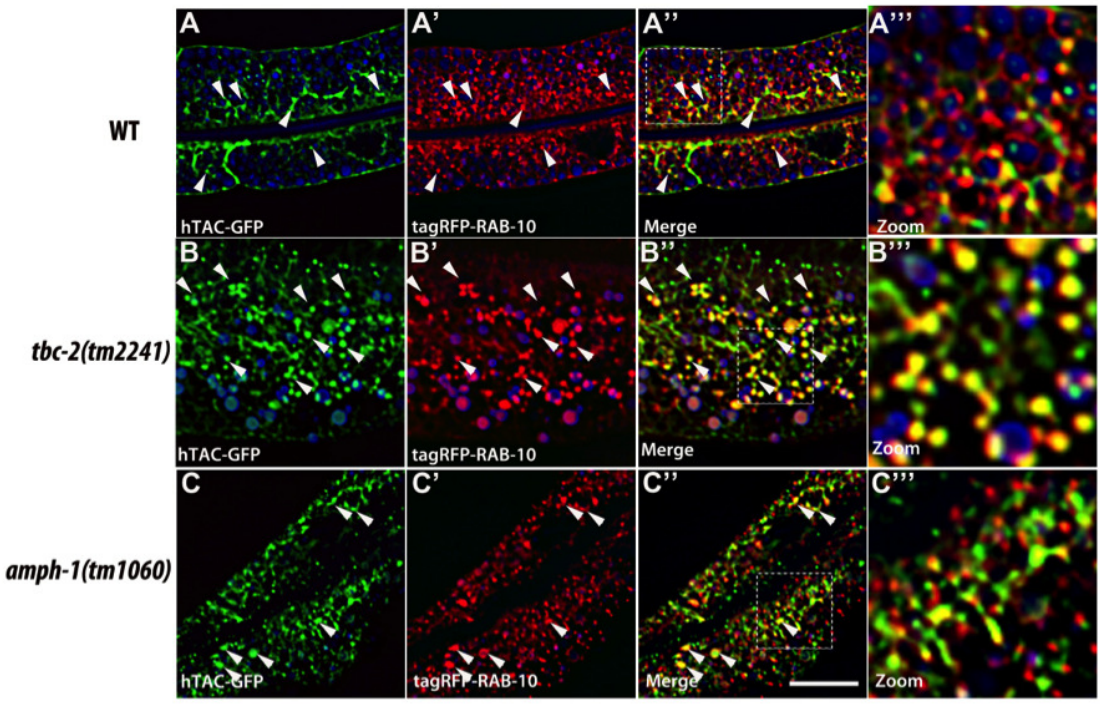
WT
tbc-2(tm2241)
amph-1(tm1060)
A
A'
A''
A'''
B
B'
B''
B'''
C
C'
C''
C'''
hTAC-GFP
tagRFP-RAB-10
Merge
Zoom

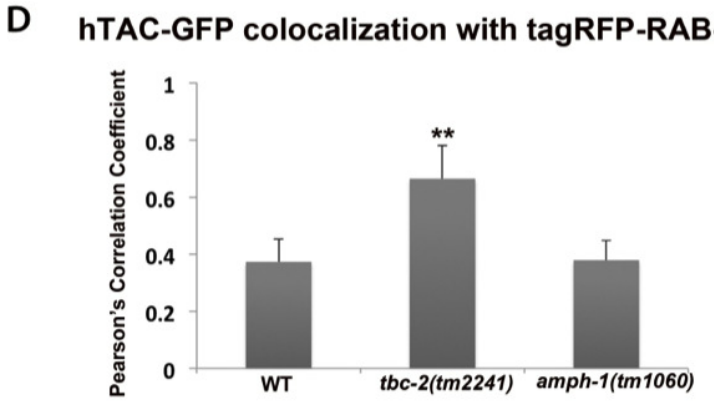
D
hTAC-GFP colocalization with tagRFP-RAB-10
Pearson's Correlation Coefficient
1
0.8
0.6
0.4
0.2
0
**
WT
tbc-2(tm2241)
amph-1(tm1060)

Figure 8: Colocalization of recycling cargo on RAB-10 labeled endosomes

All images are from deconvolved 3D confocal image stacks acquired in intact living animals expressing a GFP-tagged recycling cargo protein, the IL-2 receptor alpha-chain (hTAC-GFP) and tagRFP-RAB-10 in wild-type animals (A-A‴), *tbc-2 (tm2241)* (B-B‴) and *amph-1(tm1060)* mutants (C-C‴). (A-A‴) In wild-type animals, hTAC-GFP and tagRFP-RAB-10 colocalizes partially. (B-B‴) In *tbc-2* mutants, the degree of colocalization between hTAC- GFP and tagRFP-RAB-10 increased and they mainly overlap on punctate endosomal structures. (C-C‴) In *amph-1* mutants, no obvious change in the degree of overlap between hTAC-GFP and tagRFP-RAB-10 was detected in comparison to that in wild-type animals. In each image autofluorescent lysosome-like organelles appears in blue in all three channels, whereas GFP appears only in the green channel and RFP shows up only in the red channel. Signals observed in the green or red channels that do not overlap with signals in the blue channel are considered bone fide GFP or RFP signals respectively. (Scale bar: 10μm) (D) Pearson's correlation coefficient for colocalization of hTAC-GFP and tagRFP-RAB-10. $n = 6$. Error bars represent SEM. $^{**}P < 0.01$(student's t test).

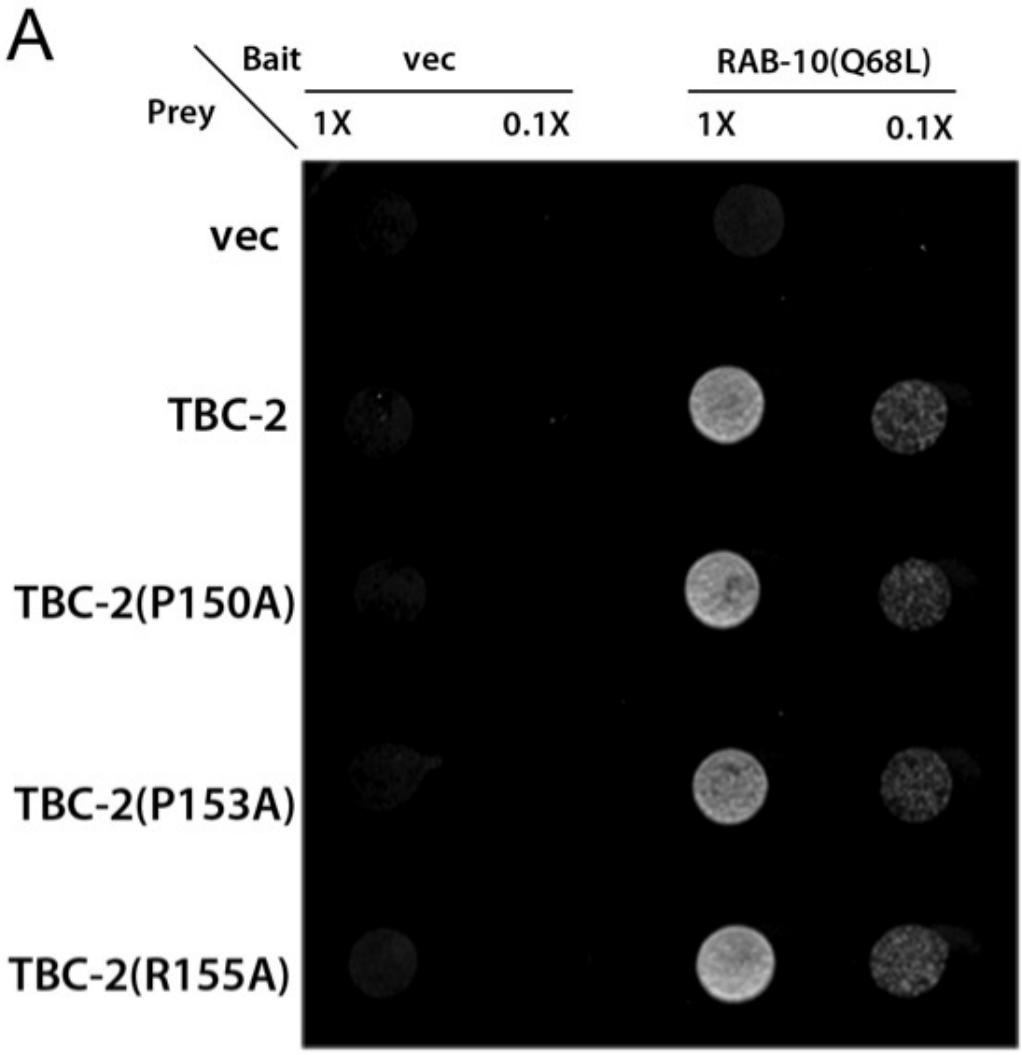
A
Bait
Prey
vec
RAB-10(Q68L)
1X
0.1X
1X
0.1X
vec
TBC-2
TBC-2(P150A)
TBC-2(P153A)
TBC-2(R155A)

Figure S1.: Mutated forms of TBC-2 (P150A, P153A, or R155A) which are incapable of binding to AMPH-1, can still interact with RAB-10 (Q68L).

(A) RAB-10(Q68L) was expressed in a yeast reporter strain as a fusion to the DNA-binding domain of LexA (bait). Mutated forms of TBC-2 (P150A, P153A or R155A) were expressed in the same yeast cells as fusions to the B42 transcriptional activation domain (prey). Interaction between bait and prey was assayed by complementation of leucine auxotrophy (LEU2 growth assay). Colonies were diluted in liquid and spotted on solid growth medium directly (1X) or after further dilution (0.1X).

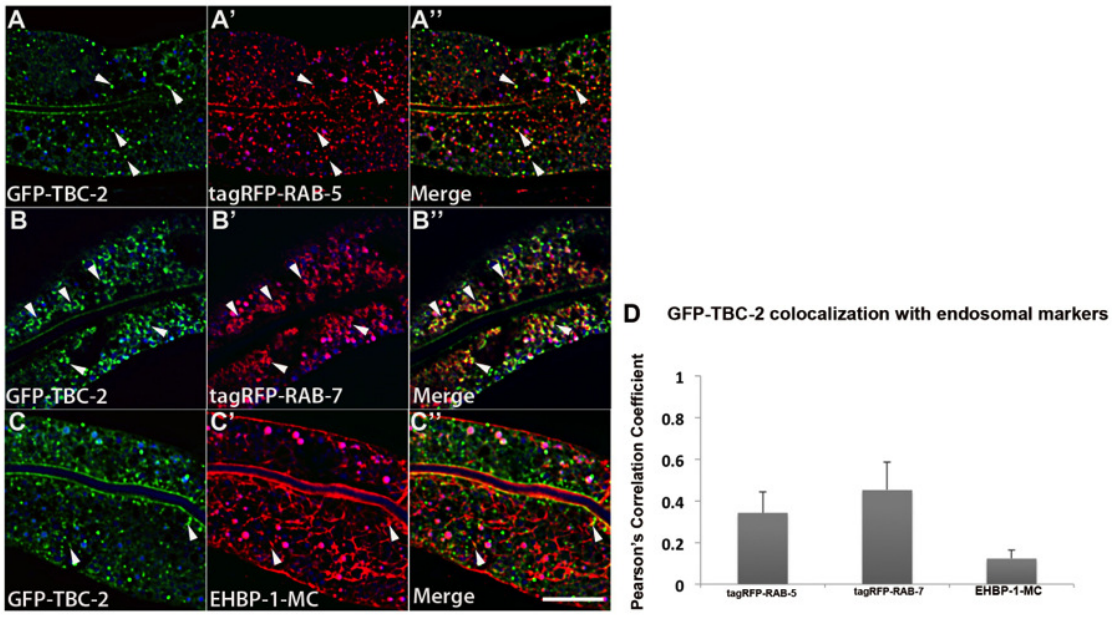
A
A'
A''
GFP-TBC-2
tagRFP-RAB-5
Merge
B
B'
B''
GFP-TBC-2
tagRFP-RAB-7
Merge
C
C'
C''
GFP-TBC-2
EHBP-1-MC
Merge
D
GFP-TBC-2 colocalization with endosomal markers
Pearson's Correlation Coefficient
1
0.8
0.6
0.4
0.2
0
tagRFP-RAB-5
tagRFP-RAB-7
EHBP-1-MC

Figure S1.: TBC-2 colocalizes partially with RAB-5 and RAB-7, and does not colocalize with EHBP-1

All images are from deconvolved 3D confocal image stacks acquired in intact living animals expressing GFP- and RFP-tagged proteins specifically in intestinal epithelial cells. (A-A″) GFP-TBC-2 colocalizes partially with tagRFP-RAB-5 on punctate endosomal structures. (B- B″) GFP-TBC-2 colocalizes partially with tagRFP-RAB-7. (C-C″) GFP-TBC-2 displays little colocalization with EHBP-1-MC. In each image autofluorescent lysosome-like organelles appears in blue in all three channels, whereas GFP appears only in the green channel and RFP shows up only in the red channel. Signals observed in the green or red channels that do not overlap with signals in the blue channel are considered bone fide GFP or RFP signals respectively. (Scale bar: 10μm) (D) Pearson's correlation coefficient for colocalization of GFP-TBC-2 with tagRFP-RAB-5, tagRFP-RAB-7, and EHBP-1-MC. $n = 6$. Error bars represent SEM.

Table S1: Transgenic and mutant strains used in this study

pwIs728[Pvha6::CNT-1::mCherry](Shi et al., 2012)

pwIs112[Pvha-6::hTAC::GFP] (Chen et al., 2006a)

pwIs717[Pvha-6::hTfR::GFP] (Sun et al., 2012b)

pwIs883[Pvha-6::EHBP-1::mCherry] (Sun et al., 2012b)

pwIs846[Pvha-6::RFP::RAB-5] (Sun et al., 2012b)

pwIs72[Pvha-6::GFP::RAB-5] (Chen et al., 2006a)

pwIs206[Pvha-6::GFP::RAB-10] (Chen et al., 2006a)

pwIs957[Pvha-6::RFP::RAB-10] (Sun et al., 2012b)

pwIs1195[Pvha-6::GFP::RAB-10(Q68L)]

pwEx142[Psnx-1::RFP::TBC-2]

pwEx143[Psnx-1::RFP::TBC-2(P150A)]

pwEx143[Psnx-1::RFP::TBC-2(288-292 AAAAA)]

vhIs12[Pvha-6::GFP::TBC-2] (Chotard et al., 2010b)

pwIs849[Pvha-6::RFP::RAB-7] (Gleason et al., 2014)

rab-10(ok1494) (Shi et al., 2012)

rab-10(q373) (Chen et al., 2006a)

tbc-2(tm2241)

amph-1(tm1060)

Chapter 4.
RAB-10-mediated regulation of endosomal phosphatidylinositol-4, 5-bisphosphate

AUTHOR CONTRIBUTIONS

This chapter was published as presented here in *Proceedings of the national academy of sciences (PNAS)* (Shi et al., 2012). I performed some *C. elegans* related experiments, biochemical studies and yeast two-hybrid analyses. (Figure 1C, Figure 2B-B″, Figure 4E-G, Figure S1B, Figure S2A-A″, S2E-G, Figure S3H-H″, S3I-I″, Figure S4D-D″, Figure S6, Figure S7B-B″, S7L-N) and contributed to writing of the paper. Dr. Anbing Shi performed some C.elegans related experiments (Figure 2A-A″, 2C-C″, Figure 3, Figure 4A-D, Figure 5, Figure S2B-M, Figure S3A-G″, Figure S4A-C, Figure S5). Sabine Koenig and Dr. Stefan Eimer performed the lipid biochemistry analysis (Figure 4H). Dr. Carlos Chen and Riju Banerjee performed some yeast two hybrid studies (Figure 1A-B, Figure S1A) Dr. Barth D. Grant and Dr. Anbing Shi wrote the paper. Dr. Barth D. Grant trained me to perform experiments.

SUMMARY

C. elegans RAB-10 and mammalian Rab10 are key regulators of endocytic recycling, especially in the basolateral recycling pathways of polarized epithelial cells. To better understand how RAB-10 contributes to recycling endosome function we sought to identify RAB-10 effectors. One novel RAB-10 binding partner that we identified, CNT-1, is the only *C. elegans* homolog of mammalian ACAP1 and ACAP2, Arf6 GTPase-activating proteins. Arf6 is known to regulate endosome to plasma membrane transport, in part through activation of type I phophatidylinositol-4-phosphate 5 kinase (PIP5KI). Here we show that CNT-1 binds to RAB-10 through its C-terminal ANK repeats and colocalizes with RAB-10 and ARF-6 on recycling endosomes *in vivo*. Furthermore, we find that RAB-10 is required for the recruitment of CNT-1 to endosomal membranes in the intestinal epithelium. Consistent with negative regulation of ARF-6 by RAB-10 and CNT-1, we found overaccumulation of endosomal phosphatidylinositol-4,5-bisphosphate (PI(4,5)P2) in *cnt-1* and *rab-10* mutants, and reduced endosomal PI(4,5)P2 levels in *arf-6* mutants. These mutants produced similar effects on endosomal recruitment of PI(4,5)P2-dependent membrane bending proteins RME-1/Ehd and SDPN-1/Syndapin/Pacsin and resulted in endosomal trapping of specific recycling cargo. Our studies identify a novel RAB-10 to ARF-6 regulatory loop required to regulate endosomal PI(4,5)P2, a key phosphoinositide in membrane traffic.

INTRODUCTION

Endocytic recycling is essential for counterbalancing endocytosis and is important for a host of higher order processes such as cytokinesis, cell migration, maintenance of polarized cell membrane domains and synaptic plasticity (Grant and Donaldson, 2009). Small GTPases of the Rab and Arf families have long been known to be key regulators of membrane traffic, and certain members of these families function specifically in endocytic recycling (Chen et al., 2006a; Donaldson, 2005; Donaldson and Honda, 2005; Linder et al., 2007; Patino-Lopez et al., 2008; Sato et al., 2008). Previous studies

in our lab indicated that RAB-10 is required for the basolateral recycling of clathrin-independent cargo such as hTAC-GFP in the *C. elegans* intestine (Chen et al., 2006a; Shi et al., 2010b). In the *C. elegans* nervous system, RAB-10 is also required for the recycling of AMPA-type glutamate receptors in postsynaptic membranes (Glodowski et al., 2007a). Accumulating evidence suggests that RAB-10 functions upstream of RME-1/Ehd, a peripheral membrane protein involved in recycling endosome tubulation and probably endosome fission (Chen et al., 2006a; Pant et al., 2009; Shi et al., 2010b). In polarized MDCK cells Rab10 also functions in basolateral recycling (Babbey et al., 2006a). Additionally, in mammalian adipocytes Rab10 was reported to regulate the insulin-dependent recycling of Glut4 glucose transporters (Sano et al., 2007b). C. elegans intestinal RAB-10-labeled endosomes are often positive for RAB-5, RAB-8, and RAB-11 (Chen et al., 2006a). Such endosomes are likely to be counterparts of the Rab10-positive common recycling endosome (CRE) in MDCK cells. CREs are thought to receive, sort, and recycle cargo received from both the apical and basolateral plasma membrane domains (Babbey et al., 2006a).

Of the Arfs, Arf6 is most closely associated with endocytic recycling regulation. The requirement for Arf6 in endosomal recycling was first documented in CHO cells, in which the expression of the dominant negative Arf6(T27N) blocked the recycling of both clathrin-dependent and independent cargos (D'Souza-Schorey et al., 1998). In HeLa cells expression of GTP hydrolysis defective Arf6(Q67L) caused PI(4,5)P2 and actin accumulation on endosomes, sequestering clathrin independent cargo proteins, but not clathrin dependent cargo TfR in the abnormal endosomes (Brown et al., 2001). While reports vary, siRNA-mediated knockdown of Arf6, or expression of dominant negative Arf6(T27N) in HeLa cells, generally affects the recycling of integral plasma membrane proteins that lack cytoplasmic clathrin adaptor sorting sequences, such as TAC, the major histocompatibility complex class I protein (MHCI), GPI anchored proteins, and certain cell adhesion molecules (Eyster et al., 2009; Naslavsky et al., 2003; Radhakrishna and Donaldson, 1997). Recycling of these cargos occurs through Arf6-positive tubules that emanate from the juxtanuclear endocytic recycling compartment (Naslavsky et al., 2003). These tubules may represent a separate recycling route from

that taken by other recycling cargo such as TfR (Naslavsky et al., 2003).

Phosphatidylinositide (PI) lipid composition defines the functional identities of distinct membrane-bound compartments. Distinct lipids are phosphorylated at different positions around the inositol rings and therefore confers different functions. Peripheral membrane proteins involved in membrane trafficking often has their preferences for a specific species of phosphoinositides. Through protein-protein and protein-lipid interactions, multiple players promoting certain step of membrane trafficking are recruited to their target sites. For each type of membrane organelle, there is usually one characteristic species of lipid that are enriched on the endosomal membrane. For example, PI(4,5)P2 are enriched on the plasma membrane and recycling endosomes, PI(4)P on Golgi, PI(3)P on early endosomes and PI(3,5)P2 on late endosomes/lysosomes. Transition from one membrane organelle to another requires proper switch of phosphorylation status of the inositol groups to provide a binding platform for the proteins that work in a certain trafficking pathway. (Di Paolo and De Camilli, 2006)

Arf6 regulates endocytic recycling, at least in part, through activation of enzymes that modify membrane lipids (D'Souza-Schorey and Chavrier, 2006). In tissue culture cells, Arf6 localizes with and activates PIP5KI (Honda et al., 1999). PIP5KI is responsible for phosphorylating PI(4)P to generate PI(4,5)P2, a major plasma membrane and recycling endosome phosphoinositide that is required to recruit and activate many peripheral membrane proteins that mediate membrane traffic and actin polymerization (Honda et al., 1999; Yin and Janmey, 2003).

In our effort to identify interacting partners of RAB-10, we recovered CNT-1, the C. elegans homolog of mammalian ACAP1/2 (Arf GAP, with Coil, ANK repeat, PH domain). ACAP1/2 (Centaurin beta 1/2) belongs to the AZAP-type of Arf GTPase-activating proteins (GAPs) (Inoue and Randazzo, 2007). Biochemical studies have suggested that ACAP1 and ACAP2 preferentially activate the GTPase activity of Arf6 over other Arfs and that the ACAPs are activated by PI(4,5)P2 binding (Jackson et al., 2000). Furthermore, PIP5KI, which is positively regulated by Arf6(GTP), seems to function with ACAP1 to enhance endosomal tubulation (Shinozaki-Narikawa et al., 2006). Here we demonstrate that CNT-1 functions as a RAB-10 effector to regulate ARF-6-dependent

endocytic recycling. Interestingly, both loss of CNT-1 or overexpression of CNT-1 results in endosomal accumulation of model ARF-6-dependent cargo protein hTAC-GFP. Our data provides evidence of a novel RAB to ARF regulatory loop influencing endosomal PI(4,5)P2 levels and the recruitment of endosomal membrane bending proteins.

RESULTS

The C-terminal ANK repeat sequence of CNT-1 is a Rab interacting domain

To better understand how RAB-10 controls endocytic recycling we sought to identify RAB-10 effectors via a yeast two-hybrid screen using a predicted constitutively active (GTPase-defective) form of RAB-10, Q68L, as bait (Shi et al., 2010b). Out of 70 clones that tested positive for interaction with RAB-10(Q68L) in Leu2 and β-galactosidase expression assays, two clones were identified that encoded full length CNT-1 (see Material and Methods). No interaction was detected between CNT-1 and a predicted GDP-bound mutant form RAB-10, T23N, or wild-type RAB-10 (Fig. 1A and Fig. S1A), suggesting that CNT-1 preferentially interacts with the active form of RAB-10.

CNT-1 was a particularly interesting candidate interactor for RAB-10, because it is the only *C. elegans* homolog of mammalian ACAP1 and ACAP2, GAPs for the class III Arf-GTPase Arf6. Binding of RAB-10 to CNT-1 suggested a link between the activities of RAB-10 and ARF-6 during endocytic recycling. Like Arf6, mammalian ACAP1 is required for the recycling of endocytic cargo proteins, and is enriched on recycling endosome tubules that contain Arf6, PIP5KI, and PI(4,5)P2 (Jackson et al., 2000; Shinozaki-Narikawa et al., 2006). Like ACAP1 and ACAP2, CNT-1 contains tandem predicted lipid binding domains (N-terminal BAR domain followed by a Pleckstrin Homology (PH) domain), in addition to a central ARF-GAP domain and C-terminal Ankyrin (ANK) repeat domain (Shinozaki-Narikawa et al., 2006).

To determine the region of CNT-1 that interacts with RAB-10 we tested various truncations of CNT-1 in the 2-hybrid assay with RAB-10(Q68L). These experiments delimited

the RAB-10 binding site within CNT-1, showing that the C-terminal ANK repeat containing segment (aa 656-826) is necessary and sufficient to mediate the interaction with RAB-10 (Fig. 1B-D). To determine the specificity of the CNT-1 interaction with RAB-10, we assayed other endocytic Rab-GTPases. While RAB-5(Q78L), RAB-7(Q68L), and RAB-11(Q70L) failed to interact with CNT-1, RAB-8(Q67L) and RAB-35(Q69L) displayed a robust interaction with CNT-1 in this assay, interacting with the same ANK repeat containing segment (aa 656-826) that interacts with RAB-10 (Fig. 1A; Fig. S1B-C). RAB-8 is the closest paralog of RAB-10 in *C. elegans* and is redundant with RAB-10 in some non-polarized cells types (Shi et al., 2010b). Like RAB-10 and RAB-8, RAB-35 is an important recycling regulator in C. elegans and mammals (Kouranti et al., 2006; Sato et al., 2008). We also tested these binding interactions using a GST-pulldown approach, using GST-only as a negative control, and a RAB-10 effector that we previously identified, EHBP-1, as a positive control (Fig. 1C). This experiment confirmed the interaction of CNT-1(ANK) with the active forms of RAB-10, RAB-8, and RAB-35, while EHBP-1 only interacted with RAB-10 and RAB-8 (Fig. 1C). Interestingly, binding of the CNT-1 ANK domain to RAB-5(Q78L) was also detected in our pulldown assay, but was not detected in the 2-hybrid assay (Fig 1C). Taken together, these results indicate that the C-terminal ANK repeats of CNT-1 provides a binding surface with the potential to interact with a subgroup of Rabs associated with endocytic recycling.

CNT-1 is enriched on endosomes

To determine if CNT-1 is associated with the same organelles as these recycling Rabs *in vivo*, we assayed the subcellular localization of functional mCherry(MC)-tagged CNT-1 fusion proteins expressed specifically in the intestinal epithelial cells (Fig. S2H-J), a tissue with well-established markers for endo-membrane compartments (Chen et al., 2006a; Shi et al., 2010b; Shi et al., 2007). CNT-1 localized strongly to intracellular puncta that were similar in size and shape to endosomes (Fig. 3A). CNT-1 also displayed enrichment on or near the basolateral and apical plasma membranes (Fig. 2A′). Consistent with our binding data, we observed extensive colocalization of CNT-1-MC

with endosomes labeled by GFP-RAB-10, GFP-RAB-8 and GFP-RAB-35 (Fig. 2A-B″, Fig. S2A-A″). In these cells RAB-10 is required for basolateral recycling, while RAB-8 has been implicated in apical transport (Chen et al., 2006a; Sato et al., 2007). RAB-10 and RAB-8 extensively colocalize on endosomes in this tissue, suggesting that this organelle sorts basolateral and apical cargos (Chen et al., 2006a; Shi et al., 2010b). This is consistent with the localization of mammalian Rab10 to the common recycling endosome (CRE) in polarized MDCK cells, an organelle that receives and sorts basolateral and apical cargos (Babbey et al., 2006a; Brown et al., 2000). RAB-35 had not been previously studied in the intestine, but we previously showed that RAB-35 is ubiquitously expressed and is required for receptor recycling in the *C. elegans* oocyte cells (Sato et al., 2008). These results are consistent with CNT-1 acting as an effector for Rab-GTPases during endocytic recycling.

Like RAB-10, CNT-1-MC showed partial colocalization with early endosome marker GFP-RAB-5, and showed little overlap with the late acting recycling endosome protein GFP-RME-1 (Fig. 2C-C‴ and Fig. S2B-B″). Likewise, little overlap was observed between CNT-1-MC and GFP-ALX-1 (Fig. S2C-C″), which labels both RME-1 positive basolateral recycling endosomes and ESCRT-enriched multivesicular endosomes (MVEs) (Shi et al., 2007). The Golgi ministack marker MANS-GFP was generally found closely juxtaposed to CNT-1-MC-labeled endosomes but with little direct overlap (Fig. S2D-D″), again similar to the localization we previously described for RAB-10 (Chen et al., 2006a; Shi et al., 2010b). Collectively, our results demonstrate that CNT-1 is enriched on recycling endosomes where it could potentially interact with RAB-10, RAB-8 and/or RAB-35 to regulate endosome-to-plasma membrane transport of cargo derived from the PM and/or the Golgi.

RAB-10 is required for CNT-1 endosomal recruitment

In many cases proteins that bind to GTP-bound Rabs are effector proteins, and such effectors are often localized and/or activated by interaction with their cognate Rab(s) (Stenmark, 2009). To determine whether CNT-1 displays such a relationship with any of the Rabs with which it can bind, we assayed for changes in the localization of

CNT-1-GFP in the relevant *rab* mutant backgrounds. We found a dramatic redistribution of CNT-1-GFP in *rab-10(q373)* mutants. CNT-1-GFP appeared very diffusive in *rab-10* mutants, displaying an almost complete loss of CNT-1-GFP endosomal localization (Fig. 3A, C, E). Loss of RAB-8 had a minor effect on CNT-1-GFP localization,displaying an average reduction in puncta intensity of about 20% in *rab-8(tm2526)* mutants (Fig. 3D, E). CNT-1-GFP localization and puncta intensity was unaffected in *rab-35(b1013)* mutants (Fig. S2E-G). The intensity of CNT-1-GFP-labeling of endosomes was mildly increased in *rme-1(b1045)* mutants that are defective in a later step in the basolateral recycling pathway (Fig. 3B, E). These results indicate that, at least in this tissue, RAB-10 is the dominant Rab GTPase recruiting CNT-1 to endosomes.

CNT-1 and RAB-10 colocalize with ARF-6 in the basolateral recycling pathway

As a first test of a functional connection of CNT-1 and RAB-10 with ARF-6 we assayed for colocalization of each protein with ARF-6 in the *C. elegans* intestine. We found that a functional ARF-6-GFP fusion proteins labels punctate and tubular membrane structures in the intestinal cells, and overlaps extensively with CNT-1-MC on endosomes (Fig. S3G-G″). Consistent with the potential connection of ARF-6 and RAB-10, we found that ARF-6-GFP also colocalized well with MC-RAB-10 on recycling endosomes (Fig. S3H-H″). To a lesser extent ARF-6-GFP also labeled the RME-1 positive recycling endosomes close to the basolateral plasma membrane, further indicating that ARF-6 is present on endosomes associated with basolateral recycling (Fig. S3I-I″).
Neither RAB-10 nor RME-1 function was required for ARF-6 endosomal recruitment. ARF-6-GFP remained localized to endosomal puncta and tubules in *rab-10* and *rme-1* mutants, and also labeled the limiting membrane of the grossly enlarged early and recycling endosomes that accumulate in *rab-10* and *rme-1* mutants, respectively (Fig. S3B, C, E). Notably, we observed an over-accumulation of ARF-6-GFP positive basolateral tubules and punctae in *cnt-1(tm2313)* mutants, suggesting in vivo relevance for CNT-1 in ARF-6 function (Fig. S3D, E). GFP-RAB-10 intensity also increased in *cnt-1 mutants* (Fig. S5B). We did not find any effect of cnt-1 mutants on late endosomal

markers GFP-RAB-7 and LMP-1-GFP, or the MVE/MVB marker HGRS-1/Hrs (Fig. S5E, H, K). The *cnt-1(tm2313)* mutant used in this analysis is a 344 base deletion and single base insertion in the ninth exon of *cnt-1*. This *cnt-1* mutation is predicted introduce a frame-shift and stop codon soon after the deletion, removing the majority of the predicted CNT-1 GAP domain, and all of the predicted ANK repeats (Δ472-826). We also tested the importance of ARF-6 in the localization of CNT-1 and RAB-10. The *arf-6* mutant *tm1447* used in these studies deletes nearly the entire *arf-6* gene, and does not produce any ARF-6 protein as judged by anti-ARF-6 Western blot (Fig. S3F). Neither CNT-1 nor RAB-10 required ARF-6 for endosomal localization. Rather we noted that both CNT-1-GFP and GFP-RAB-10 labeling of endosomes increased in intensity in *arf-6(tm1447)* mutants (Fig. S4B, C and Fig. S5C, M). Further analysis showed that CNT-1-RFP and GFP-RAB-10 remain colocalized in arf-6 mutants (Fig. S4D-D$''$). These results may reflect a block in the recycling pathway downstream of RAB-10 in *arf-6* (and *cnt-1*) mutants. We did not find any effect of *arf-6* mutants on late endosomal markers GFP-RAB-7 and LMP-1-GFP, or the MVE/MVB marker HGRS-1/Hrs (Fig. S5F, I, L). In summary, these studies establish that CNT-1, RAB-10, and ARF-6 overlap in localization on endosomes of the basolateral recycling pathway, and that loss of any of the three proteins affects the morphology of endosomes labeled by the others.

Loss of CNT-1 affects ARF-6-dependent cargo

To further test the functional relationship of CNT-1 and ARF-6 we assayed deletion alleles of *cnt-1* and *arf-6* for effects on well-defined recycling cargo proteins hTAC-GFP and hTfR-GFP (Chen et al., 2006a; Shi et al., 2007). In HeLa cells Arf6 preferentially affects recycling of CIE cargo such as TAC, while having very little effect on clathrin dependent endocytosis (CDE) cargo TfR (Naslavsky et al., 2003; Radhakrishna and Donaldson, 1997). In our previous work we showed that loss of RAB-10 preferentially traps hTAC-GFP in the endosomal system, but has very little effect on hTfR-GFP (Chen et al., 2006a; Shi et al., 2010b). Consistent with its cargo-specificity in mammals, we observed a dramatic intracellular accumulation of hTAC-GFP in the intestinal cells

of *arf-6(tm1447)* deletion mutants (Fig. 3H, O), but no such effect was found for hTfR-GFP (Fig. 3M, P). Most of the over-accumulated hTAC-GFP in *arf-6* mutants colocalized with recycling endosome marker EHBP-1-RFP (Fig S6A-A″) (Shi et al., 2010b). We observed a similar intracellular accumulation of hTAC-GFP in intestinal cells over-expressing CNT-1, a perturbation that would be expected to inactivate ARF-6 and mimic the *arf-6* loss-of-function phenotype (Fig. 3I, O).

A full Arf6 GTPase cycle is thought to be important for the efficient recycling of CIE cargo (D'Souza-Schorey and Chavrier, 2006; Radhakrishna and Donaldson, 1997). In HeLa cells MHCI and TAC recycling is also impaired upon expression of GTP-hydrolysis defective mutant ARF6(Q67L) (Naslavsky et al., 2003). Likewise, we found that expression of *C. elegans* ARF-6(Q67L) caused apparent trapping of hTAC-GFP in endosomes (Fig. 3J, O). As an ARF-6 GAP, loss of CNT-1 would be expected to result in elevated levels of ARF-6(GTP) and impaired recycling of hTAC. Indeed we observed endosomal accumulation of hTAC-GFP in *cnt-1(tm2313)* deletion mutants, and the accumulated hTAC-GFP colocalized with recycling endosome marker EHBP-1-RFP (Fig. 3G, O and Fig. S6B-B″) (Shi et al., 2010b). Our results provide *in vivo* evidence of the importance of the ARF-6 GTPase cycle in the regulation of CIE cargo recycling in *C. elegans*, and indicate a clear requirement for CNT-1 in this process.

Loss of RAB-10 leads to increased accumulation of PI(4,5)P2

Since PIP5KI is an important Arf6 effector, and CNT-1 is expected to inactivate ARF-6, loss of CNT-1 or RAB-10 would be expected to increase PI(4,5)P2 levels, while loss of ARF-6 is expected to reduce PI(4,5)P2 levels (D'Souza-Schorey and Chavrier, 2006; Honda et al., 1999; Yin and Janmey, 2003). Thus, we sought to test these predictions by assaying the subcellular distribution of PI(4,5)P2 in the *C. elegans* intestinal cells, using the PI(4,5)P2 biosensor PH(PLCδ)-GFP, which contains the PI(4,5)P2-specific binding pleckstrin homology (PH) domain of the rat phospholipase Cδ (Garcia et al., 1995). As controls, we also assayed the subcellular localization of PI(3)P and PI(3,4,5)P3 using biosensors GFP-2xFYVE(HRS) and PH(Akt)-GFP. In wild-type animals we noted that PH(PLCδ)-GFP labels the apical and basolateral plasma membrane as well as internal

puncta and tubules (Fig. 4A and Fig. S7J-J′). The PH(PLCδ)-GFP-labeled intracellular puncta and tubules colocalize extensively with functional ARF-6-MC, identifying them as endosomes along the basolateral recycling pathway (Fig. S2M, S7A-A″). Additionally, extensive overlap can be observed on the apical and lateral plasma membrane (Fig. S7B-B″). The PI(3)P marker GFP-2xFYVE(HRS) localized relatively diffusely in the intestinal cells, with only rare visible puncta (Fig. S7C). The PI(3,4,5)P3 marker PH(Akt)-GFP labeled rare cytoplasmic puncta and the apical and basolateral plasma membranes, although neither plasma membrane was as strongly labeled by the PI(3,4,5)P3 marker as by the PI(4,5)P2 marker (Fig. S7F).

In *arf-6* null mutant animals we observed a significant decrease in PH(PLCδ)-GFP labeling of endosomal puncta and tubules (Fig. 4C, D). These findings indicate that ARF-6 is important for regulation of endosomal PI(4,5)P2 levels. Conversely, we found that in *cnt-1* and *rab-10* mutants PH(PLCδ)-GFP labeling on the basolateral endosomal puncta and tubules was increased, as would be expected if ARF-6 activity is increased in these mutant backgrounds (Fig. 4B, D and F, G). However, the apparent increase of PI(4,5)P2 labeling in *rab-10* mutants was greater than that in *cnt-1* mutants, suggesting that only part of the effect of RAB-10 on PI(4,5)P2 could be accounted for by failure in recruiting CNT-1 to membranes. We also detected an increase in PH(PLCδ)-GFP labeling in the intestine of *rab-8* mutant animals (Fig S7L-N), consistent with the mildly reduced endosomal recruitment of CNT-1 observed in *rab-8* mutants (Fig 3D, E). In this case however, the increased PI(4,5)P2 biosensor labeling was near the apical membranes, consistent with a proposed role for RAB-8 in apical transport (Sato et al., 2007). As shown in Fig. S7, the levels of PI(3)P (labeled by GFP- 2xFYVE) and PI(3,4,5)P3 (labeled by PH(Akt)-GFP) appeared unperturbed in *cnt-1* and *arf-6* mutants (Fig S7C-I), indicating the specificity of the effects. Interestingly, PH(PLCδ)-GFP labeling intensity in *rme-1* mutants was not detectably altered, although some of the endosomes labeled by PH(PLCδ)-GFP were grossly enlarged in *rme-1* mutants (Fig. S7J-K′).

We also sought to confirm the results derived from imaging methods using biochemical methods. Thus we measured PI(4,5)P2 levels in whole animal lipid extracts, comparing

rab-10, *cnt-1*, and *arf-6* mutants with wild-type controls, using thin-layer chromatography followed by gas chromatography (Konig et al., 2008). To account for differences in lipid extraction efficiency between samples, we normalized the measured PI(4,5)P2 levels in the samples relative to the more abundant phospholipids phosphatidylcholine and phosphatidylinositol.

In agreement with the imaging data, our bulk lipid analysis detected elevated PI(4,5)P2 levels in *rab-10* mutants, and reduced PI(4,5)P2 levels in *arf-6* mutants (Fig 4H). Furthermore, we found that loss of ARF-6 reduced the elevated PI(4,5)P2 levels found in *rab-10* mutants by about 40%, further indicating that ARF-6 contributes to the effects of RAB-10 on PI(4,5)P2 (Fig 4H). However, the bulk lipid analysis did not detect a clear difference in PI(4,5)P2 levels between wild-type animals and *cnt-1* mutants (Fig. 4H). This may reflect a difference in the sensitivity of the two methods, or may reflect the inability of the bulk lipid analysis approach to detect differences in specific phospholipid pools that can be detected using the imaging approach. For instance CNT-1 may affect only certain organelles (i.e. endosome versus plasma membrane pools) and/or tissues.

Endosomal recruitment of membrane bending proteins is aberrant in *cnt-1* and *arf-6* mutants

Changes in endosomal PI(4,5)P2 levels in *cnt-1* and *arf-6* mutants would be expected to affect the endosomal recruitment of endosomal PI(4,5)P2-binding proteins such as RME-1 and SDPN-1 (*C. elegans* ortholog of Syndapin/Pacsin), endosomal proteins that are required for basolateral recycling in the intestine through their membrane bending activities (Pant et al., 2009; Shi et al., 2007). Consistent with this prediction, GFP-RME-1 and GFP-SDPN-1 endosomal labeling increased in *cnt-1* mutants, and decreased in *arf-6* mutants (Fig. 5). Altered recruitment of these proteins and others like them, that participate in the recycling process could explain the defects in recycling that we observed in *cnt-1* and *arf-6* mutants.

Clathrin and CNT-1 co-accumulate on the enlarged endosomes of *arf-6* mutants

ACAP1 has been reported to be part of a clathrin complex that functions on endosomes to promote the recycling of the insulin responsive glucose transporter Glut4, and the adhesion molecule β-integrin (Li et al., 2007). This work also indicated that endosomal clathrin accumulates when ACAP1 is over-expressed, but no previous studies have tested if this effect on endosomal clathrin requires Arf6 (Li et al., 2007). We found that CNT-1-GFP over- accumulates on endosomes in *arf-6* mutants (Fig. S4B). We further found that functional GFP-tagged clathrin heavy chain (GFP-CHC-1) showed a similar strong intracellular accumulation in *arf-6* mutants (Fig. S8B). Importantly we noted that CNT-1-MC colocalizes with GFP-CHC-1 in wild-type animals (Fig. S8C-C″), and that CNT-1-MC and GFP-CHC-1 co-accumulate on the enlarged endosomes of *arf-6* null mutant animals (Fig. S8D-D″). While we do not yet understand the precise role of this pool of endosomal clathrin, our results do suggest that the endosomal clathrin could interact with CNT-1 and/or ARF-6 during endocytic sorting and recycling, although our data do not fit with a simple model in which ARF-6 acts to assemble endosomal clathrin.

DISCUSSION

In this study, we further investigated the role of the RAB-10 GTPase in endocytic recycling, identifying an important link to endosomal PI(4,5)P2 regulation, in part through a newly identified interaction of RAB-10 with the ACAP homolog CNT-1. We defined the RAB-10 binding region within CNT-1 as the C-terminal ANK repeat domain, and provided evidence that RAB-10 is required for the endosomal recruitment of CNT-1. Our results suggest that RAB-10 is the dominant Rab recruiting CNT-1 to endosomes in the intestinal epithelium. Thus CNT-1 is likely to provide a functional connection between members of different GTPase classes (RAB-10 and ARF-6) that are vital for endocytic recycling regulation. We went on to show mis-regulation of endosomal

PI(4,5)P2 levels in *rab-10*, *cnt-1*, and *arf-6* mutants, and showed that part of the effect of RAB-10 on PI(4,5)P2 depends upon ARF-6. Indeed, certain PI(4,5)P2-binding proteins of the recycling endosome that are implicated in membrane bending and membrane fission are aberrantly recruited upon perturbation of any of these components. However, the effects of RAB-10 on endosomal PI(4,5)P2 were stronger than those of CNT-1, and not all of the increased levels of PI(4,5)P2 detected in *rab-10* mutants could be suppressed by loss of ARF-6, indicating that RAB-10 also affects endosomal PI(4,5)P2 via additional mechanisms that remain to be identified. One possibility is that RAB-10 interacts with additional ARF regulators such as CNT-2. Alternatively RAB-10 may interact with additional effectors that control PI(4,5)P2 levels by a completely different mechanism.

RAB-10 appears to function at the interface of early endosomes and recycling endosomes, as reflected by its partial colocalization with early and recycling endosome markers, and the defects in morphology observed in both endosome types in *rab-10* mutants (Chen et al., 2006a; Shi et al., 2010b). Given the importance of phosphoinositide species in determining distinct organelle identities, the control of endosomal PI(4,5)P2 by RAB-10 likely contributes to the biogenesis and/or maintenance of the basolateral recycling endosome compartment (Di Paolo and De Camilli, 2006; Grant and Donaldson, 2009). It remains unclear if such recycling endosomes form by the remodeling of early endosome fission products, which might be viewed as a maturation process. RAB-10 could act to promote early endosome to recycling endosome maturation, or RAB-10 could act to define the identity of a particular subdomain within a complex, longer-lived, recycling organelle.

Studies in mammals suggest that a complete Arf6 GTPase cycle (activation of Arf6 via GDP- to-GTP exchange, and Arf6 inactivation through GTP-to-GDP hydrolysis) is necessary for functional transport, since expression of GDP or GTP locked forms of Arf6 impairs cargo recycling, albeit at different steps in the transport process (Brown et al., 2001; D'Souza- Schorey et al., 1998). Our results, showing intracellular accumulation of hTAC-GFP in an *arf-6* null mutant, or under conditions predicted to cause over-accumulation of ARF-6(GTP), agree with this model. Loss of CNT-1 is

expected to reduce GTP hydrolysis by ARF-6, leading to an increased level of active ARF-6-GTP, interfering with receptor recycling, as was observed upon expression of GTPase defective Arf6. Over-accumulation of PI(4,5)P2 in *rab-10* and *cnt-1* mutants, and partial suppression of this defect in combination with *arf-6* mutants is consistent with accumulation of abnormally high levels of ARF-6-GTP.

RAB-10 effector CNT-1 may also contribute additional functions to the recycling process. CNT-1 harbors an N-terminal BAR domain. Proteins with BAR domains such as amphiphysin, endophilins, and sorting nexins have been reported to sense membrane curvature and to induce positive curvature, features that are important in membrane budding and tubulation (Casal et al., 2006). Recruited to the membrane by RAB-10, CNT-1 could be further localized to high-curvature regions of budding vesicles or tubules through its BAR domain, or could help to remodel functional subdomains or buds on endosomes, facilitating sequestration of recycling cargo.

Recent studies suggest that Rab to Arf signaling is an evolutionarily conserved process. Kanno et al, recently identified binding of another recycling associated Rab GTPase, Rab35, to ACAP2 in mammalian cells (Kanno et al., 2010). The Kanno et al. study also identified the ACAP2 ANK repeats as the Rab-binding domain for Rab35-mediated recruitment of ACAP2 to the plasma membrane (Kanno et al., 2010). In mammalian macrophages it was demonstrated that Rab35, together with ACAP2, regulates phagocytosis (Egami et al., 2011). In addition, in PC12 cells, ACAP2 can be recruited by Rab35 to Arf6 positive endosomes, and ACAP2's Arf6-GAP activity is required for NGF-induced neurite outgrowth (Kobayashi and Fukuda, 2012). None of these recent Rab35 studies directly assayed for effects on endosomal PI(4,5)P2 levels, effects on the recruitment of PI(4,5)P2-binding membrane bending/fission proteins, or the requirement for Arf6 in these changes, but could very well proceed via such mechanisms. Indeed, our studies also demonstrated that CNT-1 has the potential to interact with RAB-35 in *C. elegans*. Although the RAB-35 interaction with CNT-1 did not appear physiologically important in the intestinal epithelium, both proteins are widely expressed and thus may interact functionally in another tissue or at another developmental time. Rab35 has been proposed to regulate PI(4,5)P2 at the intercellular bridge

of cells during mitosis, but that regulation was proposed to be through interaction of Rab35 and the OCRL lipid phosphatase (Dambournet et al., 2011). It will be interesting to determine if a Rab35/ACAP/Arf6 cascade also contributes to the abscission process.

Rab/Arf functional interactions can also be reciprocal. In HeLa cell, Chesneau et al. showed that Arf6-GTP can interact with Rab35 GAP EPI64B, negatively regulating Rab35 activity during cytokinesis (Chesneau et al., 2012). Together with our results, these observations provide compelling evidence that Rab to Arf, and Arf to Rab, regulatory loops represent a general mechanism for the coordinate regulation of Rabs and Arfs during membrane trafficking. Rab/Arf cross-talk is likely important for many higher-level processes that depend upon tight regulation of recycling endosome function.

Previous studies in mammals demonstrated a role for ACAP1 in Glut4 and integrin recycling (Dai et al., 2004; Li et al., 2005). Furthermore, ACAP1 was reported to be part of a clathrin coat complex on endosomes (Li et al., 2007). Although clathrin coats have been suggested to participate in the recycling process (van Dam and Stoorvogel, 2002), the role of clathrin coats in endocytic recycling remains controversial. In our studies we found that GFP-CHC-1 colocalizes with CNT-1-MC on endosomes, and that GFP-CHC-1 and CNT-1-MC co- accumulate on the enlarged endosomes of *arf-6* mutants, consistent with the idea of a conserved clathrin-ACAP interaction. However the traditional role of an Arf protein is in recruiting clathrin adaptors, and thus loss of the Arf would be expected to reduce clathrin accumulation (Krauss et al., 2003). Indeed, recent work indicated endosomal recruitment of the epithelial cell-specific clathrin adaptor complex AP-1B by Arf6 (Shteyn et al., 2011). Rather, we observed increased accumulation of endosomal clathrin in *arf-6* null mutant *C. elegans*. Thus our data does not fit with a simple recruitment model for endosomal clathrin via ARF-6.

While the budding of clathrin-coated vesicles has been suggested to contribute to endocytic recycling, a flat clathrin lattice on endosomes has been suggested to create and/or maintain degradative subdomains on endosomes associated with HRS and ESCRT proteins, regulating the sorting of ubiquitinated cargo proteins in the endosome

(Raiborg et al., 2001; Raiborg et al., 2006; Shi et al., 2009). Thus another possibility is that ACAPs could interact with clathrin in the flat lattice to affect the balance in degradation and recycling that must be maintained in the endosomal system.

MATERIALS AND METHODS

General Methods and Strains

All *C. elegans* strains were derived originally from the wild-type Bristol strain N2. Worm cultures, genetic crosses, and other *C. elegans* husbandry were performed according to standard protocols (Brenner, 1974). Strains expressing transgenes were grown at 20℃. A complete list of strains used in this study can be found in Supplementary Table 1.

Antibodies

The mouse anti-HA monoclonal antibody (16B12) was purchased from Covance Research Products (Berkeley, CA). The rabbit polyclonal antibody against C. elegans ARF-6 was produced against a peptide (CSTGDGLHEGLTWLSQN) corresponding to ARF-6 amino acids 157-172 coupled to keyhole limpet hemocyanin. The resulting serum was affinity purified using standard methods against the same peptide coupled to a HiTrap NHS-activated HP Column (GE Healthcare). The resulting purified antibodies were tested for specificity on Western blots of wild-type, *arf-6* null, and ARF-6-GFP expressing animals.

Yeast Two-hybrid Analyses

Yeast two-hybrid screen for candidates of RAB-10 interacting proteins was performed according to the procedure of the DupLEX-A yeast two-hybrid system (OriGene Technologies, Rockville MD). The cDNA sequences of *C. elegans* rab-10(Q68L) in the entry vector pDONR221 were cloned into the pEG202-Gtwy bait vector by Gateway recombination cloning (Invitrogen, Carlsbad, CA) to generate N-terminal fusions with the LexA DNA binding domain. The pEG202-rab-5(Q78L), rab-7(Q68L), rab-8(Q67L),

rab-10(+), rab-10(T23N), rab-11(Q70L) and rab-35(Q69L) were constructed accordingly. The preprylation motifs for membrane attachment at the C-terminal ends of RAB were also deleted to improve entry of bait fusion proteins into the yeast nucleus. The *C. elegans* cDNA library was purchased from the DupLEX-A yeast two-hybrid system (OriGene Technologies, Rockville MD).

The LexA-based DupLEX-A yeast two-hybrid system (OriGene Technologies Inc., Rockville, MD) was used for all subsequent truncation analysis. All two-hybrid plasmids were generated as PCR products with Gateway attB.1 and attB.2 sequence extensions, and were introduced into the Gateway entry vector pDONR221 by BP reaction. The bait vector pEG202-Gtwy and target vector pJG4-5-Gtwy have been described previously (Sato et al., 2008). Origene plasmid pSH18-34 [URA3, 8 ops.-LacZ] was used as reporter in all the yeast two-hybrid experiments. Constructs were introduced into the yeast strain EGY48 [MAT trp1 his3 ura3 leu2::6 LexAop-LEU2] included in the system. Transformants were selected on plates lacking leucine, histidine, tryptophan and uracil, containing 2% galactose/1% raffinose at 30℃ for 3 days and assayed for the expression of the *LEU2* reporter. Blue/white β-galactosidase assays confirmed results shown for growth assays, according to manufacturer's instructions.

Protein Expression and Coprecipitation Assays

rab-5(Q78L), rab-7(Q68L), rab-8(Q67L), rab-10(Q68L) and *rab-35(Q69L)* cDNA clones were transferred into an in-house modified vector pcDNA3.1 (+) (Invitrogen, Carlsbad, CA) with 2xHA epitope tag and Gateway cassette (Invitrogen, Carlsbad, CA) for *in vitro* transcription/translation experiments. For GST pull-down experiments an equivalent *ehbp-1(aa 662-901)* and *cnt-1(aa 656-826)* PCR products were introduced in frame into vector pGEX-2T (GE Healthcare Life Sciences, Piscataway, NJ) modified with a Gateway cassette.

N-terminally hemagglutinin (HA)-tagged proteins, RAB-5(Q78L), RAB7(Q68L), RAB-8(Q67L), and RAB-10(Q68L), RAB-35(Q69L) were synthesized in vitro using the TNT-

coupled transcription-translation system (Promega, Madison, WI) using DNA templates pcDNA3.1-2xHA-RAB-5(Q78L), pcDNA3.1-2xHA-RAB-7(Q68L), pcDNA3.1-2xHA-RAB- 8(Q67L), and pcDNA3.1-2xHA-RAB10(Q68L) and pcDNA3.1-2xHA-RAB-35(Q69L) respectively (1 μg/50 μl reaction). The reaction cocktail was incubated at 30℃ for 90 min. Negative control glutathione S-transferase (GST) was expressed in NEB Express I^q Competent *E. coli* cells (NEB BioLabs, Ipswich, MA). GST-CNT-1(aa 656-826) and GST- EHBP-1(aa 662-901) fusion proteins were expressed in the *ArcticExpress*^{TM} strain of *E. coli* (Stratagene, La Jolla, CA). Bacterial pellets of GST and GST-EHBP-1(aa 662-901) were lysed in 20 ml B-PER Bacterial Protein Extraction Reagent (Pierce, Rockford, ILL) with Complete Protease Inhibitor Cocktail Tablets (Roche, Indianapolis, IN). Bacterial pellets of GST-CNT-1 (aa 656-826) was lysed with Avestin EmulsiFlex-C3 homogenizer (AVESTIN, Ottawa, Canada) at 15,000 psi in 40ml bacterial lysis buffer (50mM Tris-HCL, pH 8.0, 20% sucrose, 10% glycerol, 2mM dithiothreitol) with Complete Protease Inhibitor Cocktail Tablets (Roche, Indianapolis, IN). Extracts were cleared by centrifugation, and supernatants were incubated with glutathione-Sepharose 4B beads (Amersham Pharmacia, Piscataway, NJ) at 4℃ for 3 hours. Beads were then washed six times with cold STET buffer (10 mM Tris-HCl, pH 8.0, 150 mM NaCl, 1 mM EDTA, 0.1% Tween-20). *In vitro* synthesized HA-tagged protein (10 μl TNT mix diluted in 500 μl STET) was added to the beads and allowed to bind at 4℃ for 1h. After six additional washes in STET, the proteins were eluted by boiling in 70 μl of 2X SDS-PAGE sample buffers. Eluted proteins were separated on SDS-PAGE (12% polyacrylamide), blotted to nitrocellulose, stained with Ponceau S to detect GST fusion proteins. After blocking, the blot was then probed with anti-HA (16B12) antibody.

Plasmids and Transgenic Strains

To construct GFP or RFP/mCherry fusion transgenes for expression specifically in the worm intestine, a previously described *vha-6* promoter driven vector modified with a Gateway cassette inserted at the Asp718I site just upstream of the GFP or RFP coding region was used. The sequences of *C. elegans cnt-1(cDNA)* (a gift from H. A. Baylis,

University of Cambridge) and *C. elegans* arf-6(genomic DNA) lacking a stop codon were cloned into entry vector pDONR221 by PCR and BP reaction, and then transferred into intestinal expression vectors by Gateway recombination cloning LR reaction to generate C-terminal fusions (Chen et al., 2006a). Complete plasmid sequences are available on request. Low copy integrated transgenic lines for all of these plasmids were obtained by the microparticle bombardment method (Praitis et al., 2001).

Microscopy and Image Analysis

Live worms were mounted on 2% agarose pads with 10 mM levamisole as described previously (Sato et al., 2005). Multi-wavelength fluorescence images were obtained using an Axiovert 200M (Carl Zeiss MicroImaging, Oberkochen, Germany) microscope equipped with a digital CCD camera (C4742-12ER, Hamamatsu Photonics, Hamamatsu, Japan), captured using Metamorph software ver 6.3r2 (Universal Imaging, West Chester, PA), and then deconvolved using AutoDeblur Gold software ver 9.3 (AutoQuant Imaging, Watervliet, NY). Images taken in the DAPI channel were used to identify broad-spectrum intestinal autofluorescence caused by lipofuscin-positive lysosome-like organelles (Clokey and Jacobson, 1986; Hermann et al., 2005). To obtain images of GFP fluorescence without interference from autofluorescence, we used argon 488nm excitation and the spectral fingerprinting function of the Zeiss LSM510 Meta confocal microscope system (Carl Zeiss MicroImaging) as described previously (Chen et al., 2006a). Quantification of images was performed with Metamorph software ver 6.3r2 (Universal Imaging). Most GFP/RFP colocalization experiments were performed on L3 and L4 larvae expressing GFP and RFP-markers as previously described.

Whole animal lipid extracting, thin-layer chromatography and gas chromatography

All *C. elegans* strains for lipid analysis were maintained at 20°C using standard methods. For each strain animals were harvested from growth plates using M9 buffer and worms were isolated by centrifugation. Pellets were ground in liquid N2 to a fine powder using mortar and pestle. Phospholipids were extracted under acidic conditions as described

in König et al. 2008 (König *et al.*, 2008). Phosphatidylinositol lipid standards were purchased from Avanti Polar Lipids (Alabaster, AL, USA). Phosphatidylcholine was purchased from MoBiTec (Göttingen, Germany).

ACKNOWLEDGEMENTS

We thank Howard A Baylis and Shohei Mitani for important reagents, and Robin Chan and Gilbert DiPoalo for very helpful advice and discussions. We thank Peter Schweinsberg and Zui Pan for their generous advice and technical assistance. R.B. was supported by Aresty Research Center grant. S. E. was supported by the German Research Foundation Research Center for Molecular Physiology of the Brain. This work was supported by NIH Grants GM067237 and 3R01GM067237-07S1 to B.D.G.

FIGURES

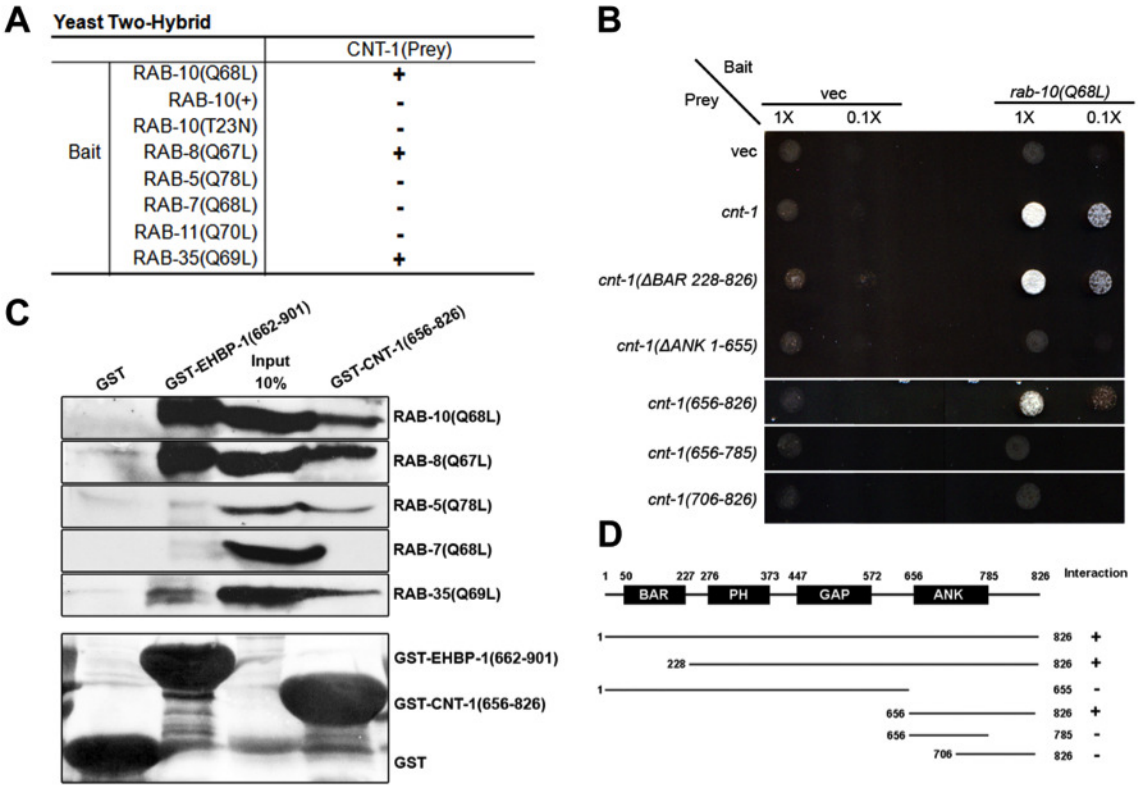
A
Yeast Two-Hybrid
CNT-1(Prey)
Bait
RAB-10(Q68L) +
RAB-10(+) -
RAB-10(T23N) -
RAB-8(Q67L) +
RAB-5(Q78L) -
RAB-7(Q68L) -
RAB-11(Q70L) -
RAB-35(Q69L) +
B
Bait
Prey
vec
rab-10(Q68L)
1X
0.1X
1X
0.1X
vec
cnt-1
cnt-1(ΔBAR 228-826)
cnt-1(ΔANK 1-655)
cnt-1(656-826)
cnt-1(656-785)
cnt-1(706-826)
C
GST
GST-EHBP-1(662-901)
Input 10%
GST-CNT-1(656-826)
RAB-10(Q68L)
RAB-8(Q67L)
RAB-5(Q78L)
RAB-7(Q68L)
RAB-35(Q69L)
GST-EHBP-1(662-901)
GST-CNT-1(656-826)
GST
D
1 50 227 276 373 447 572 656 785 826
Interaction
BAR
PH
GAP
ANK
1 826 +
228 826 +
1 655 -
656 826 +
656 785 -
706 826 -

Figure 1: CNT-1 physically interacts with RAB-10(Q68L).

(A) Binding specificity of CNT-1 with RAB-8, RAB-10 and RAB-35. Using full-length CNT-1 as prey, Rabs with reported endosomal trafficking involvement were used as bait in the yeast two-hybrid assays, including active RAB-5(Q78L), RAB-7(Q68L), RAB-8(Q67L), RAB-10(Q68L), RAB-10(+), RAB-10(T23N), RAB-11(Q70L), RAB-35(Q69L).

(B) The interaction between CNT-1 and RAB-10(Q68L) requires CNT-1 C-terminal ANK repeat containing segment. RAB-10(Q68L) was expressed in a yeast reporter strain as a fusion with the DNA-binding domain of LexA (bait). CNT-1 truncated forms were expressed in the same yeast cells as fusions with the B42 transcriptional activation domain (prey). Interaction between bait and prey was assayed by complementation of leucine auxotrophy (LEU2 growth assay). Colonies were diluted in liquid and spotted on solid growth medium directly or after further 0.1x dilutions.

(C) Glutathione beads loaded with recombinant GST, GST-EHBP-1(aa 662-901), GST-CNT-1(aa 656-826) were incubated with *in vitro* expressed HA-tagged RAB-5(Q78L), RAB-7(Q68L), RAB-8(Q67L), RAB-10(Q68L) and RAB-35(Q69L), and then washed to remove unbound proteins. Eluted proteins were separated on SDS-PAGE and stained with Ponceau S to detect GST fusion proteins (bottom). Bound proteins were eluted and analyzed by western blot using anti-HA (top). Input lanes contain *in vitro* expressed HA-tagged RABs used in the binding assays (10%).

(D) (D) Schematic representations of CNT-1 domains and the truncated fragments used in the Y2H analysis. Protein domains are displayed as dark boxes above protein sequence used in the study (shown as dark lines). Amino acid numbers are indicated.

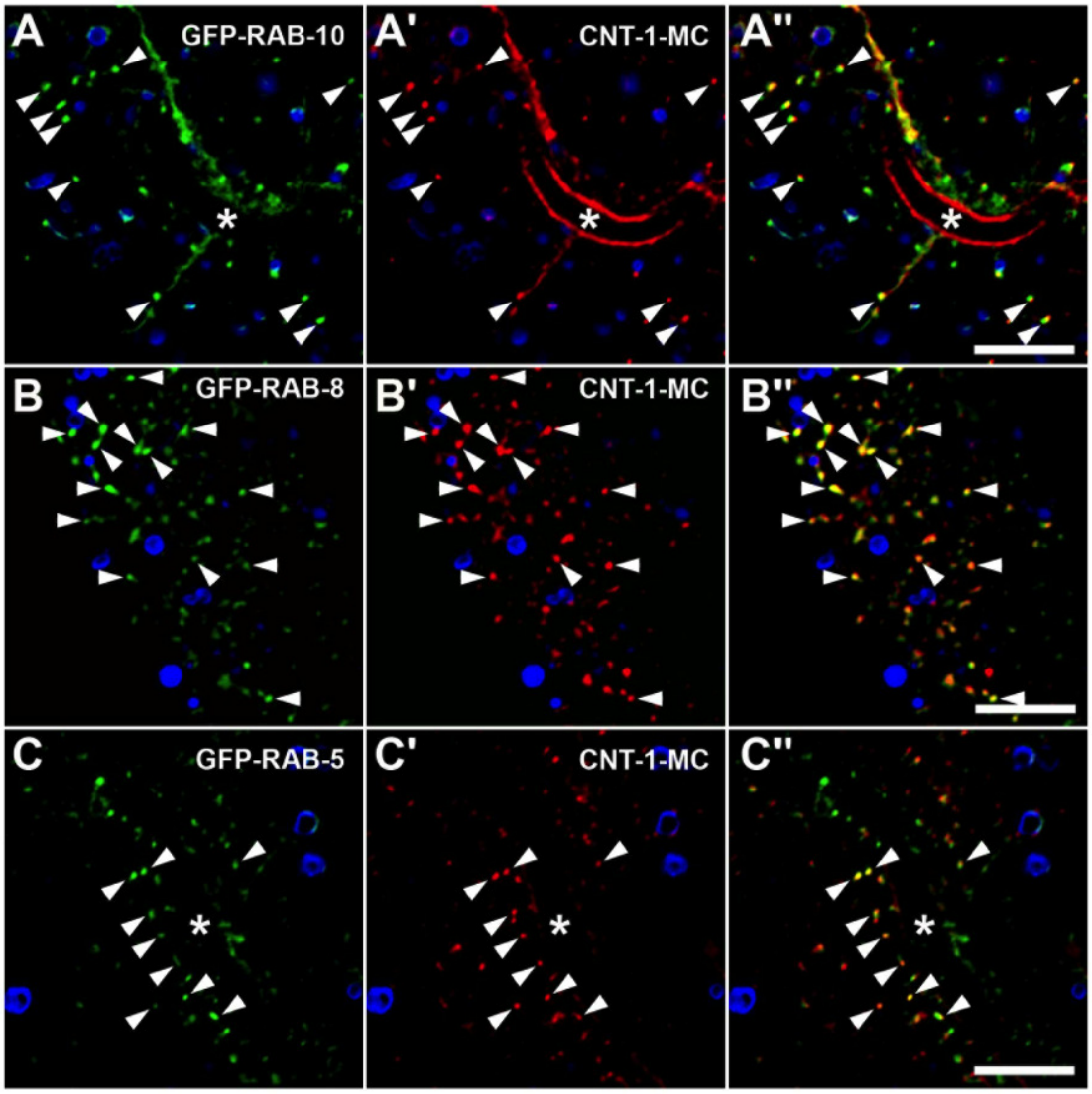
A
GFP-RAB-10
A'
CNT-1-MC
A''
B
GFP-RAB-8
B'
CNT-1-MC
B''
C
GFP-RAB-5
C'
CNT-1-MC
C''

Figure 2: CNT-1 colocalizes with RAB-10 on endosomes.

(A-C″) Colocalization images are from deconvolved 3-D image stacks acquired in intact living animals expressing GFP and mCherry tagged proteins specifically in intestinal epithelial cells. (A-A″) CNT-1-MC colocalizes with GFP-RAB-10. Arrowheads indicate endosomes labeled by both CNT-1-MC and GFP-RAB-10. (B-B″) CNT-1-MC colocalizes with GFP-RAB-8 on endosomal structures. Arrowheads indicate endosomes labeled by both CNT-1-MC and GFP-RAB-8. (C-C″) CNT-1-MC partially colocalizes with GFP-RAB-5 on endosomal structures. Arrowheads indicate endosomes labeled by both CNT-1-MC and GFP-RAB-5. In each image autofluorescent lysosome-like organelles can be seen in all three channels with the strongest signal in blue, whereas GFP appears only in the green channel and mCherry only in the red channel. Signals observed in the green or red channels that do not overlap with signals in the blue channel are considered bone fide GFP or RFP signals, respectively. Asterisk indicates intestinal lumen. Scale bar represents 10 μm.

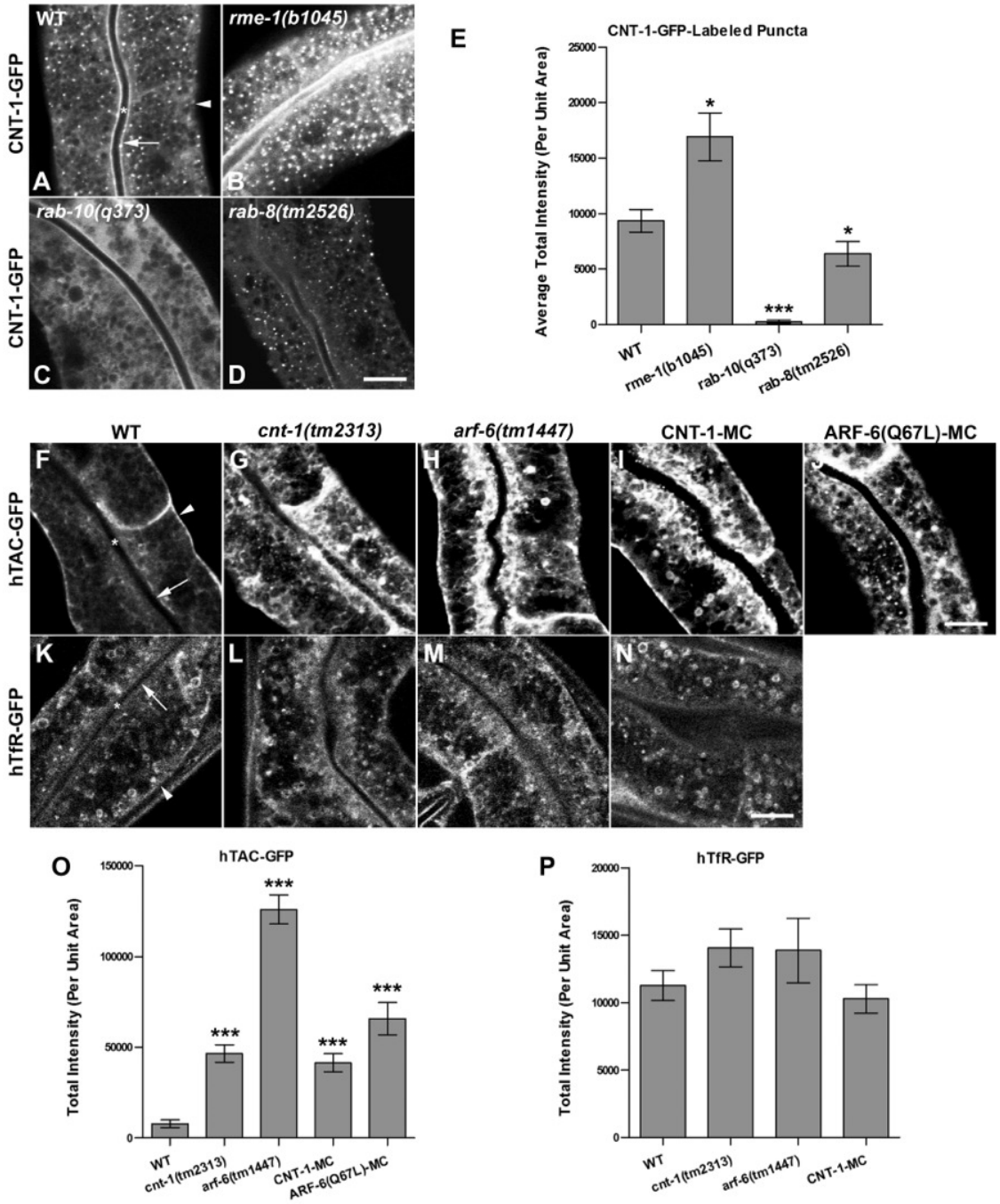
WT
rme-1(b1045)
rab-10(q373)
rab-8(tm2526)
CNT-1-GFP
CNT-1-GFP
A
B
C
D
E
CNT-1-GFP-Labeled Puncta
Average Total Intensity (Per Unit Area)
25000
20000
15000
10000
5000
0
*
*
***
WT
rme-1(b1045)
rab-10(q373)
rab-8(tm2526)
WT
cnt-1(tm2313)
arf-6(tm1447)
CNT-1-MC
ARF-6(Q67L)-MC
hTAC-GFP
hTfR-GFP
F
G
H
I
J
K
L
M
N
O
hTAC-GFP
Total Intensity (Per Unit Area)
150000
100000
50000
0
***
***
***
***
WT
cnt-1(tm2313)
arf-6(tm1447)
CNT-1-MC
ARF-6(Q67L)-MC
P
hTfR-GFP
Total Intensity (Per Unit Area)
20000
15000
10000
5000
0
WT
cnt-1(tm2313)
arf-6(tm1447)
CNT-1-MC

Figure 3: CNT-1 lost its endosomal association in *rab-10(q373)* mutants.

Representative confocal images are shown for CNT-1-GFP in wild-type animals, *rme-1(b1045)*, *rab-10(q373)* and *rab-8(tm2526)* mutants. Average total intensity of CNT-1-GFP in unit area was quantified in (E). Loss of functional RAB-10 disrupts CNT-1 endosomal association (C and E). Instead, depletion of RME-1 induces greatly accumulated CNT-1-GFP positive puncta, approximate 2-fold average total intensity (per unit area) increase (B and E). (D and E) Loss of RAB-8 had a minor effect on CNT-1-GFP localization, displaying an average reduction in puncta intensity of about 20% in *rab-8(tm2526)* mutants.

(F-P) Loss of CNT-1 induces endocytic recycling defects of hTAC in the *C. elegans* intestine. Confocal images of the worm intestine expressing GFP-tagged cargo proteins that recycle via the recycling endosome, the human transferrin receptor (hTfR-GFP) and the IL-2 receptor alpha chain (hTAC-GFP) in wild type, *cnt-1(tm2313)* and *arf-6(tm1447)* mutant animals. Compared with wild type animals (F), hTAC-GFP significantly accumulates on the intestinal cytosolic endosomal structures ($\tilde{6}$-fold increase) in *cnt-1(tm2313)* and increases in *arf-6(tm1447)* ($\tilde{5}$0-fold increase), respectively (G, H and O). hTfR-GFP was not affected in *cnt-1(tm2313)* and *arf-6(tm1447)* mutants (L, M and P). (I and O) Intracellular hTAC-GFP accumulates in intestinal cells with CNT-1 over-expressed. (J and O) Expression of *C. elegans* ARF-6 GTPase-defective form ARF-6(Q67L) greatly impaired hTAC-GFP localization and caused trapping of hTAC-GFP in endosomes.

In panel A, F, and K, asterisks indicate intestinal lumen, arrows indicate apical membrane, and arrowheads indicate basolateral membrane. Error bars are SEM ($n = 18$ each, 6 animals of each genotype sampled in three different regions of each intestine defined by a 100×100 (pixl^2) box positioned at random). Asterisks indicate significant differences in the one-tailed Students t-test ($^*p < 0.01$, $^{***}p < 0.001$). Scale bar represents 10 μm.

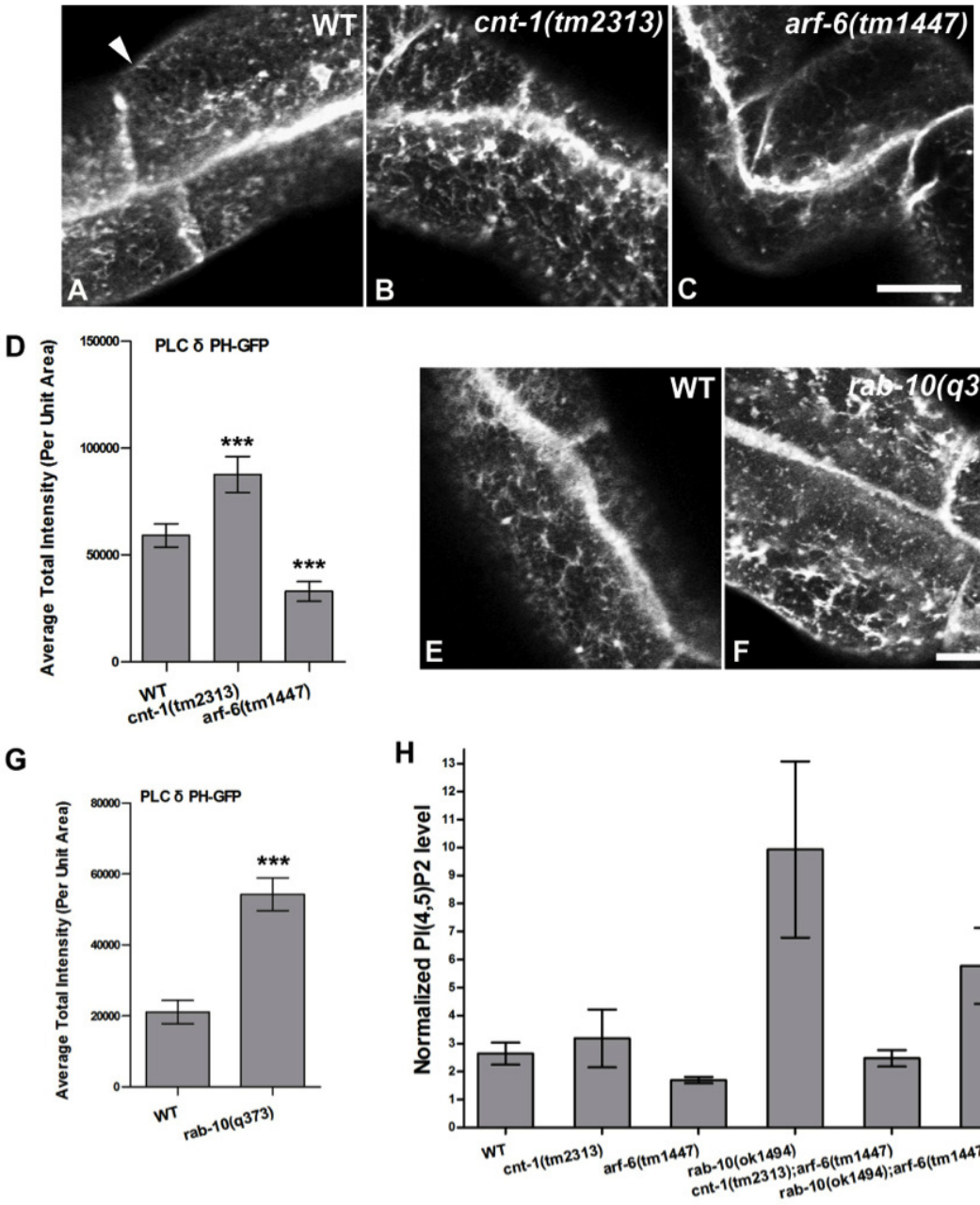
WT
cnt-1(tm2313)
arf-6(tm1447)
A
B
C
D
PLC δ PH-GFP
Average Total Intensity (Per Unit Area)
150000
100000
50000
0
***
***
WT
cnt-1(tm2313)
arf-6(tm1447)
WT
rab-10(q373)
E
F
G
PLC δ PH-GFP
Average Total Intensity (Per Unit Area)
80000
60000
40000
20000
0
***
WT
rab-10(q373)
H
Normalized PI(4,5)P2 level
13
12
11
10
9
8
7
6
5
4
3
2
1
0
WT
cnt-1(tm2313)
arf-6(tm1447)
rab-10(ok1494)
cnt-1(tm2313);arf-6(tm1447)
rab-10(ok1494);arf-6(tm1447)

Figure 4: PH-GFP increased in *cnt-1* or *rab-10* mutants and decreased in *arf-6* mutants

(A-C, E-F) Subcellular PH-GFP (PI(4,5)P2) were up-regulated in *cnt-1(tm2313)* and *rab-10(q373)* mutants, however, down-regulated in *arf-6(tm1447)* mutants. Representative confocal images are shown for PH-GFP in wild-type animals, *cnt-1(tm2313)*, *arf-6(tm1447)* and *rab-10(q373)* mutants. Average total intensity of PH-GFP in unit area was quantified in (D and G). In panel A, arrowhead indicates basolateral membrane. Error bars are SEM ($n = 18$ each, 6 animals of each genotype sampled in three different regions of each intestine defined by a 100×100 (pixl^2) box positioned at random). Asterisks indicate significant differences in the one-tailed Students t-test ($^{***}p < 0.001$). Scale bar represents 10 μm.

(H) PI(4,5)P2 levels in *cnt-1(tm2313)*, *arf-6(tm1447)*, *rab-10(q373)* and *cnt-1(tm2313)*;*arf-6(tm1447)*, *rab-10(q373)*;*arf-6(tm1447)* double mutants. Whole animal lipid extracts were prepared using thin-layer chromatography and analyzed by gas chromatography. PI(4,5)P2 measurements were normalized to the abundant phospholipids (phosphatidylcholine and phosphatidylinositol) in each sample respectively. Membrane PI(4,5)P2 are present in both *cnt-1* and *rab-10* mutants at levels higher than WT. Notably, consistent with subcellular PH-GFP quantification result in (G), PI(4,5)P2 level is substantially higher in rab-10 mutants than WT. Conversely, *arf-6* mutants PI(4,5)P2 level shows moderate (35%) decrease compared with WT. In *cnt-1(tm2313)*;*arf-6(tm1447)* double mutants, PI(4,5)P2 level appears fairly normal. Whereas, *rab-10(q373)*;*arf-6(tm1447)* double mutants PI(4,5)P2 level is 2-fold higher than WT, loss-of-ARF-6 reduces the elevated PI(4,5)P2 levels in *rab-10* mutants by about 40%. The mean values and SEM from three independent experiments are shown.

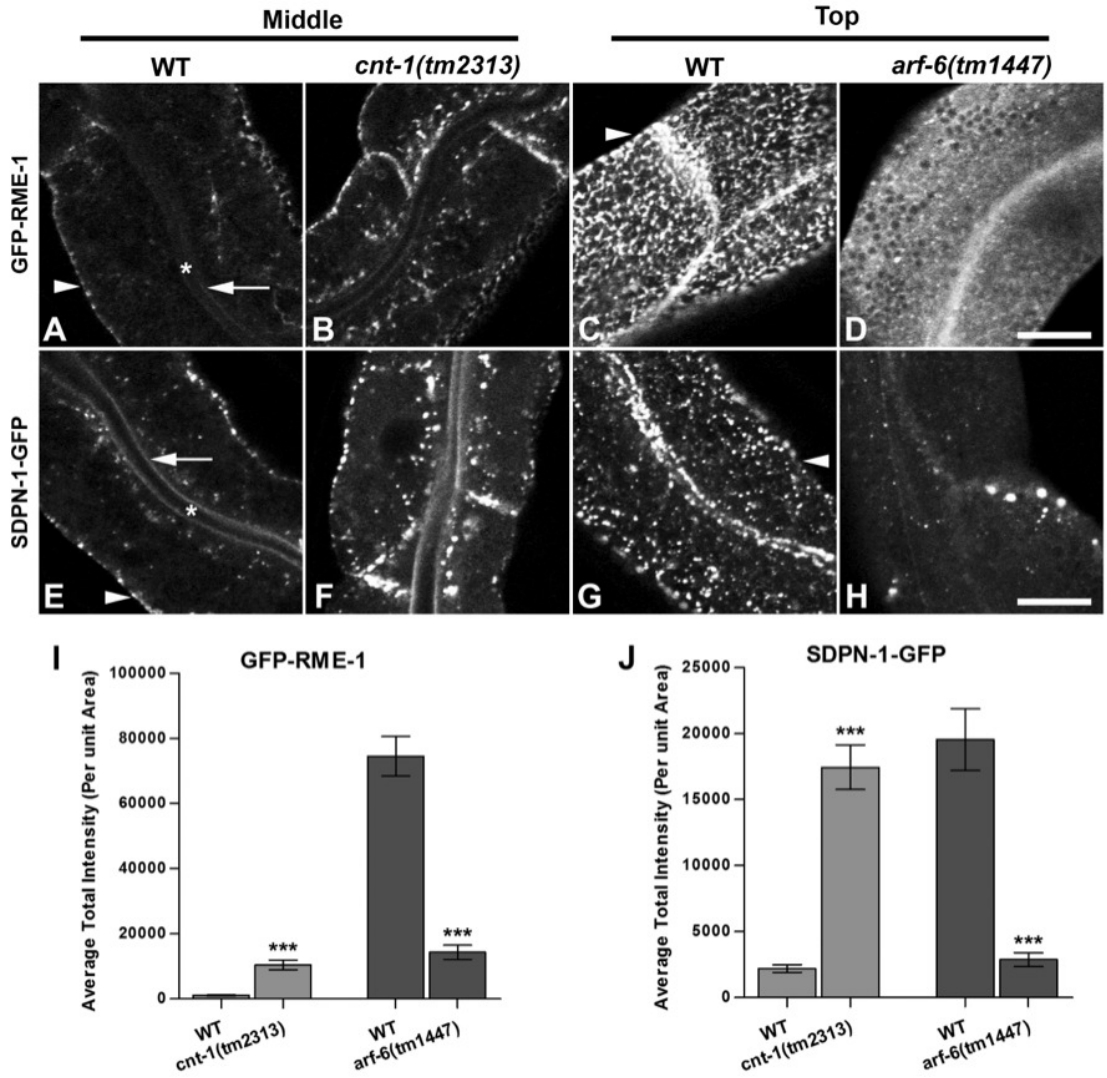
Middle
Top
WT
cnt-1(tm2313)
WT
arf-6(tm1447)
GFP-RME-1
SDPN-1-GFP
A
B
C
D
E
F
G
H
I
GFP-RME-1
Average Total Intensity (Per unit Area)
100000
80000
60000
40000
20000
0
***
***
WT
cnt-1(tm2313)
WT
arf-6(tm1447)
J
SDPN-1-GFP
Average Total Intensity (Per unit Area)
25000
20000
15000
10000
5000
0
***
***
WT
cnt-1(tm2313)
WT
arf-6(tm1447)

Figure 5: Aberrant subcellular distribution of PI(4,5)P2-binding proteins GFP-RME-1 and GFP- SDPN-1 in *cnt-1* and *arf-6* mutants.

(A-D) GFP-RME-1 medial endosomal labeling increased in *cnt-1* mutants, while its basolateral tubular and puncta labeling greatly decreased in *arf-6* mutants. Average total intensity of GFP-RME-1 in unit area was quantified in (I). (E-H) Similar to GFP-RME-1, recycling endosomal marker GFP-SDPN-1 medial endosomal labeling increased in cnt-1 mutants. Whereas, SDPN-1 basolateral tubular and puncta labeling greatly decreased in *arf-6* mutants. Average total intensity of GFP-SDPN-1 in unit area were quantified in (J).

In panels A, C, E, and G, asterisks indicate intestinal lumen, arrows indicate apical membrane, and arrowheads indicate basolateral membrane. Error bars are SEM ($n =$ 18 each, 6 animals of each genotype sampled in three different regions of each intestine defined by a 100×100 (pixl^2) box positioned at random). Asterisks indicate significant differences in the one-tailed Student's t-test ($^{***}p < 0.001$). Scale bar represents 10 μm.

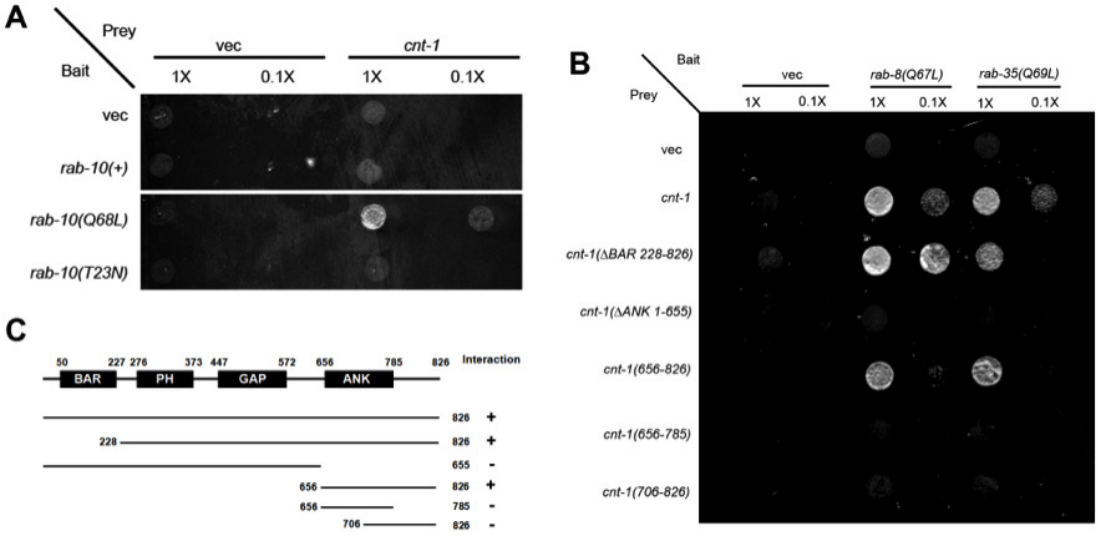
A
Prey
Bait
vec
cnt-1
1X
0.1X
1X
0.1X
vec
rab-10(+)
rab-10(Q68L)
rab-10(T23N)
B
Bait
Prey
vec
rab-8(Q67L)
rab-35(Q69L)
1X
0.1X
1X
0.1X
1X
0.1X
vec
cnt-1
cnt-1(ΔBAR 228-826)
cnt-1(ΔANK 1-655)
cnt-1(656-826)
cnt-1(656-785)
cnt-1(706-826)
C
50
227
276
373
447
572
656
785
826
Interaction
BAR
PH
GAP
ANK
826 +
228
826 +
655 -
656
826 +
656
785 -
706
826 -

Figure S1: CNT-1 interacts with RAB-10, RAB-8, and RAB-35.

(A) CNT-1 interacts with GTP bound active form of RAB-10 preferentially. RAB-10, RAB- 10(Q68L) and RAB-10(T23N) were expressed in a yeast reporter strain as a fusion with the DNA-binding domain of LexA (bait). CNT-1 truncated forms were expressed in the same yeast cells as fusions with the B42 transcriptional activation domain (prey). Interaction between bait and prey was assayed by complementation of leucine auxotrophy (LEU2 growth assay). Colonies were diluted in liquid and spotted on solid growth medium directly or after further 0.1 × dilutions.

(B-C) CNT-1 physically interacts with RAB-8(Q67L) and RAB-35(Q69L), and the interaction between CNT-1 and RAB-8(Q67L) and RAB-35(Q69L) requires CNT-1 C-terminal ANK repeat containing segment. RAB-8(Q67L) and RAB-35(Q69L) were expressed in as bait, and CNT-1 truncated forms were expressed as prey. (C) Schematic representations of CNT-1 domains and the truncated fragments used in the Y2H analysis. Protein domains are displayed as dark boxes above protein sequence used in the study (shown as dark lines). Amino acid numbers are indicated.

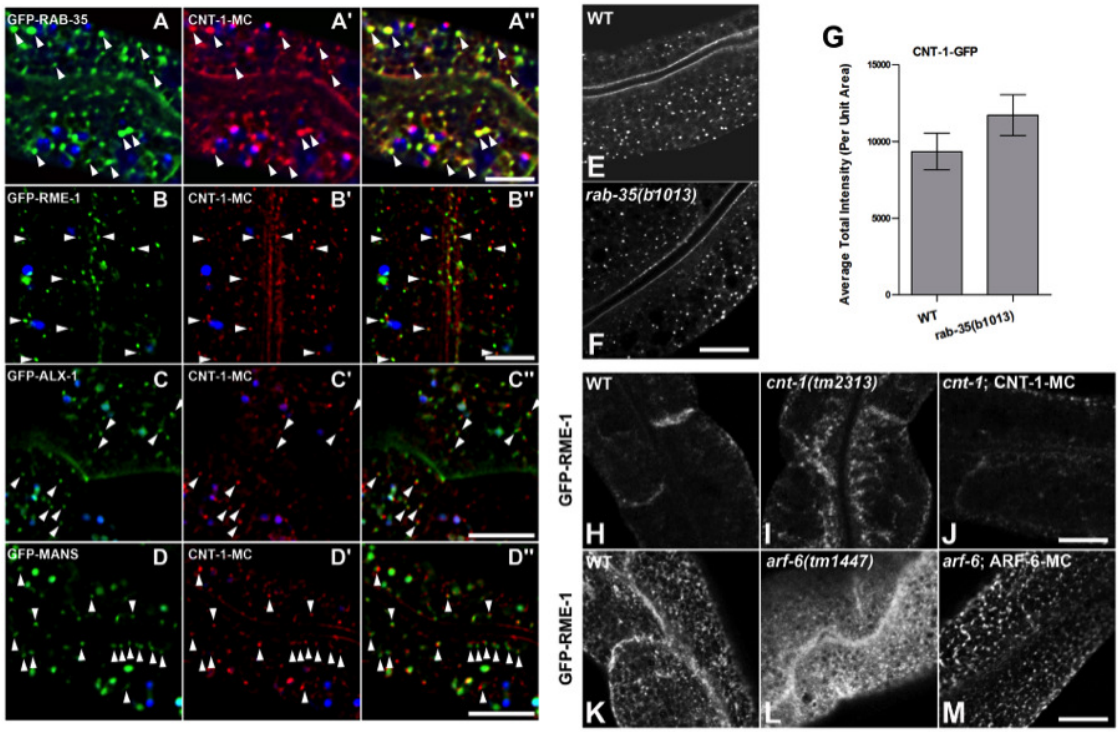
GFP-RAB-35
A
CNT-1-MC
A'
A''
GFP-RME-1
B
CNT-1-MC
B'
B''
GFP-ALX-1
C
CNT-1-MC
C'
C''
GFP-MANS
D
CNT-1-MC
D'
D''
WT
E
rab-35(b1013)
F
G
CNT-1-GFP
Average Total Intensity (Per Unit Area)
15000
10000
5000
0
WT
rab-35(b1013)
GFP-RME-1
WT
cnt-1(tm2313)
cnt-1; CNT-1-MC
H
I
J
GFP-RME-1
WT
arf-6(tm1447)
arf-6; ARF-6-MC
K
L
M

Figure S2: CNT-1 colocalizes with RAB-35 but not affected by *rab-35* mutants

(A-D″) Colocalization images are from deconvolved 3-D image stacks acquired in intact living animals expressing GFP and mCherry tagged proteins specifically in intestinal epithelial cells. (A-A″) CNT-1-MC colocalizes with GFP-RAB-35. Arrowheads indicate endosomes labeled by both CNT-1-MC and GFP-RAB-35. (B-B″) CNT-1-MC partially colocalizes with recycling endosome marker GFP-RME-1. Arrowheads indicate endosomes labeled by both CNT-1-MC and GFP-RME-1. (C-C″) CNT-1-MC partially colocalizes with GFP- ALX-1. Arrowheads indicate CNT-1-MC positive endosomes partially overlapped with GFP- ALX-1 labeled structures. (D-D″) CNT-1-MC does not colocalize with Golgi marker GFP- Mannosidase. In each image autofluorescent lysosome-like organelles can be seen in all three channels with the strongest signal in blue, whereas GFP appears only in the green channel and mCherry only in the red channel. Signals observed in the green or red channels that do not overlap with signals in the blue channel are considered bone fide GFP or RFP signals, respectively. Scale bar represents 10 μm.

(E-F) Loss of RAB-35 had no effect on CNT-1-GFP localization. Average total intensity of CNT-1-GFP in unit area was quantified in (G). Error bars are SEM ($n = 18$ each, 6 animals of each genotype sampled in three different regions of each intestine defined by a 100×100 (pixl^2) box positioned at random). Scale bar represents 10 μm.

(H-J) GFP-RME-1 medial endosomal accumulation phenotype in *cnt-1(tm2313)* mutants can be rescued by expression of MC-tagged CNT-1 driven by the intestine-specific *vha-6* promoter. (K-M) GFP-RME-1 basolateral tubular and puncta labeling decrease phenotype in *arf-6(tm1447)* mutants can be rescued by intestinal expression of MC-ARF-6. Scale bar represents 10 μm.

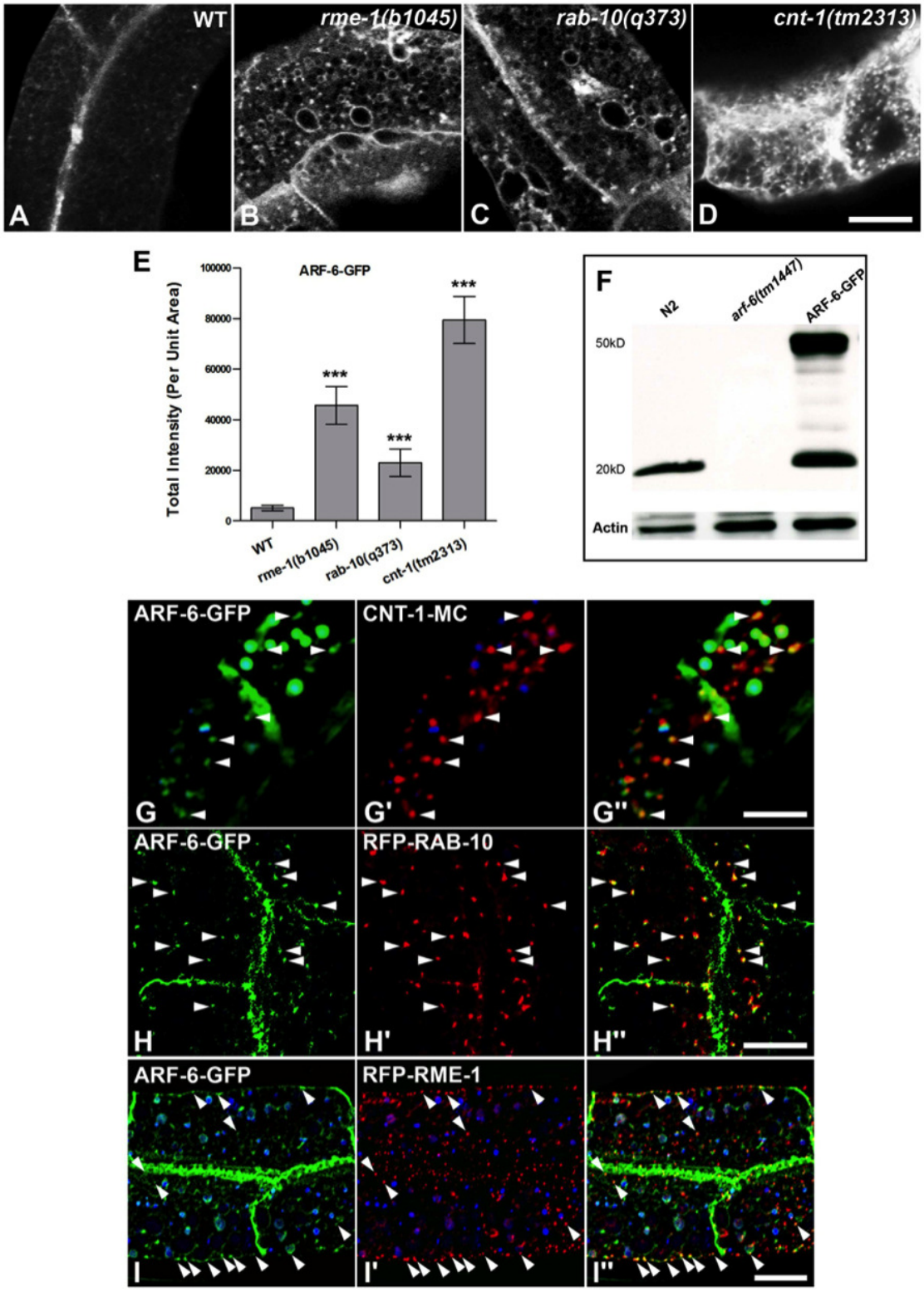
WT
rme-1(b1045)
rab-10(q373)
cnt-1(tm2313)
A
B
C
D
E
ARF-6-GFP
Total Intensity (Per Unit Area)
100000
80000
60000
40000
20000
0
***
***
***
WT
rme-1(b1045)
rab-10(q373)
cnt-1(tm2313)
F
N2
arf-6(tm1447)
ARF-6-GFP
50kD
20kD
Actin
ARF-6-GFP
CNT-1-MC
G
G'
G''
ARF-6-GFP
RFP-RAB-10
H
H'
H''
ARF-6-GFP
RFP-RME-1
I
I'
I''

Figure S3: ARF-6 labels recycling endosomes and accumulates on enlarged endosomes in recycling defective mutants

(A-E) ARF-6-GFP labels recycling endosomes and accumulates on enlarged endosomes in recycling defective mutants. (A-D) Representative confocal images are shown for ARF-6- GFP in wild-type animals, *rme-1(b1045)*, *rab-10(q373)* and *cnt-1(tm2313)* mutants. Total intensity of ARf-6-GFP in unit area was quantified in (E).

(F) ARF-6 levels in wild-type, *arf-6(tm1447)* and ARF-6-GFP expressing transgenic animals. Protein ARF-6 was not detected in *arf-6(tm1447)* mutant animals.

(G-I″) Colocalization images are from deconvolved 3-D image stacks acquired in intact living animals expressing fluorophore tagged proteins specifically in intestinal epithelial cells. (G- G″) CNT-1-MC colocalizes with ARF-6-GFP. Arrowheads indicate endosomes labeled by both CNT-1-MC and ARF-6-GFP. (H-H″) ARF-6-GFP colocalizes with RFP-RAB-10. Arrowheads indicate ARF-6-GFP positive endosomes overlapped with RFP-RAB-10 labeled puncta. (I-I″) Recycling endosomal marker RFP-RME-1 mainly colocalizes with ARF-6-GFP on puncta close to basolateral membrane. Arrowheads indicate endosomes labeled by both RFP-RME- 1 and ARF-6-GFP. Scale bar represents 10 μm.

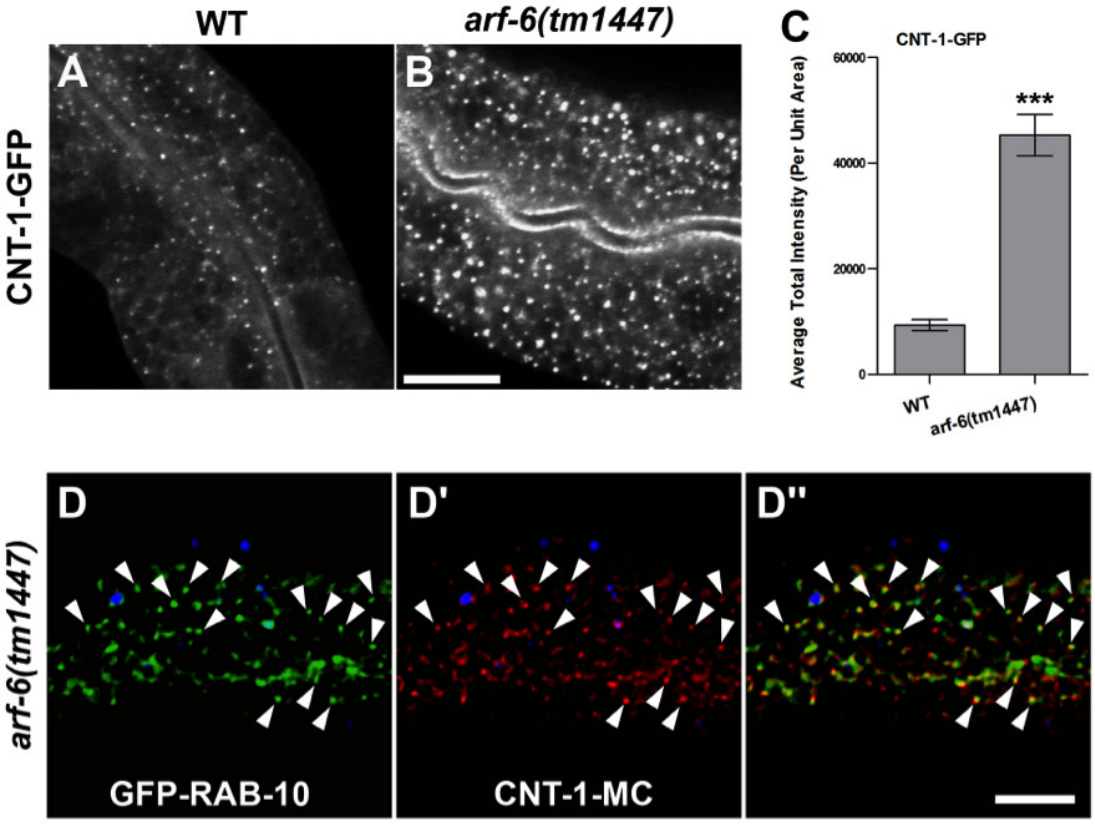
WT
arf-6(tm1447)
A
B
CNT-1-GFP
C
CNT-1-GFP
Average Total Intensity (Per Unit Area)
60000
40000
20000
0
***
WT
arf-6(tm1447)
D
D'
D''
arf-6(tm1447)
GFP-RAB-10
CNT-1-MC

Figure S4: CNT-1 accumulates on recycling endosomes in *arf-6* mutants

(A-C) CNT-1 accumulates on endosomal structures in *arf-6* mutants. Depletion of ARF-6 induces greatly accumulated CNT-1-GFP positive puncta, approximate 4-fold average total intensity (per unit area) increase (C). Error bars are SEM ($n = 18$ each, 6 animals of each genotype sampled in three different regions of each intestine defined by a 100×100 (pixl^2) box positioned at random). Asterisks indicate significant differences in the one-tailed Student's t-test ($^{***}p < 0.001$). Scale bar represents 10 μm. (D-D$''$) RAB-10 and CNT-1 co- accumulate on endosomes in *arf-6* mutants. Arrowheads indicate endosomes labeled by both CNT-1-MC and GFP-RAB-10. Scale bar represents 10 μm.

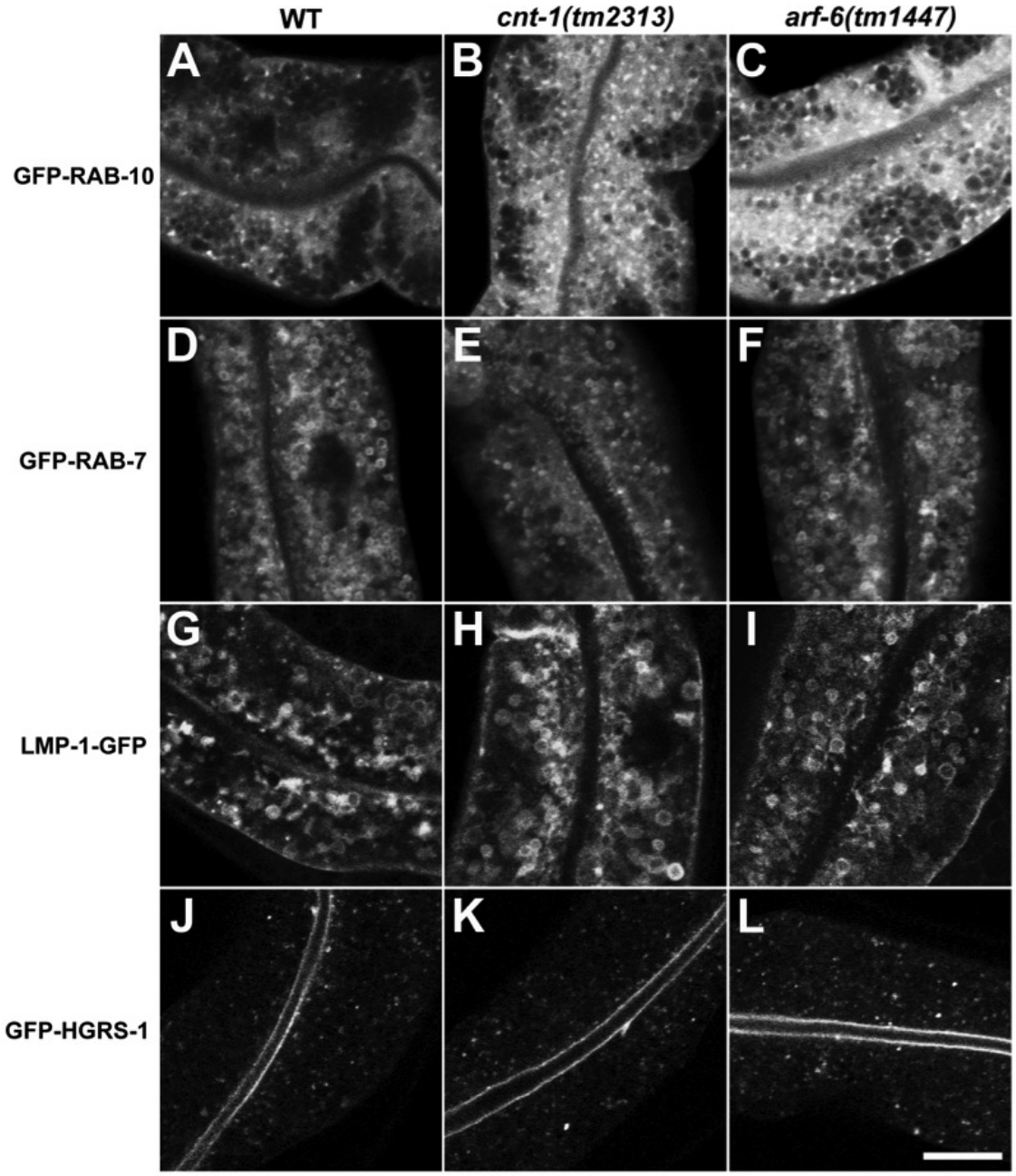
WT
cnt-1(tm2313)
arf-6(tm1447)
A
B
C
GFP-RAB-10
D
E
F
GFP-RAB-7
G
H
I
LMP-1-GFP
J
K
L
GFP-HGRS-1

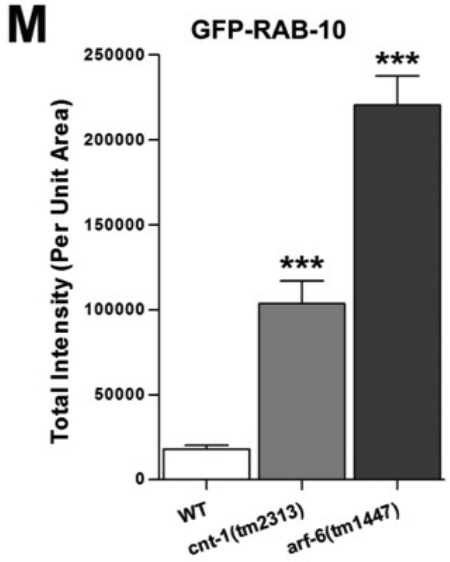
M
GFP-RAB-10
Total Intensity (Per Unit Area)
250000
200000
150000
100000
50000
0
***
***
WT
cnt-1(tm2313)
arf-6(tm1447)

Figure S5: RAB-10 accumulates in *cnt-1* and *arf-6* mutants

(A-C) GFP-RAB-10-labeled recycling endosomes increase in number in cnt-1 and arf-6 mutant intestinal cells. (M) Quantification of GFP-labeled puncta total intensity per unit area. Error bars are SEM ($n = 18$ each, 6 animals of each genotype sampled in three different regions of each intestine defined by a 100×100 (pixl^2) box positioned at random). Asterisks indicate significant differences in the one-tailed Student's t-test ($^{***}p < 0.001$).

(D-F) GFP-RAB-7 labeled late endosomes were not detectably altered in *cnt-1* and *arf-6* mutant intestinal cells. (G-I) LMP-1-GFP labeled late endosomes were not afftected in *cnt-1* and *arf-6* mutant intestinal cells. (J-L) MVE/MVB marker HGRS-1/Hrs appears normal in *cnt-1* and *arf-6* mutants. Scale bar represents 10 μm.

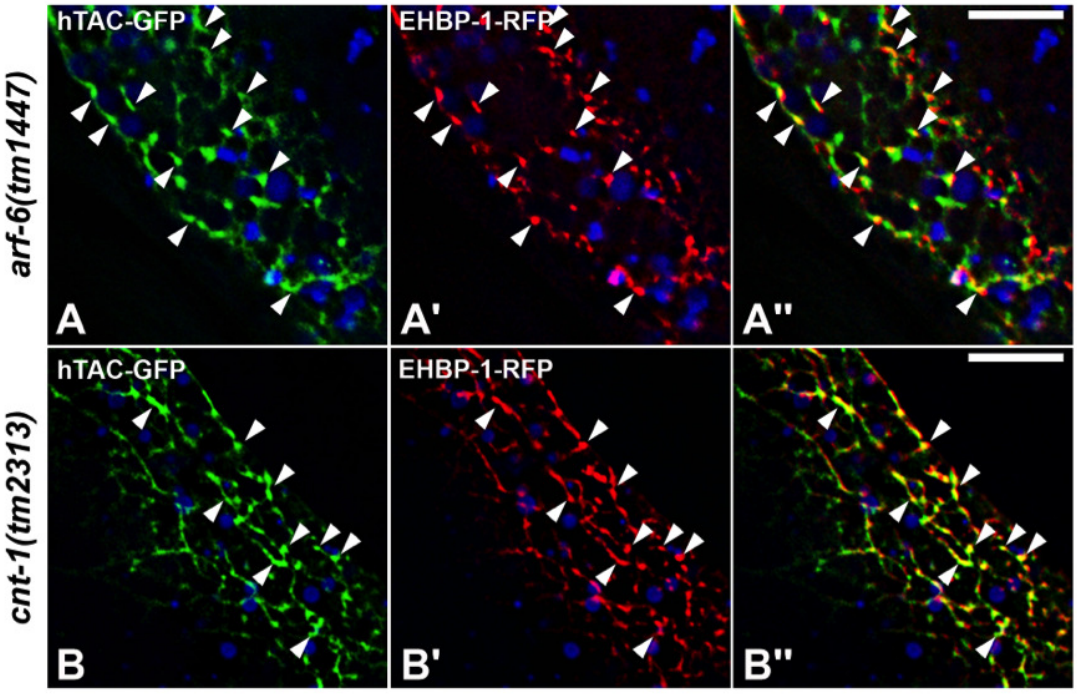
arf-6(tm1447)
cnt-1(tm2313)
hTAC-GFP
EHBP-1-RFP
A
A'
A''
B
B'
B''

Figure S6: GFP-hTAC accumulates on recycling endosome in *cnt-1* and *arf-6* mutants

(A-A") GFP-hTAC co-accumulates on endosomes with EHBP-1-RFP endosomes in *cnt-1* mutants. Arrowheads indicate endosomes labeled by both GFP-hTAC and EHBP-1-RFP. (B- B″) GFP-hTAC co-accumulates on endosomes with EHBP-1-RFP endosomes in *arf-6* mutants. Arrowheads indicate endosomes labeled by both GFP-hTAC and EHBP-1-RFP. Arrowheads indicate basolateral/apical membrane labeled by both GFP-hTAC and EHBP-1-RFP. Scale bar represents 10 μm.

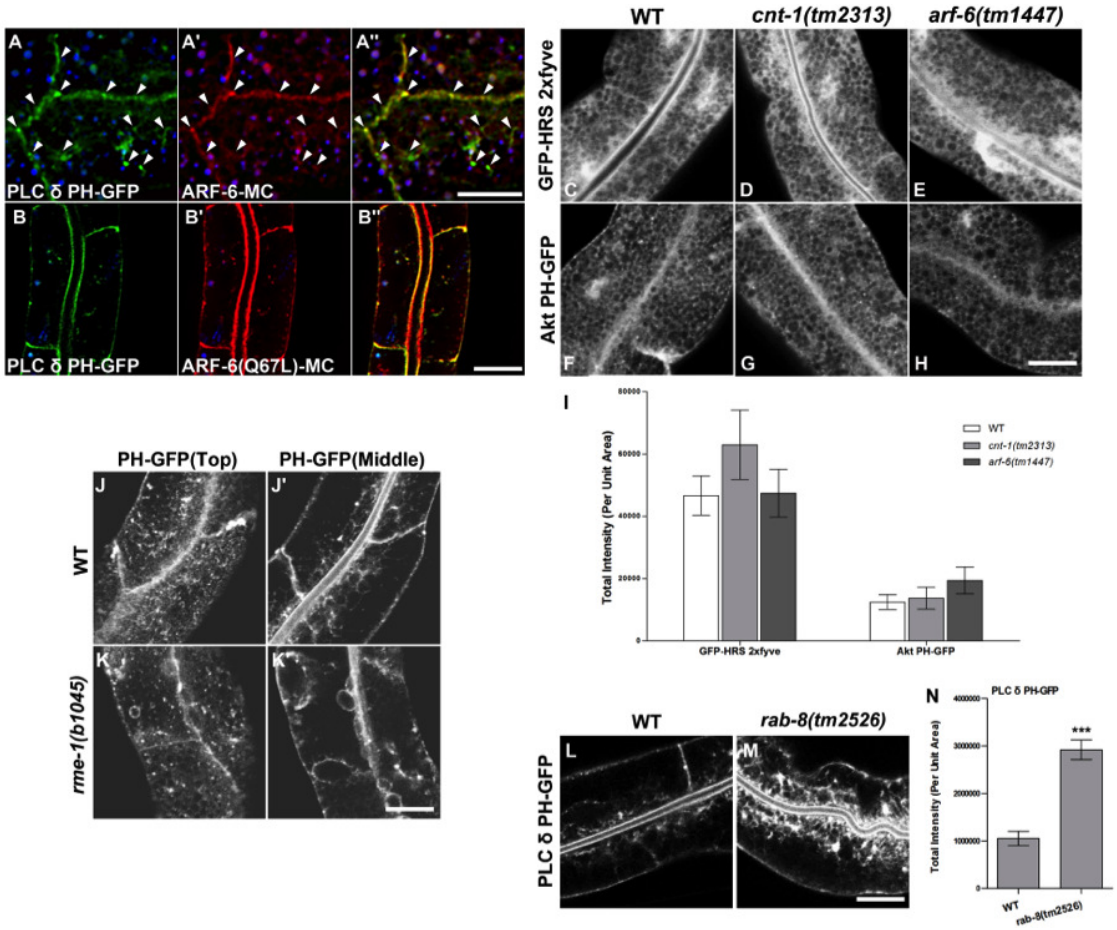
A
A'
A''
PLC δ PH-GFP
ARF-6-MC
B
B'
B''
PLC δ PH-GFP
ARF-6(Q67L)-MC
WT
cnt-1(tm2313)
arf-6(tm1447)
GFP-HRS 2xfyve
Akt PH-GFP
C
D
E
F
G
H
I
Total Intensity (Per Unit Area)
WT
cnt-1(tm2313)
arf-6(tm1447)
GFP-HRS 2xfyve
Akt PH-GFP
PH-GFP(Top)
PH-GFP(Middle)
WT
rme-1(b1045)
J
J'
K
K'
WT
rab-8(tm2526)
PLC δ PH-GFP
L
M
N
PLC δ PH-GFP
Total Intensity (Per Unit Area)
***
WT
rab-8(tm2526)

Figure S7: ARF-6 colocalizes with PH-GFP and accumulates in *rab-8* mutants

(A-A″) ARF-6 colocalizes with PH-GFP on basolateral tubular and puncta. (B-B″) ARF- 6(Q67L) colocalizes with PH-GFP on apical and lateral plasma membrane. Arrowheads indicate tubular and puncta labeled by both ARF-6-MC and PH-GFP. Scale bar represents 10 μm.

(C-I) Levels of PI(3)P (labeled by GFP-2xFYVE) and PI(3,4,5)P3 (labeled by PH(Akt)-GFP) were unperturbed in *cnt-1* and *arf-6* mutants. Error bars are SEM ($n = 18$ each, 6 animals of each genotype sampled in three different regions of each intestine defined by a 100×100 (pixl^2) box positioned at random). Scale bar represents 10 μm.

(J-K″) PH(PLCδ)-GFP labeling in *rme-1* mutants was not detectably altered. Some of the endosomes labeled by PH(PLCδ)-GFP were grossly enlarged in *rme-1* mutants. Scale bar represents 10 μm.

(L-M) Loss of RAB-8 causes significant cytosolic accumulation of PH-GFP. Total intensity of PH-GFP in unit area was quantified in (N). Error bars are SEM ($n = 18$ each, 6 animals of each genotype sampled in three different regions of each intestine defined by a 100×100 (pixl^2) box positioned at random). Scale bar represents 10 μm.

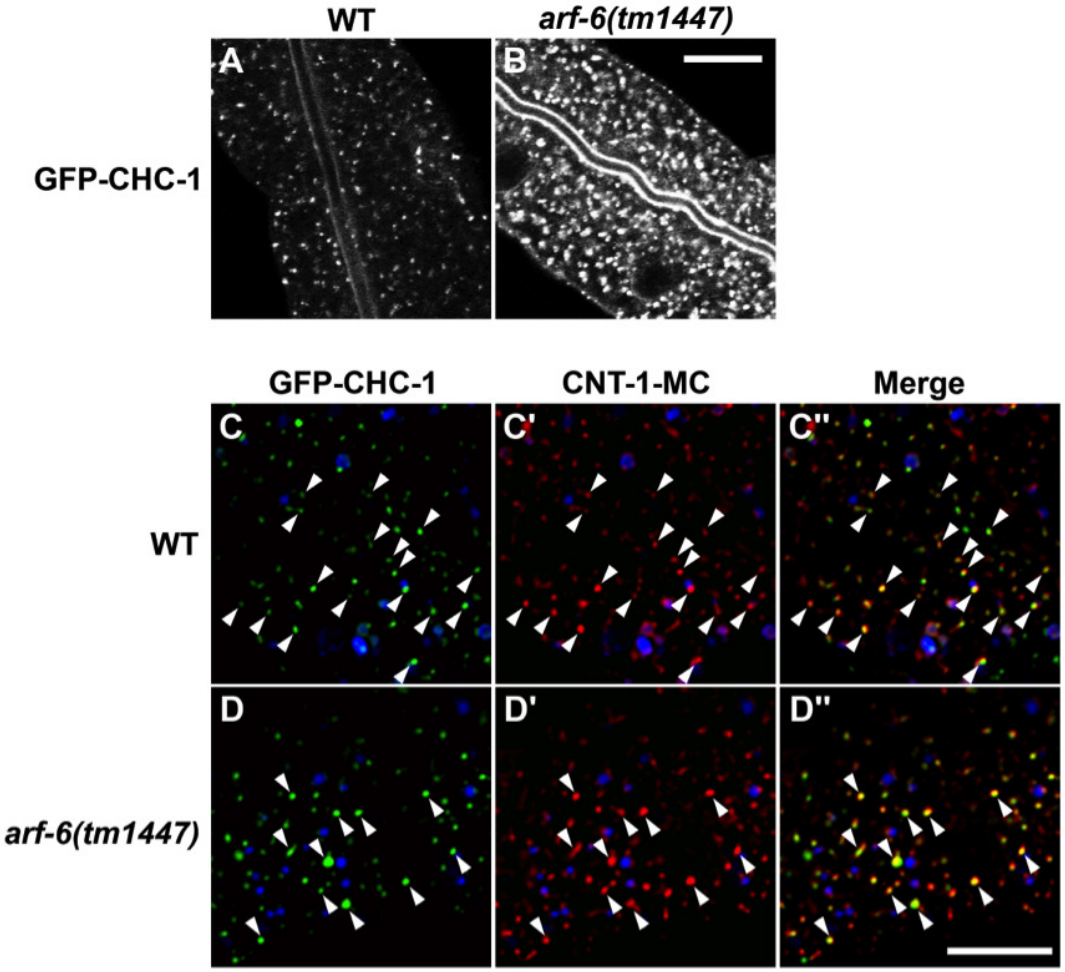
WT
arf-6(tm1447)
A
B
GFP-CHC-1
GFP-CHC-1
CNT-1-MC
Merge
C
C'
C''
WT
D
D'
D''
arf-6(tm1447)

Figure S8: Clathrin accumulates and overlaps with CNT-1 on enlarged endosomes in *arf-6* mutants.

(A-B) Representative confocal images are shown for GFP-tagged clathrin heavy chain (GFP- CHC-1) in wild-type animals and *arf-6(tm1447)* mutants. Scale bar represents 10 μm.

(C-D″) Colocalization images of CHC-1 and CNT-1 in both WT and *arf-6* mutant background are from deconvolved 3-D image stacks acquired in intact living animals expressing GFP and mCherry tagged proteins specifically in intestinal epithelial cells. (C-C″) CNT-1-MC colocalizes with GFP-CHC-1 in wild type animals. Arrowheads indicate representative endosomes labeled by both CNT-1-MC and GFP-CHC-1. (D-D″) CNT-1-MC colocalizes with GFP-CHC-1 on enlarged endosomal structures in *arf-6* mutants. Arrowheads indicate enlarged puncta labeled by both CNT-1-MC and GFP-CHC-1. In each image autofluorescent lysosome-like organelles can be seen in all three channels with the strongest signal in blue. Scale bar represents 10 μm.

Supplemental Table

Table 1: Transgenic and Mutant Strains Used in This Study

pwIs724[pvha6::CNT-1::GFP]

pwIs728[pvha6::CNT-1::mCherry]

pwIs601[pvha6::ARF-6::GFP]

pwIs206[pvha6::GFP::RAB-10](Chen et al., 2006a)

pwIs72[pvha6::GFP::RAB-5] (Chen et al., 2006a)

pwIs87[pvha6::GFP::RME-1](Chen et al., 2006a)

pwIs524[pvha6::GFP::ALX-1](Shi et al., 2007)

pwIs481[pvha6::MANS::GFP](Chen et al., 2006a)

pwIs112[pvha6::hTAC::GFP](Chen et al., 2006a)

pwIs90[pvha6::hTfR::GFP](Chen et al., 2006a)

pwIs722[pvha6::SDPN-1::GFP](Pant et al., 2009)

pwIs170[pvha6::GFP::RAB-7](Chen et al., 2006a)

pwIs50[plmp-1::LMP-1::GFP](Treusch et al., 2004)

pwIs518[pvha6::GFP::HGRS-1](Shi et al., 2007)

pwIs446[pvha6::PH::GFP]

pwIs140[pvha6::GFP::2xFYVE]

pwIs890[pvha6::Akt-PH::GFP]

dkIs8 [pvha6::GFP::CHC-1](Sato, 2008)

pwIs68[pvha6::GFP::RAB-8]

pwIs625[pvha6::ARF-6::mCherry]

rme-1(b1045)(Grant et al., 2001b)

rab-10(q373)(Chen et al., 2006a)

alx-1 (gk275)(Shi et al., 2007)

rab-10(ok1494) (From C. elegans Gene Knockout Consortium)

cnt-1(tm2313) (Dr. Shohei Mitani, Japanese National Bioresource Project for the Experimental Animal "Nematode C. elegans")

arf-6(tm1447) (Dr. Shohei Mitani, Japanese National Bioresource

Project for the Experimental Animal "Nematode C. elegans")

Chapter 5.

Conclusion and discussion

One of the main focuses of research in our lab is to investigate how the recycling cargos are sorted from the early endosome and returned back to the plasma membrane along the endocytic recycling pathway. The small GTPase RAB-10 has been identified as a key resident and regulator of the basolateral recycling endosome. *rab-10* mutants causes large vacuoles in the intestine which are detectable at the dissecting-microscope level. And since these vacuoles accumulate fluid-phase endocytic markers including ssGFP secreted from body wall muscle and fluorescent BSA microinjected into the body cavity, we learned that RAB-10 functions at the basolateral recycling step. In the worm intestine, RAB-10 partially colocalizes with early endosome marker RAB-5 and loss of RAB-10 caused accumulation of RAB-5. In addition, our lab uses the previously characterized CIE-dependent cargo hTAC and CDE-dependent cargo hTFR as model cargo to study the basolateral recycling pathway. *rab-10* mutant caused CIE-dependent cargo hTAC to accumulate in the worm intestine (Chen et al., 2006a).

Another key component of the basolateral recycling endosome is RME-1. RME-1 was first discovered in a screen for Receptor Mediated Endocytosis in which defects in the uptake of intestinally secreted yolk protein YP170A by oocytes were screened for. *rme-1* mutant animals displayed deficiency in yolk uptake by oocytes which turned out to be due to poor recycling of yolk receptor RME-2 in oocytes. *rme-1* mutants also have vacuoles in the intestine which can be recognized under the dissecting microscope. The enlarged vacuoles in *rme-1* mutant also accumulated fluid-phase basolateral endocytic markers and model basolateral recycling cargos hTFR and hTAC (Chen et al., 2006a; Grant et al., 2001b). *rme-1* mutant caused accumulation of RAB-10 and the enlarged structures of rme-1 labeled for ARF-6 but not RAB-5 (Chen et al., 2006a; Shi et al., 2010b). Under wild-type conditions, RME-1 labels a tubulovesicular meshwork of endosomes that is close to the basolateral membrane. However, in *rab-10* mutants, RME-1 labeled structures becomes diffusive. In mammalian cells, the RME-1 homolog EHD1 was also found to label endocytic recycling compartment and mediate the transport from recycling endosome to plasma membrane (Caplan et al., 2002; Lin et al., 2001). All these lines of evidence suggest that RME-1 could function at a step of the basolateral recycling pathway that is close to the plasma membrane and downstream of RAB-10

function. We could also infer from the results mentioned above that RAB-10 functions from the interface between early endosome and recycling endosome and at a later step that connects with RME-1 function that recycles cargo back to plasma membrane.

Encountered with continuous flow of proteins and membranes along the endocytic and exocytic pathways, cells face a formidable challenge in achieving accurate intracellular transport of membrane cargo. After internalization into the cell from plasma membrane, cargos arrive at the early endosome to be sorted for different destinations: (1) direct return plasma membrane through rapid recycling pathway (2) recycle through the recycling endosomes for further sorting and returned back to plasma membrane (Grant and Donaldson, 2009; Hsu and Prekeris, 2010b). (3) cycle from endosomes to the Golgi through retrograde pathway (Bonifacino and Rojas, 2006) (4) transport from early endosomes to late endosomes and finally to lysosomes for degradation (Raiborg and Stenmark, 2009). Such transport is likely to require tight regulation that enforces the directionality of sequential flow between membranous compartments (Hutagalung and Novick, 2011a).

Our keen interest rests on how is the recycling pathway branched from the sorting station, i.e. how do recycling cargo achieve the transition from early endosome to recycling endosome. We learned from previous work in the field that Rab GTPases serve as master regulators of membrane trafficking by controlling the structural and functional characteristics of intracellular organelles (Hutagalung and Novick, 2011a). The ability to switch between the "on" and "off" states through the Rab GTP/GDP cycle empowers Rab proteins to control the spatial and temporal regulation of cargo transport (Barr and Lambright, 2010). An ordered relay of cargo between sequentially acting compartments is thought to entail coordination of Rab activation states, coordinating changes in organelle maturation and/or allowing distinct compartments to interact at the right time and the right place for cargo transfer (Wandinger-Ness and Zerial, 2014). A Rab cascade model has been proposed that likely defines a general principle in membrane transport. This model proposes that an upstream GTP-loaded Rab protein recruits the GEF for the next Rab- GTPase along a transport pathway, activating the downstream Rab. In turn a countercurrent activity is initiated by the downstream GTP-loaded Rab,

which recruits the GAP for the upstream Rab to deactivate it (Hutagalung and Novick, 2011a). Therefore, we approached this problem on transition from the early endosome compartment to the recycling compartment from potential interaction between the key Rab proteins that labels these two endosomal compartment, RAB-5 and RAB-10, respectively.

In Chapter 2, we identified that TBC-2 plays a role in cargo recycling most likely by acting as a GAP protein for RAB-5. *tbc-2* mutant animals display accumulation of both CIE recycling cargo hTAC and CDE recycling cargo hTFR. Consistent with TBC-2 potentially act as a GAP protein to inactivate RAB-5, expression of RAB-5 in the nonhydrolyzable GTP-locked form mimics the loss of TBC-2 phenotype in recycling pathways in the fact that it causes even more dramatic accumulation of both recycling cargos hTAC and hTFR in the worm intestine. This work also revealed that the Rho-family GTPase CED-10, likely to be activated by the CED-5/CED-12 bipartite GEF, serves to bring TBC-2 onto endosomes to dampen the activity of RAB-5. CED-10 functions upstream of TBC-2 in the recycling pathway and its action in promoting cargo recycling is mainly through TBC-2 as overexpression of fluorescently tagged TBC-2 can bypass the deficiency in cargo recycling caused by loss of CED-10. CED-10 has some overlap with a small subset of RAB-5 labeled endosome and has the strongest overlap with the recycling endosome regulator RAB-10 and has less colocalization with the later acting recycling endosome protein RME-1. In addition, the GFP-RAB-5 and GFP-RAB-10 labeled puncta intensities increased in *ced-10* mutants. The recycling cargo hTAC was found to accumulate on EHBP-1 positive tubular recycling endosomes in *ced-10*, *ced-12* or *tbc-2* mutants. This work demonstrates how the crosstalk between Rho-family GTPase CED- 10 and Rab-family GTPase RAB-5 mediated by RABGAP protein TBC-2 can regulate the early-to-recycling pathway.

In Chapter 3, further work is done to investigate on how the transition from early endosome to recycling endosome is achieved from the RAB-5/RAB-10 interaction perspective. In this study, we showed that the downstream Rab, RAB-10, in its GTP-bound form, binds to RAB-5 GAP TBC-2 and is required for its recruitment to endosomes. This is consistent with the Rab cascade model where a RAB-10 works as

a downstream Rab to inactivate the upstream RAB-5 through a negative regulatory loop via the RAB-5 GAP TBC-2. Furthermore we have shown that loss of TBC-2 or RAB-10 increases association of RAB-5 with membranes, indicating abnormally high RAB-5 activation. Lack of TBC-2 also causes a dramatic morphological change in the RAB-5 labeled early endosomes. We observed accumulation of abnormally large, RAB-5-positive, pleomorphic endosome structures, many of which displayed increased overlap with RAB-10. Thus we reasoned that TBC-2 could serve as a bridge in the interaction between RAB-10 and RAB-5. This model suggests that without TBC-2, RAB-5 cannot be inactivated as part of the recycling pathway, and RAB-10 endosomes cannot properly separate from RAB-5 endosomes. Our cargo localization analysis shows that in *tbc-2* mutants the recycling cargo hTAC is mostly trapped in RAB-5 positive endosomes, indicating a defect in the exit of recycling cargo from early endosomes that cannot inactivate RAB-5. These results are reminiscent of the a counter-current GAP cascade in Saccharomyces cerevisiae that is required to restrict the spatial overlap of early and late Golgi Rabs Ypt1p and Ypt32p (Rivera-Molina and Novick, 2009).

Our study also showed that cargo transition from early endosomes to recycling endosomes requires the coordination of another regulator of the recycling pathway, BAR-domain protein AMPH-1. Our previous work also showed that AMPH-1 is involved in the endocytic recycling pathway potentially by binding to RME-1, a later acting player in the basolateral recycling pathway. (Pant et al., 2009). The AMPH-1 BAR domain binds directly to PI(4,5)P2 enriched membranes, can potentially sense membrane curvature, and can promote tubule formation (Pant et al., 2009). Like RAB-10, AMPH-1 contributes to endosomal recruitment of TBC-2. We also detected failure in proper separation of RAB-5 and RAB-10 and failure in the exit of recycling cargo from early endosomes in *amph-1* mutants, although the endosomes did not appear as grossly enlarged as in *tbc-2* mutants. An interesting possibility is that AMPH-1 derived membrane tubules could be directly involved in cargo transfer and AMPH-1 might act in the recycling pathway for a longer journey, possibly starting from the RAB-5/RAB-10 interface to the later acting RAB-10/RME-1 interface or even longer towards the tubules branching towards the plasma membrane.

Our current study delineated distinct regions of TBC-2 bound by RAB-10 binding and AMPH-1, favoring a cooperative rapport between RAB-10 and AMPH-1 in terms of interacting with TBC-2 and promote early-to-recycling transition over a competitive model between the two proteins.

Combining our work in Chapter 2 and Chapter 3, our observations indicate that TBC-2 is a key feedback regulator of RAB-5, acting as a molecular nexus that integrates signals from recycling endosome regulators RAB-10, AMPH-1, and CED-10. To ensure correct localization of peripheral membrane proteins at a certain transport step, multiple weak physical interactions are usually needed, perhaps to more precisely position such proteins at points where multiple binding partners converge, a concept sometimes called coincidence sensing. Such localization mechanisms may also be easily reversible, an important characteristic in dynamic situations.

We conclude here that recruitment of TBC-2 to endosomes during recycling is likely to be quite important in the complex process of endosomal transport, where RAB-5 activity is essential for early aspects of the pathway but needs to be deactivated for later events.

In wild-type animals our data showed that RAB-5-labeled endosomes and RAB-10-labeled endosomes appear as distinct puncta that show partial overlap, suggesting that only a subpopulation of RAB-5 and RAB-10 labeled endosomes is interacting at any given time. This could imply the existence of transient interactions between RAB-5 and RAB-10 labeled endosomes that function to transfer recycling cargo. Such transient interactions between early and recycling endosomes have been proposed in other systems, although the detailed mechanisms remain obscure (Rodal et al., 2011). Interestingly that work also indicated a BAR domain protein (Nwk) was involved in early endosome to recycling endosome transport, perhaps indicating cargo transfer via membrane tubules.

In Chapter 4, we further explored on how RAB-10 regulates the recycling endosome by studying a RAB-10 effector, CNT-1, which is the only *C. elegans* homolog of mammalian ACAP1 and ACAP2, Arf6 GTPase-activating proteins. Arf6 regulates endosome to

plasma membrane transport, in part through activation of type I phophatidylinositol-4-phosphate 5 kinase (PIP5KI). Our study indicates that CNT-1 binds to RAB-10 through its C-terminal ANK repeats and colocalizes with RAB-10 and ARF-6 on recycling endosomes *in vivo*. Furthermore RAB-10 recruits CNT-1 to endosomes to negatively regulate ARF-6. We found overaccumulation of endosomal phosphatidylinositol-4,5-bisphosphate (PI(4,5)P2) in *cnt-1* and *rab-10* mutants, and reduced endosomal PI(4,5)P2 levels in *arf-6* mutants. These mutants produced similar effects on endosomal recruitment of PI(4,5)P2-dependent membrane bending proteins RME-1/Ehd and SDPN-1/Syndapin/Pacsin and resulted in endosomal trapping of specific recycling cargo. Our studies identified a novel RAB-10 to ARF-6 regulatory loop required to regulate endosomal PI(4,5)P2, a key phosphoinositide in membrane traffic.

One future direction would be to understand the dynamic interactions between early and recycling endosomes that mediate cargo transfer. One speculation is that the early-to-recycling endosome transition might differ from the better-known mechanism for early-to-late endosome maturation. This is likely due to the morphological difference between late endosome and the recycling endosome. In the worm intestine, late endosome often labels round ring-like structures which could provide a better platform for the subdomain model in which RAB-5 is gradually removed from its domain of occupation and RAB-7 is recruited and expand its localization onto the round endosomal structures as early endosome mature into late endosome. The recycling endosome need to form a network of tubular vesicular structures which facilitates long distance transport. With the key Rab protein RAB-10 labeling mostly small punctate endosomal structures, we suspect that RAB-10 moves dynamically to contact and inactivate RAB-5, and this dynamic interaction and separation of RAB-5 and RAB-10 is necessary for formation of tubular recycling endosomes and the transfer of cargos from early endosome to recycling endosome. A recently study has casted some light onto the dynamic between RAB-10 and recycling cargo hTAC tubules supports this idea that RAB-10's dynamic movement could serve to guide the formation of hTAC tubules (Chen et al., 2014). Further work is needed to study the dynamic rapport between early endosome and recycling endosome.

References

[1] Babbey, C.M., Ahktar, N., Wang, E., Chen, C.C.-H., Grant, B.D., and Dunn, K.W. (2006). Rab10 Regulates Membrane Transport through Early Endosomes of Polarized Madin-Darby Canine Kidney Cells. Molecular Biology of the Cell 17, 3156-3175.

[2] Babbey, C.M., Ahktar, N., Wang, E., Chen, C.C., Grant, B.D., and Dunn, K.W. (2006a). Rab10 regulates membrane transport through early endosomes of polarized Madin-Darby canine kidney cells. Molecular biology of the cell 17, 3156-3175.

[3] Babbey, C.M., Ahktar, N., Wang, E., Chen, C.C.-H., Grant, B.D., and Dunn, K.W. (2006b). Rab10 Regulates Membrane Transport through Early Endosomes of Polarized Madin-Darby Canine Kidney Cells. Molecular Biology of the Cell 17, 3156-3175.

[4] Barr, F., and Lambright, D.G. (2010). Rab GEFs and GAPs. Current opinion in cell biology 22, 461-470.

[5] Bernards, A. (2003). GAPs galore! A survey of putative Ras superfamily GTPase activating proteins in man and Drosophila. Biochimica et biophysica acta 1603, 47-82.

[6] Bonifacino, J.S., and Rojas, R. (2006). Retrograde transport from endosomes to the trans- Golgi network. Nat Rev Mol Cell Biol 7, 568-579.

[7] Brenner, S. (1974). The genetics of Caenorhabditis elegans. Genetics 77, 71-94.

[8] Brown, F.D., Rozelle, A.L., Yin, H.L., Balla, T., and Donaldson, J.G. (2001). Phosphatidylinositol 4,5-bisphosphate and Arf6-regulated membrane traffic. The Journal of cell biology 154, 1007-1017.

[9] Brown, P.S., Wang, E., Aroeti, B., Chapin, S.J., Mostov, K.E., and Dunn, K.W. (2000). Definition of distinct compartments in polarized Madin-Darby canine kidney (MDCK) cells for membrane-volume sorting, polarized sorting and apical recycling. Traffic (Copenhagen, Denmark) 1, 124-140.

[10] Brugnera, E., Haney, L., Grimsley, C., Lu, M., Walk, S.F., Tosello-Trampont, A.C., Macara, I.G., Madhani, H., Fink, G.R., and Ravichandran, K.S. (2002). Unconventional Rac-GEF activity is mediated through the Dock180-ELMO complex. Nat Cell Biol 4, 574-582.

[11] Bucci, C., Parton, R.G., Mather, I.H., Stunnenberg, H., Simons, K., Hoflack, B., and Zerial, M. (1992). The small GTPase rab5 functions as a regulatory factor in the early endocytic pathway. Cell 70, 715-728.

[12] Cabello, J., Neukomm, L.J., Gunesdogan, U., Burkart, K., Charette, S.J., Lochnit, G., Hengartner, M.O., and Schnabel, R. (2010). The Wnt pathway controls cell death engulfment, spindle orientation, and migration through CED-10/Rac. PLoS Biol 8, e1000297.

[13] Caplan, S., Naslavsky, N., Hartnell, L.M., Lodge, R., Polishchuk, R.S., Donaldson, J.G., and Bonifacino, J.S. (2002). A tubular EHD1-containing compartment involved in the recycling of major histocompatibility complex class I molecules to the plasma membrane. The EMBO journal 21, 2557-2567.

[14] Cardoso, C.M., Jordao, L., and Vieira, O.V. (2010). Rab10 regulates phagosome maturation and its overexpression rescues Mycobacterium-containing phagosomes maturation. Traffic 11, 221-235.

[15] Carney, D.S., Davies, B.A., and Horazdovsky, B.F. (2006). Vps9 domain-containing proteins: activators of Rab5 GTPases from yeast to neurons. Trends in cell biology 16, 27-35.

[16] Casal, E., Federici, L., Zhang, W., Fernandez-Recio, J., Priego, E.M., Miguel, R.N., DuHadaway, J.B., Prendergast, G.C., Luisi, B.F., and Laue, E.D. (2006). The crystal structure of the BAR domain from human Bin1/amphiphysin II and its implications for molecular recognition. Biochemistry 45, 12917-12928.

[17] Casanova, J.E., Wang, X., Kumar, R., Bhartur, S.G., Navarre, J., Woodrum, J.E., Altschuler, Y., Ray, G.S., and Goldenring, J.R. (1999). Association of Rab25 and Rab11a with the apical recycling system of polarized Madin-Darby canine kidney cells. Molecular biology of the cell 10, 47-61.

[18] Chen, C.C., Schweinsberg, P.J., Vashist, S., Mareiniss, D.P., Lambie, E.J., and Grant, B.D. (2006a). RAB-10 is required for endocytic recycling in the Caenorhabditis elegans intestine. Molecular biology of the cell 17, 1286-1297.

[19] Chen, C.C.-H., Schweinsberg, P.J., Vashist, S., Mareiniss, D.P., Lambie, E.J., and Grant, B.D. (2006b). RAB-10 Is Required for Endocytic Recycling in the Caenorhabditis elegans Intestine. Mol Biol Cell 17, 1286-1297.

[20] Chen, S., Li, L., Li, J., Liu, B., Zhu, X., Zheng, L., Zhang, R., and Xu, T. (2014). SEC-10 and RAB- 10 coordinate basolateral recycling of clathrin-independent cargo through endosomal tubules in Caenorhabditis elegans. Proceedings of the National Academy of Sciences of the United States of America 111, 15432-15437.

[21] Chen, Y., Wang, Y., Zhang, J., Deng, Y., Jiang, L., Song, E., Wu, X.S., Hammer, J.A., Xu, T., and Lippincott-Schwartz, J. (2012). Rab10 and myosin-Va mediate insulin-stimulated GLUT4 storage vesicle translocation in adipocytes. The Journal of cell biology 198, 545-560.

[22] Chesneau, L., Dambournet, D., Machicoane, M., Kouranti, I., Fukuda, M., Goud, B., and Echard, A. (2012). An ARF6/Rab35 GTPase cascade for endocytic recycling and successful cytokinesis. Curr Biol 22, 147-153.

[23] Chotard, L., Mishra, A.K., Sylvain, M.-A., Tuck, S., Lambright, D.G., and Rocheleau, C.E. (2010a). TBC-2 Regulates RAB-5/RAB-7-mediated Endosomal Trafficking in Caenorhabditis elegans. Molecular Biology of the Cell 21, 2285-2296.

[24] Chotard, L., Mishra, A.K., Sylvain, M.A., Tuck, S., Lambright, D.G., and Rocheleau, C.E. (2010b). TBC-2 regulates RAB-5/RAB-7-mediated endosomal trafficking in Caenorhabditis elegans. Mol Biol Cell 21, 2285-2296.

[25] Chotard, L., Skorobogata, O., Sylvain, M.A., Shrivastava, S., and Rocheleau, C.E. (2010c). TBC- 2 is required for embryonic yolk protein storage and larval survival during L1 diapause in Caenorhabditis elegans. PLoS One 5, e15662. Clokey, G.V., and Jacobson, L.A. (1986). The autofluorescent "lipofuscin granules" in the intestinal cells of Caenorhabditis elegans are secondary lysosomes. Mechanisms of ageing and development 35, 79-94.

[26] D'Souza-Schorey, C., and Chavrier, P. (2006). ARF proteins: roles in membrane traffic and beyond. Nature reviews 7, 347-358.

[27] D'Souza-Schorey, C., van Donselaar, E., Hsu, V.W., Yang, C., Stahl, P.D., and Peters, P.J. (1998). ARF6 targets recycling vesicles to the plasma membrane: insights from an ultrastructural investigation. The Journal of cell biology 140, 603-616.

[28] Dai, J., Li, J., Bos, E., Porcionatto, M., Premont, R.T., Bourgoin, S., Peters, P.J., and Hsu, V.W. (2004). ACAP1 promotes endocytic recycling by recognizing recycling sorting signals. Developmental cell 7, 771-776.

[29] Dambournet, D., Machicoane, M., Chesneau, L., Sachse, M., Rocancourt, M., El Marjou, A., Formstecher, E., Salomon, R., Goud, B., and Echard, A. (2011). Rab35 GTPase and OCRL phosphatase remodel lipids and F-actin for successful cytokinesis. Nat Cell Biol 13, 981-988.

[30] de Renzis, S., Sonnichsen, B., and Zerial, M. (2002). Divalent Rab effectors regulate the sub- compartmental organization and sorting of early endosomes. Nature cell biology 4, 124-133.

[31] Del Conte-Zerial, P., Brusch, L., Rink, J.C., Collinet, C., Kalaidzidis, Y., Zerial, M., and Deutsch, A. (2008). Membrane identity and GTPase cascades regulated by toggle and cut-out switches. Molecular systems biology 4, 206.

[32] Deneka, M., Neeft, M., Popa, I., van Oort, M., Sprong, H., Oorschot, V., Klumperman, J., Schu, P., and van der Sluijs, P. (2003). Rabaptin-5alpha/rabaptin-4 serves as a linker between rab4 and gamma(1)-adaptin in membrane recycling from endosomes. Embo J 22, 2645-2657.

[33] Deng, C.Y., Lei, W.L., Xu, X.H., Ju, X.C., Liu, Y., and Luo, Z.G. (2014). JIP1 mediates anterograde transport of Rab10 cargos during neuronal polarization. The Journal of neuroscience : the official journal of the Society for Neuroscience 34, 1710-1723.

[34] Di Paolo, G., and De Camilli, P. (2006). Phosphoinositides in cell regulation and membrane dynamics. Nature 443, 651-657.

[35] Donaldson, J.G. (2005). Arfs, phosphoinositides and membrane traffic. Biochemical Society transactions 33, 1276-1278.

[36] Donaldson, J.G., and Honda, A. (2005). Localization and function of Arf family GTPases. Biochemical Society transactions 33, 639-642.

[37] Donaldson, J.G., Porat-Shliom, N., and Cohen, L.A. (2009). Clathrin-independent endocytosis: a unique platform for cell signaling and PM remodeling. Cell Signal 21, 1-6.

[38] Eaton, S., and Martin-Belmonte, F. (2014). Cargo sorting in the endocytic pathway: a key regulator of cell polarity and tissue dynamics. Cold Spring Harbor perspectives in biology 6, a016899.

[39] Echard, A., Jollivet, F., Martinez, O., Lacapre, J.-J., Rousselet, A., Janoueix-Lerosey, I., and Goud, B. (1998). Interaction of a Golgi-Associated Kinesin-Like Protein with Rab6. Science 279, 580-585.

[40] Egami, Y., Fukuda, M., and Araki, N. (2011). Rab35 regulates phagosome formation through recruitment of ACAP2 in macrophages during FcgammaR-mediated phagocytosis. Journal of cell science 124, 3557-3567.

[41] Eyster, C.A., Higginson, J.D., Huebner, R., Porat-Shliom, N., Weigert, R., Wu, W.W., Shen, R.F., and Donaldson, J.G. (2009). Discovery of new cargo proteins that enter cells through clathrin-independent endocytosis. Traffic (Copenhagen, Denmark) 10, 590-599.

[42] Folsch, H., Mattila, P.E., and Weisz, O.A. (2009). Taking the scenic route: biosynthetic traffic to the plasma membrane in polarized epithelial cells. Traffic 10, 972-981.

[43] Frasa, M.A., Maximiano, F.C., Smolarczyk, K., Francis, R.E., Betson, M.E., Lozano, E., Goldenring, J., Seabra, M.C., Rak, A., Ahmadian, M.R., et al. (2010a). Armus is a Rac1 effector that inactivates Rab7 and regulates E-cadherin degradation. Current biology : CB 20, 198- 208.

[44] Frasa, M.A.M., Maximiano, F.C., Smolarczyk, K., Francis, R.E., Betson, M.E., Lozano, E., Goldenring, J., Seabra, M.C., Rak, A., Ahmadian, M.R., et al. (2010b). Armus Is a Rac1 Effector that Inactivates Rab7 and Regulates E-Cadherin Degradation. Current Biology 20, 198-208.

[45] Friedland, A.E., Tzur, Y.B., Esvelt, K.M., Colaiacovo, M.P., Church, G.M., and Calarco, J.A. (2013). Heritable genome editing in C. elegans via a CRISPR-Cas9 system. Nature methods 10, 741-743.

[46] Garcia, P., Gupta, R., Shah, S., Morris, A.J., Rudge, S.A., Scarlata, S., Petrova, V., McLaughlin, S., and Rebecchi, M.J. (1995). The pleckstrin homology domain of phospholipase C-delta 1 binds with high affinity to phosphatidylinositol 4,5-bisphosphate in bilayer membranes. Biochemistry 34, 16228-16234.

[47] Gleason, R.J., Akintobi, A.M., Grant, B.D., and Padgett, R.W. (2014). BMP signaling requires retromer-dependent recycling of the type I receptor. Proceedings of the National Academy of Sciences of the United States of America 111, 2578-2583.

[48] Glodowski, D.R., Chen, C.C., Schaefer, H., Grant, B.D., and Rongo, C. (2007a). RAB-10 regulates glutamate receptor recycling in a cholesterol-dependent endocytosis pathway. Molecular biology of the cell 18, 4387-4396.

[49] Glodowski, D.R., Chen, C.C.-H., Schaefer, H., Grant, B.D., and Rongo, C. (2007b). RAB-10 Regulates Glutamate Receptor Recycling in a Cholesterol-dependent Endocytosis Pathway. Molecular Biology of the Cell 18, 4387-4396.

[50] Grant, B., Zhang, Y., Paupard, M.-C., Lin, S.X., Hall, D.H., and Hirsh, D. (2001a). Evidence that RME-1, a conserved C. elegans EH-domain protein, functions in endocytic recycling. Nat Cell Biol 3, 573-579.

[51] Grant, B., Zhang, Y., Paupard, M.C., Lin, S.X., Hall, D.H., and Hirsh, D. (2001b). Evidence that RME-1, a conserved C. elegans EH-domain protein, functions in endocytic recycling. Nature cell biology 3, 573-579.

[52] Grant, B.D., and Caplan, S. (2008). Mechanisms of EHD/RME-1 protein function in endocytic transport. Traffic 9, 2043-2052.

[53] Grant, B.D., and Donaldson, J.G. (2009). Pathways and mechanisms of endocytic recycling. Nat Rev Mol Cell Biol 10, 597-608.

[54] Grosshans, B.L., Ortiz, D., and Novick, P. (2006a). Rabs and their effectors: achieving specificity in membrane traffic. Proceedings of the National Academy of Sciences of the United States of America 103, 11821-11827.

[55] Grosshans, B.L., Ortiz, D., and Novick, P. (2006b). Rabs and their effectors: Achieving specificity in membrane traffic. Proceedings of the National Academy of Sciences 103, 11821-11827.

[56] Guilherme, A., Soriano, N.A., Bose, S., Holik, J., Bose, A., Pomerleau, D.P., Furcinitti, P., Leszyk, J., Corvera, S., and Czech, M.P. (2004a). EHD2 and the Novel EH Domain Binding Protein EHBP1 Couple Endocytosis to the Actin Cytoskeleton. Journal of Biological Chemistry 279, 10593-10605.

[57] Guilherme, A., Soriano, N.A., Furcinitti, P.S., and Czech, M.P. (2004b). Role of EHD1 and EHBP1 in Perinuclear Sorting and Insulin-regulated GLUT4 Recycling in 3T3-L1 Adipocytes. Journal of Biological Chemistry 279, 40062-40075.

[58] Guilherme, A., Soriano, N.A., Furcinitti, P.S., and Czech, M.P. (2004c). Role of EHD1 and EHBP1 in perinuclear sorting and insulin-regulated GLUT4 recycling in 3T3-L1 adipocytes. The Journal of biological chemistry 279, 40062-40075.

[59] Hermann, G.J., Schroeder, L.K., Hieb, C.A., Kershner, A.M., Rabbitts, B.M., Fonarev, P., Grant, B.D., and Priess, J.R. (2005). Genetic analysis of lysosomal trafficking in Caenorhabditis elegans. Molecular biology of the cell 16, 3273-3288.

[60] Honda, A., Nogami, M., Yokozeki, T., Yamazaki, M., Nakamura, H., Watanabe, H., Kawamoto, K., Nakayama, K., Morris, A.J., Frohman, M.A., et al. (1999). Phosphatidylinositol 4-phosphate 5-kinase alpha is a downstream effector of the small G protein ARF6 in membrane ruffle formation. Cell 99, 521-532.

[61] Hoogenraad, C.C., Popa, I., Futai, K., Martinez-Sanchez, E., Wulf, P.S., van Vlijmen, T., Dortland, B.R., Oorschot, V., Govers, R., Monti, M., et al. (2010). Neuron specific Rab4 effector GRASP-1 coordinates membrane specialization and maturation of recycling endosomes. PLoS Biol 8, e1000283.

[62] Howes, M.T., Mayor, S., and Parton, R.G. (2010). Molecules, mechanisms, and cellular roles of clathrin-independent endocytosis. Current Opinion in Cell Biology 22, 519-527.

[63] Hsu, V.W., and Prekeris, R. (2010a). Transport at the recycling endosome. Curr Opin Cell Biol 22, 528-534.

[64] Hsu, V.W., and Prekeris, R. (2010b). Transport at the recycling endosome. Current Opinion in Cell Biology 22, 528-534.

[65] Hutagalung, A.H., and Novick, P.J. (2011a). Role of Rab GTPases in membrane traffic and cell physiology. Physiol Rev 91, 119-149.

[66] Hutagalung, A.H., and Novick, P.J. (2011b). Role of Rab GTPases in Membrane Traffic and Cell Physiology. Physiological Reviews 91, 119-149.

[67] Inoue, H., and Randazzo, P.A. (2007). Arf GAPs and their interacting proteins. Traffic (Copenhagen, Denmark) 8, 1465-1475.

[68] Itoh, T., Satoh, M., Kanno, E., and Fukuda, M. (2006). Screening for target Rabs of TBC (Tre- 2/Bub2/Cdc16) domain-containing proteins based on their Rab-binding activity. Genes to Cells 11, 1023-1037.

[69] Jackson, L.P., Kelly, B.T., McCoy, A.J., Gaffry, T., James, L.C., Collins, B.M., Höning, S., Evans, P.R., and Owen, D.J. (2010). A Large-Scale Conformational Change Couples Membrane Recruitment to Cargo Binding in the AP2 Clathrin Adaptor Complex. Cell 141, 1220-1229.

[70] Jackson, T.R., Brown, F.D., Nie, Z., Miura, K., Foroni, L., Sun, J., Hsu, V.W., Donaldson, J.G., and Randazzo, P.A. (2000). ACAPs are arf6 GTPase-activating proteins that function in the cell periphery. The Journal of cell biology 151, 627-638.

[71] Jou, T.S., Leung, S.M., Fung, L.M., Ruiz, W.G., Nelson, W.J., and Apodaca, G. (2000). Selective alterations in biosynthetic and endocytic protein traffic in Madin-Darby canine kidney epithelial cells expressing mutants of the small GTPase Rac1. Mol Biol Cell 11, 287-304.

[72] Kanno, E., Ishibashi, K., Kobayashi, H., Matsui, T., Ohbayashi, N., and Fukuda, M. (2010). Comprehensive screening for novel Rab-binding proteins by GST pull-down assay using 60 different mammalian Rabs. Traffic (Copenhagen, Denmark).

[73] Kelly, B.T., and Owen, D.J. (2011). Endocytic sorting of transmembrane protein cargo. Current Opinion in Cell Biology 23, 404-412.

[74] Kinchen, J.M., and Ravichandran, K.S. (2007). Journey to the grave: signaling events regulating removal of apoptotic cells. J Cell Sci 120, 2143-2149.

[75] Kinchen, J.M., and Ravichandran, K.S. (2010). Identification of two evolutionarily conserved genes regulating processing of engulfed apoptotic cells. Nature 464, 778-782.

[76] Kobayashi, H., and Fukuda, M. (2012). Rab35 regulates Arf6 activity through centaurin beta2/ACAP2 during neurite outgrowth. Journal of cell science. Konig, S., Hoffmann, M., Mosblech, A., and Heilmann, I. (2008). Determination of content and fatty acid composition of unlabeled phosphoinositide species by thin-layer chromatography and gas chromatography. Anal Biochem 378, 197-201.

[77] Koo, T.H., Eipper, B.A., and Donaldson, J.G. (2007). Arf6 recruits the Rac GEF Kalirin to the plasma membrane facilitating Rac activation. BMC Cell Biol 8, 29.

[78] Kouranti, I., Sachse, M., Arouche, N., Goud, B., and Echard, A. (2006). Rab35 regulates an endocytic recycling pathway essential for the terminal steps of cytokinesis. Curr Biol 16, 1719-1725.

[79] Krauss, M., Kinuta, M., Wenk, M.R., De Camilli, P., Takei, K., and Haucke, V. (2003). ARF6 stimulates clathrin/AP-2 recruitment to synaptic membranes by activating phosphatidylinositol phosphate kinase type Igamma. The Journal of cell biology 162, 113-124.

[80] Li, J., Ballif, B.A., Powelka, A.M., Dai, J., Gygi, S.P., and Hsu, V.W. (2005). Phosphorylation of ACAP1 by Akt regulates the stimulation-dependent recycling of integrin beta1 to control cell migration. Developmental cell 9, 663-673.

[81] Li, J., Peters, P.J., Bai, M., Dai, J., Bos, E., Kirchhausen, T., Kandror, K.V., and Hsu, V.W. (2007). An ACAP1-containing clathrin coat complex for endocytic recycling. The Journal of cell biology 178, 453-464.

[82] Li, W., Zou, W., Zhao, D., Yan, J., Zhu, Z., Lu, J., and Wang, X. (2009). C. elegans Rab GTPase activating protein TBC-2 promotes cell corpse degradation by regulating the small GTPase RAB-5. Development 136, 2445-2455.

[83] Lin, S.X., Grant, B., Hirsh, D., and Maxfield, F.R. (2001). Rme-1 regulates the distribution and function of the endocytic recycling compartment in mammalian cells. Nature cell biology 3, 567-572.

[84] Linder, M.D., Uronen, R.L., Holtta-Vuori, M., van der Sluijs, P., Peranen, J., and Ikonen, E. (2007). Rab8-dependent recycling promotes endosomal cholesterol removal in normal and sphingolipidosis cells. Molecular biology of the cell 18, 47-56.

[85] Lundquist, E.A., Reddien, P.W., Hartwieg, E., Horvitz, H.R., and Bargmann, C.I. (2001). Three C. elegans Rac proteins and several alternative Rac regulators control axon guidance, cell migration and apoptotic cell phagocytosis. Development 128, 4475-4488.

[86] Manders, E.M., Stap, J., Brakenhoff, G.J., van Driel, R., and Aten, J.A. (1992). Dynamics of three-dimensional replication patterns during the S-phase, analysed by double labelling of DNA and confocal microscopy. Journal of cell science 103 (Pt 3), 857-862.

[87] McGhee, J.D. (2007). The C. elegans intestine. In WormBook, T.C.e.R. Community, ed. (WormBook).

[88] Melendez, A., and Levine, B. (2009). Autophagy in C. elegans. WormBook : the online review of *C. elegans* biology, 1-26.

[89] Mello, C., and Fire, A. (1995). DNA transformation. Methods in cell biology 48, 451-482.

[90] Naslavsky, N., Weigert, R., and Donaldson, J.G. (2003). Convergence of non-clathrin- and clathrin-derived endosomes involves Arf6 inactivation and changes in phosphoinositides. Molecular biology of the cell 14, 417-431.

[91] Naslavsky, N., Weigert, R., and Donaldson, J.G. (2004). Characterization of a nonclathrin endocytic pathway: membrane cargo and lipid requirements. Mol Biol Cell 15, 3542-3552.

[92] Nordmann, M., Cabrera, M., Perz, A., Brocker, C., Ostrowicz, C., Engelbrecht-Vandre, S., and Ungermann, C. (2010). The Mon1-Ccz1 complex is the GEF of the late endosomal Rab7 homolog Ypt7. Curr Biol 20, 1654-1659.

[93] Paix, A., Wang, Y., Smith, H.E., Lee, C.Y., Calidas, D., Lu, T., Smith, J., Schmidt, H., Krause, M.W., and Seydoux, G. (2014). Scalable and versatile genome editing using linear DNAs with microhomology to Cas9 Sites in Caenorhabditis elegans. Genetics 198, 1347-1356.

[94] Palamidessi, A., Frittoli, E., Garre, M., Faretta, M., Mione, M., Testa, I., Diaspro, A., Lanzetti, L., Scita, G., and Di Fiore, P.P. (2008). Endocytic trafficking of Rac is required for the spatial restriction of signaling in cell migration. Cell 134, 135-147.

[95] Pan, C.L., Baum, P.D., Gu, M., Jorgensen, E.M., Clark, S.G., and Garriga, G. (2008). C. elegans AP-2 and retromer control Wnt signaling by regulating mig-14/Wntless. Dev Cell 14, 132- 139.

[96] Pant, S., Sharma, M., Patel, K., Caplan, S., Carr, C.M., and Grant, B.D. (2009). AMPH- 1/Amphiphysin/Bin1 functions with RME-1/Ehd1 in endocytic recycling. Nature cell biology 11, 1399-1410.

[97] Patino-Lopez, G., Dong, X., Ben-Aissa, K., Bernot, K.M., Itoh, T., Fukuda, M., Kruhlak, M.J., Samelson, L.E., and Shaw, S. (2008). Rab35 and its GAP EPI64C in T cells regulate receptor recycling and immunological synapse formation. The Journal of biological chemistry 283, 18323-18330.

[98] Poteryaev, D., Datta, S., Ackema, K., Zerial, M., and Spang, A. (2010). Identification of the switch in early-to-late endosome transition. Cell 141, 497-508.

[99] Praitis, V., Casey, E., Collar, D., and Austin, J. (2001). Creation of low-copy integrated transgenic lines in Caenorhabditis elegans. Genetics 157, 1217-1226.

[100] Radhakrishna, H., Al-Awar, O., Khachikian, Z., and Donaldson, J.G. (1999). ARF6 requirement for Rac ruffling suggests a role for membrane trafficking in cortical actin rearrangements. J Cell Sci 112 (Pt 6), 855-866.

[101] Radhakrishna, H., and Donaldson, J.G. (1997). ADP-ribosylation factor 6 regulates a novel plasma membrane recycling pathway. The Journal of cell biology 139, 49-61.

[102] Raiborg, C., Bache, K.G., Mehlum, A., Stang, E., and Stenmark, H. (2001). Hrs recruits clathrin to early endosomes. The EMBO journal 20, 5008-5021.

[103] Raiborg, C., and Stenmark, H. (2009). The ESCRT machinery in endosomal sorting of ubiquitylated membrane proteins. Nature 458, 445-452.

[104] Raiborg, C., Wesche, J., Malerod, L., and Stenmark, H. (2006). Flat clathrin coats on endosomes mediate degradative protein sorting by scaffolding Hrs in dynamic microdomains. Journal of cell science 119, 2414-2424.

[105] Reddien, P.W., and Horvitz, H.R. (2000). CED-2/CrkII and CED-10/Rac control phagocytosis and cell migration in Caenorhabditis elegans. Nat Cell Biol 2, 131-136.

[106] Rink, J., Ghigo, E., Kalaidzidis, Y., and Zerial, M. (2005). Rab conversion as a mechanism of progression from early to late endosomes. Cell 122, 735-749.

[107] Rivera-Molina, F.E., and Novick, P.J. (2009). A Rab GAP cascade defines the boundary between two Rab GTPases on the secretory pathway. Proceedings of the National Academy of Sciences of the United States of America 106, 14408-14413.

[108] Rodal, A.A., Blunk, A.D., Akbergenova, Y., Jorquera, R.A., Buhl, L.K., and Littleton, J.T. (2011). A presynaptic endosomal trafficking pathway controls synaptic growth signaling. The Journal of cell biology 193, 201-217.

[109] Sano, H., Eguez, L., Teruel, M.N., Fukuda, M., Chuang, T.D., Chavez, J.A., Lienhard, G.E., and McGraw, T.E. (2007a). Rab10, a Target of the AS160 Rab GAP, Is Required for Insulin- Stimulated Translocation of GLUT4 to the Adipocyte Plasma Membrane. Cell Metabolism 5, 293-303.

[110] Sano, H., Eguez, L., Teruel, M.N., Fukuda, M., Chuang, T.D., Chavez, J.A., Lienhard, G.E., and McGraw, T.E. (2007b). Rab10, a target of the AS160 Rab GAP, is required for insulin- stimulated translocation of GLUT4 to the adipocyte plasma membrane. Cell metabolism 5, 293-303.

[111] Sasidharan, N., Sumakovic, M., Hannemann, M., Hegermann, J., Liewald, J.F., Olendrowitz, C., Koenig, S., Grant, B.D., Rizzoli, S.O., Gottschalk, A., et al. (2012). RAB-5 and RAB-10 cooperate to regulate neuropeptide release in Caenorhabditis elegans. Proceedings of the National Academy of Sciences of the United States of America 109, 18944-18949.

[112] Sato, K., Norris, A., Sato, M., and Grant, B.D. (2014). C. elegans as a model for membrane traffic. WormBook : the online review of *C. elegans* biology, 1-47.

[113] Sato, K.e.a. (2008). Differential requirements for clathrin in receptor-mediated endocytosis and maintenance of synaptic vesicle pools. Proceedings of the National Academy of Sciences, USA.

[114] Sato, M., Sato, K., Fonarev, P., Huang, C.J., Liou, W., and Grant, B.D. (2005). Caenorhabditis elegans RME-6 is a novel regulator of RAB-5 at the clathrin-coated pit. Nature cell biology 7, 559-569.

[115] Sato, M., Sato, K., Liou, W., Pant, S., Harada, A., and Grant, B.D. (2008). Regulation of endocytic recycling by C. elegans Rab35 and its regulator RME-4, a coated-pit protein. The EMBO journal 27, 1183-1196.

[116] Sato, T., Mushiake, S., Kato, Y., Sato, K., Sato, M., Takeda, N., Ozono, K., Miki, K., Kubo, Y., Tsuji, A., et al. (2007). The Rab8 GTPase regulates apical protein localization in intestinal cells. Nature 448, 366-369.

[117] Schindelin, J., Arganda-Carreras, I., Frise, E., Kaynig, V., Longair, M., Pietzsch, T., Preibisch, S., Rueden, C., Saalfeld, S., Schmid, B., et al. (2012). Fiji: an open-source platform for biological- image analysis. Nature methods 9, 676-682.

[118] Schuck, S., Gerl, M.J., Ang, A., Manninen, A., Keller, P., Mellman, I., and Simons, K. (2007a). Rab10 is involved in basolateral transport in polarized Madin-Darby canine kidney cells. Traffic 8, 47-60.

[119] Schuck, S., Gerl, M.J., Ang, A., Manninen, A., Keller, P., Mellman, I., and Simons, K. (2007b). Rab10 is Involved in Basolateral Transport in Polarized Madin-Darby Canine Kidney Cells. Traffic 8, 47-60.

[120] Shi, A., Chen, C.C., Banerjee, R., Glodowski, D., Audhya, A., Rongo, C., and Grant, B.D. (2010a). EHBP-1 functions with RAB-10 during endocytic recycling in Caenorhabditis elegans. In Mol Biol Cell, pp. 2930-2943.

[121] Shi, A., Chen, C.C., Banerjee, R., Glodowski, D., Audhya, A., Rongo, C., and Grant, B.D. (2010b). EHBP-1 functions with RAB-10 during endocytic recycling in Caenorhabditis elegans. Molecular biology of the cell 21, 2930-2943.

[122] Shi, A., Chen, C.C.-H., Banerjee, R., Glodowski, D., Audhya, A., Rongo, C., and Grant, B.D. (2010c). EHBP-1 Functions with RAB-10 during Endocytic Recycling in Caenorhabditis elegans. Mol Biol Cell 21, 2930-2943.

[123] Shi, A., Liu, O., Koenig, S., Banerjee, R., Chen, C.C., Eimer, S., and Grant, B.D. (2012). RAB-10- GTPase-mediated regulation of endosomal phosphatidylinositol-4,5-bisphosphate. Proceedings of the National Academy of Sciences of the United States of America 109, E2306-2315.

[124] Shi, A., Pant, S., Balklava, Z., Chen, C.C., Figueroa, V., and Grant, B.D. (2007). A novel requirement for C. elegans Alix/ALX-1 in RME-1-mediated membrane transport. Curr Biol 17, 1913-1924.

[125] Shi, A., Sun, L., Banerjee, R., Tobin, M., Zhang, Y., and Grant, B.D. (2009). Regulation of endosomal clathrin and retromer-mediated endosome to Golgi retrograde transport by the J-domain protein RME-8. Embo J 28, 3290-3302.

[126] Shinozaki-Narikawa, N., Kodama, T., and Shibasaki, Y. (2006). Cooperation of phosphoinositides and BAR domain proteins in endosomal tubulation. Traffic (Copenhagen, Denmark) 7, 1539-1550.

[127] Shteyn, E., Pigati, L., and Folsch, H. (2011). Arf6 regulates AP-1B-dependent sorting in polarized epithelial cells. The Journal of cell biology 194, 873-887.

[128] Sobajima, T., Yoshimura, S., Iwano, T., Kunii, M., Watanabe, M., Atik, N., Mushiake, S., Morii, E., Koyama, Y., Miyoshi, E., et al. (2014). Rab11a is required for apical protein localisation in the intestine. Biology open 4, 86-94.

[129] Sonnichsen, B., De Renzis, S., Nielsen, E., Rietdorf, J., and Zerial, M. (2000). Distinct membrane domains on endosomes in the recycling pathway visualized by multicolor imaging of Rab4, Rab5, and Rab11. J Cell Biol 149, 901-914.

[130] Stenmark, H. (2009). Rab GTPases as coordinators of vesicle traffic. Nature reviews Molecular cell biology 10, 513-525.

[131] Stenmark, H., Parton, R.G., Steele-Mortimer, O., Lutcke, A., Gruenberg, J., and Zerial, M. (1994). Inhibition of *rab5* GTPase activity stimulates membrane fusion in endocytosis. Embo J 13, 1287-1296.

[132] Struckhoff, E.C., and Lundquist, E.A. (2003). The actin-binding protein UNC-115 is an effector of Rac signaling during axon pathfinding in C. elegans. Development 130, 693-704.

[133] Sun, L., Liu, O., Desai, J., Karbassi, F., Sylvain, M.-A., Shi, A., Zhou, Z., Rocheleau, C.E., and Grant, B.D. (2012a). CED-10/Rac1 Regulates Endocytic Recycling through the RAB-5 GAP TBC-2. PLoS Genet 8, e1002785.

[134] Sun, L., Liu, O., Desai, J., Karbassi, F., Sylvain, M.A., Shi, A., Zhou, Z., Rocheleau, C.E., and Grant, B.D. (2012b). CED-10/Rac1 regulates endocytic recycling through the RAB-5 GAP TBC-2. PLoS genetics 8, e1002785.

[135] Thompson, A., Nessler, R., Wisco, D., Anderson, E., Winckler, B., and Sheff, D. (2007). Recycling endosomes of polarized epithelial cells actively sort apical and basolateral cargos into separate subdomains. Mol Biol Cell 18, 2687-2697.

[136] Traub, L.M. (2009). Tickets to ride: selecting cargo for clathrin-regulated internalization. Nature reviews Molecular cell biology 10, 583-596.

[137] Treusch, S., Knuth, S., Slaugenhaupt, S.A., Goldin, E., Grant, B.D., and Fares, H. (2004). Caenorhabditis elegans functional orthologue of human protein h-mucolipin-1 is required for lysosome biogenesis. Proceedings of the National Academy of Sciences of the United States of America 101, 4483-4488.

[138] van Dam, E.M., and Stoorvogel, W. (2002). Dynamin-dependent transferrin receptor recycling by endosome-derived clathrin-coated vesicles. Molecular biology of the cell 13, 169-182.

[139] Wandinger-Ness, A., and Zerial, M. (2014). Rab proteins and the compartmentalization of the endosomal system. Cold Spring Harbor perspectives in biology 6, a022616.

[140] Wang, D., Lou, J., Ouyang, C., Chen, W., Liu, Y., Liu, X., Cao, X., Wang, J., and Lu, L. (2010). Ras- related protein Rab10 facilitates TLR4 signaling by promoting replenishment of TLR4 onto the plasma membrane. Proceedings of the National Academy of Sciences of the United States of America 107, 13806-13811.

[141] Wang, E., Brown, P.S., Aroeti, B., Chapin, S.J., Mostov, K.E., and Dunn, K.W. (2000). Apical and basolateral endocytic pathways of MDCK cells meet in acidic common endosomes distinct from a nearly-neutral apical recycling endosome. Traffic 1, 480-493.

[142] Wang, T., Liu, Y., Xu, X.H., Deng, C.Y., Wu, K.Y., Zhu, J., Fu, X.Q., He, M., and Luo, Z.G. (2011). Lgl1 activation of rab10 promotes axonal membrane trafficking underlying neuronal polarization. Developmental cell 21, 431-444.

[143] Wang, W., and Ferro-Novick, S. (2002). A Ypt32p exchange factor is a putative effector of Ypt1p. Molecular biology of the cell 13, 3336-3343.

[144] Weigert, R., Yeung, A.C., Li, J., and Donaldson, J.G. (2004). Rab22a regulates the recycling of membrane proteins internalized independently of clathrin. Mol Biol Cell 15, 3758-3770.

[145] Xin, X., Gfeller, D., Cheng, J., Tonikian, R., Sun, L., Guo, A., Lopez, L., Pavlenco, A., Akintobi, A., Zhang, Y., et al. (2013). SH3 interactome conserves general function over specific form. Molecular systems biology 9, 652.

[146] Yang, P.T., Lorenowicz, M.J., Silhankova, M., Coudreuse, D.Y., Betist, M.C., and Korswagen, H.C. (2008). Wnt signaling requires retromer-dependent recycling of MIG-14/Wntless in Wnt- producing cells. Dev Cell 14, 140-147.

[147] Yin, H.L., and Janmey, P.A. (2003). Phosphoinositide regulation of the actin cytoskeleton. Annual review of physiology 65, 761-789.

[148] Zeigerer, A., Gilleron, J., Bogorad, R.L., Marsico, G., Nonaka, H., Seifert, S., Epstein-Barash, H., Kuchimanchi, S., Peng, C.G., Ruda, V.M., et al. (2012). Rab5 is necessary for the biogenesis of the endolysosomal system in vivo. Nature 485, 465-470.

[149] Zhou, Y., Toth, M., Hamman, M.S., Monahan, S.J., Lodge, P.A., Boynton, A.L., and Salgaller, M.L. (2002). Serological cloning of PARIS-1: a new TBC domain-containing, immunogenic tumor antigen from a prostate cancer cell line. Biochemical and biophysical research communications 290, 830-838.